

FEDERAL UNIVERSITY OF ABC  
Center for Natural and Human Sciences  
Postgraduate Program in Nanoscience and Advanced Materials

Jose Eduardo Ulloa Rojas

**Preparation and characterization of fibroin hydrogels for potential  
application in photodynamic therapy**

Santo André-SP 2017



FEDERAL UNIVERSITY OF ABC  
Center for Natural and Human Sciences

Postgraduate Program in Nanoscience and Advanced Materials

**Preparation and characterization of fibroin hydrogels for potential  
application in photodynamic therapy**

Candidate: Jose Eduardo Ulloa Rojas

Advisor: Prof. Dr. Wendel Andrade Alves

Santo André, São Paulo 2017

Jose Eduardo Ulloa Rojas

**Preparation and characterization of fibroin hydrogels for potential application in photodynamic therapy**

*Dissertação apresentada ao Centro de Ciências Naturais e Humanas da Universidade Federal do ABC para obtenção do Título de Mestre em nanociência e materiais avançados*

*Orientador: Prof. Dr. Wendel Andrade Alves*

Santo André

Mês /2014

**Sistema de Bibliotecas da Universidade Federal do ABC**  
Elaborada pelo Sistema de Geração de Ficha Catalográfica da UFABC  
com os dados fornecidos pelo(a) autor(a).

Ulloa Rojas, Jose Eduardo

Preparation and characterization of fibroin hydrogels for potential  
application in photodynamic therapy / Jose Eduardo Ulloa Rojas. — 2017.

103 fls.

Orientador: Wendel Andrade Alves

Dissertação (Mestrado) — Universidade Federal do ABC, Programa de Pós  
Graduação em Nanociências e Materiais Avançados, Santo Andre, 2017.

1. Fibroína. 2. Hidrogéis. 3. Fototerapia. 4. Nanociências. I. Andrade  
Alves, Wendel. II. Programa de Pós-Graduação em Nanociências e Materiais  
Avançados, 2017. III. Título.

Este exemplar foi revisado e alterado em relação à versão original, de acordo com as observações levantadas pela banca no dia da defesa, sob responsabilidade única do autor e com a anuência de seu orientador.

Santo André, 28 de agosto de 2017.

Assinatura do autor: Jose Eduardo Villos Rojas

Assinatura do orientador: 





**MINISTÉRIO DA EDUCAÇÃO**  
**Fundação Universidade Federal do ABC**  
**Programa de Pós-Graduação em Nanociências e Materiais Avançados**  
Avenida dos Estados, 5001 – Bairro Santa Terezinha – Santo André – SP  
CEP 09210-580 · Fone: (11) 4996-0017  
ppg.nanomat@ufabc.edu.br

## FOLHA DE ASSINATURAS

Assinaturas dos membros da Banca Examinadora que avaliou e aprovou a Defesa de Dissertação de Mestrado do candidato Jose Eduardo Ulloa Rojas, realizada em 30 de junho de 2017:

Prof.(a) Dr.(a) **Wendel Andrade Alves** (Universidade Federal do ABC) – Presidente

Prof.(a) Dr.(a) **Danilo Justino Carastan** (Universidade Federal do ABC) – Membro Titular

Prof.(a) Dr.(a) **Frank Herbert Quina** (Universidade de São Paulo) – Membro Titular

Prof.(a) Dr.(a) **Amedea Barozzi Seabra** (Universidade Federal do ABC) – Membro Suplente

Prof.(a) Dr.(a) **Iseli Lourenço Nantes** (Universidade Federal do ABC) – Membro Suplente

Prof.(a) Dr.(a) **Rosangela Itri** (Universidade de São Paulo) – Membro Suplente

Prof.(a) Dr.(a) **Herculano da Silva Martinho** (Universidade Federal do ABC) – Membro Suplente



Universidade Federal do ABC

# Agradecimentos

Ao Prof. Dr. Wendel Andrade Alves pela orientação e pela oportunidade concedida.

À doutoranda Valéria Sandra, pela orientação e pelos ensinamentos que tem me passado. E por toda a assistência prestada nestes dois anos.

À Prof. Francesca Giuntini pela ajuda e pela orientação.

À UFABC, ao Grupo Comibra de Universidades Brasileiras e a OEA pela bolsa de Mestrado.

Ao FAPESP e CNPq, pelo auxílio financeiro.

A todos aqueles que de forma direta ou indireta contribuíram para a conclusão deste trabalho.

“Greatness is a transitory experience. It is never consistent. It depends in part upon the myth-making imagination of humankind. The person who experiences greatness must have a feeling for the myth he is in. He must reflect what is projected upon him. And he must have a strong sense of the sardonic. This is what uncouples him from belief in his own pretensions. The sardonic is all that permits him to move within himself. Without this quality, even occasional greatness will destroy a man.”

- Frank Herbert

“We’re all stories, in the end.  
Just make it a good one, eh?”

— The Doctor



## Abstract

The research in to natural materials has notably increased in recent years due to the opportunity of combining biocompatibility with exceptional physical, mechanical, and chemical properties, which would be arduous to obtain following a synthetic route. Among these natural polymers, silk fibroin is attractive because of its optical transparency, outstanding mechanical robustness and compatibility with living systems, with the formation of non-inflammatory degradation products. In this study, we were capable to form translucent hydrogels from raw silk fibers at different concentrations and used them as matrix to incorporate a photosensitive molecule - sodium (4,4',4''-(20-(4-(3-carboxypropanamido) phenyl) porphyrin-5,10,15-triyl) tribenzenesulfonate - for future use in photodynamic therapy. The obtained hydrogels were characterized by different rheology techniques and spectrophotometry analysis to study the factors that are involved in the formation of the hydrogel, and to have information about silk fibroin (SF) properties after adding the porphyrin molecule to the matrix. The set of obtained results showed that the SF hydrogels have a shear thinning behavior, where the viscosity of the gel decrease whit the increase of the shear rate, and that it can be classified as thixotropic materials. This mean that the structure of the material needs time to recover after experience shear deformation. Also, we observed that the secondary structure of the fibroin is not affected by the addition of porphyrin in any concentration, it was confirmed by the negative Cotton signal around 220 nm in the circular dichroism spectra. The hybrid porphyrin-fibroin nanofibers were capable to generate singlet oxygen after gelification, and we proved that silk fibroin hydrogels are an excellent matrix to encapsulate other molecules to application in photodynamic therapy and photothermal therapy, leading to the formation of self-assembled peptide nanostructures with controllable phototherapeutic effects.

**Key words:** Porphyrin, fibroin, hydrogels, photodynamic therapy, crosslinking, rheology, singlet oxygen.

## Resumo

A pesquisa em materiais naturais aumentou notavelmente nos últimos anos devido à oportunidade de combinar biocompatibilidade com propriedades físicas, mecânicas e químicas excepcionais, o que seria árduo para obter seguindo uma rota sintética. Entre estes polímeros naturais, a fibroína de seda é atraente por sua transparência óptica, excelente robustez mecânica e compatibilidade com sistemas vivos, com a formação de produtos de degradação não inflamatória. Neste estudo, fomos capazes de formar hidrogéis translúcidos a partir de fibras de seda crua em diferentes concentrações e usamos como matriz para incorporar uma molécula fotossensível : sódio (4,4', 4' - (20-(4- (3-carboxipropanamido ) Fenil) porfirina-5,10,15-triil) tribenzenossulfonato - para uso futuro na terapia fotodinâmica. Os hidrogéis obtidos foram caracterizados por diferentes técnicas de reologia e análise de espectrofotometria para estudar os fatores envolvidos na formação do hidrogel e para obter informações sobre propriedades da fibroína da seda (SF) após a adição da molécula de porfirina na matriz. O conjunto de resultados obtidos mostrou que os hidrogéis SF têm um comportamento de desbaste de cisalhamento, onde a viscosidade do gel diminui com o aumento da taxa de cisalhamento e que pode ser classificado como materiais tixotrópicos, o que significa que a estrutura do material precisa de tempo para se recuperar após a deformação de cisalhamento da experiência. Além disso, observamos que a estrutura secundária da fibroína não é afetado pela adição de porfirina em qualquer concentração, foi confirmado pelo sinal negativo de Cotom em torno de 220 nm nos espectros de dicroísmo circular. As nanofibras de fibroína porfirina híbridas foram capazes de gerar oxigênio singlete após a gelificação, e provamos que os hidrogéis de fibroína de seda são uma excelente matriz para encapsular outras moléculas para aplicação em terapia fotodinâmica e terapia fototérmica, levando à formação de nanoestruturas de péptido auto-montadas com efeitos fototerapêuticos controláveis.

**Palavras-Chave:** Porfirina, fibroína, hidrogéis, terapia fotodinâmica, reticulação, reologia, oxigênio singlete.

## Figures Index

Figure 1 .Silk fibroin structure diagrams a) Silk fibroin $\beta$ -sheet crystal secondary structure, b) Silk fibroin fibers structures (JOANA; VASCONCELOS, 2010). ....	5
Figure 2.Silk Fibroin is purified from silk sericin and dissolved whit inorganic salts as LiBr to form silk fibroin solutions (HARDY; LEAL-EGAÑA; SCHEIBEL, 2013). ....	7
Figure 3. Schematic of material forms fabricated from silk fibroin (ROCKWOOD et al., 2011). ....	8
Figure 4. Applications of different silk material formats in photonics, drug delivery, electronic devices, textiles and tissue scaffolds. (LIU; ZHANG, 2014). ....	9
Figure 5. Schematic of the pentacene OTFT with silk fibroin as the gate dielectric developed by Wang et al. 2011. ....	10
Figure 6. Modulation of silk fibroin properties through protein secondary structure formation using methanol (PRITCHARD et al., 2014) ....	12
Figure 7. a) Schematic diagram of a parallel-plate rheometer, one of the plates is moved with a velocity U relative to the second stationary plate, causing thinnest layers of the liquid to be displaced between the plates, b) Parallel plate model (OSSWALD, 2015). ....	13
Figure 8. Relationship between microstructure and viscosity of shear thinning-shear thickening transition in hard-sphere colloidal suspensions. ....	15
Figure 9 . Hysteresis loop of a thixotropic material (CHIARI et al., 2012) . ....	16
Figure 10 . a) Descriptive outline about the general PDT mechanism a) Type I reaction and Type II reaction PDT mechanism. (SINGH et al., 2014). ....	19
Figure 11 . Classification of photosensitizers as porphyrin-based or nonporphyrin-based molecules. post-treatment. (O'CONNOR; GALLAGHER; BYRNE, 2009) ....	21
Figure 12 . Porphin basic structure formed by a porphyrin ring of twenty carbon atoms composed by four pyrrole molecules connected by methane bridges. ....	22
Figure 13.Frisson Silk degumming process in a 0.02 M (2g/L) of Na <sub>2</sub> CO <sub>3</sub> solution at 85 °C for 30 min for three times. ....	24
Figure 14 .General degummed Frisson fibroin dissolving process with LiBr 9.5M. ....	25
Figure 15. Methodology used for the Preparation of fibroin - ethanol-water Hydrogels from a 61 mg/mL fibroin solution (6.1% m/v). ....	27
Figure 16 .Structure, formula and molecular weight of the water-soluble porphyrin added to the fibroin hydrogel matrix. ....	28
Figure 17. Preparation of SF and porphyrin hydrogels at different concentration of porphyrin. ....	29
Figure 18.Franz's cell apparatus used in the permeability test. ....	34
Figure 19. Fibroin solutions obtained by four different dispersion methods, A) CaCl <sub>2</sub> -EtOH- H <sub>2</sub> O, 1:2:8 (molar), B) LiCl-H <sub>2</sub> O 9.5 M. C) LiCl-EtOH-H <sub>2</sub> O, 10:18:72 (w/w), D) LiBr 9.3 M. ....	37
Figure 20 . Fibroin hydrogels obtained by adding different ratios of ethanol to the silk fibroin solutions: A) SFS1000, B) SFS750, C) SFS500 and D) SFS250. ....	40
Figure 21 . Fibroin hydrogels with different porphyrin concentrations: A)1mg/ml, B)0,5mg/ml, C)0,25 mg/ml, D)0,1 mg/ml, C) 0,05 mg/ml and D) 0,025 mg/ml. ....	41
Figure 22 . Fibroin hydrogels(3,9mg/ml) with different porphyrin concentrations: A)1mg/ml, B)0,5mg/ml, C)0,25 mg/ml, D)0,1 mg/ml, C) 0,05 mg/ml and D) 0,025 mg/ml. ....	41
Figure 23 . LVER curve of a Fibroin Hydrogel with different concentrations of fibroin solutions (●) 15.2 mg/mL, (○)15.2 mg/mL, (■) 7.5 mg/mL, (□) 7.5 mg/mL, (▲) 2.5 mg/mL,(Δ) 2.5 mg/mL. . Closed symbols represent the G' value and open symbols the G'' value. ....	42
Figure 24 . Frequency sweep of the fibroin hydrogels with different ratios of silk fibroin solution and ethanol 50% solution . Closed symbols represent the G' value and open symbols the G'' value. (●) 750F-250EtOH 50%, (○)750F-250EtOH 50%, (■) 500F-500EtOH 50%, (□) 500F-500EtOH 50%, (◆) 250F-750EtOH. ....	44

Figure 25. Frequency sweep of the fibroin hydrogels with different content of fibroin. Closed symbols represent the $G'$ value and open symbols the $G''$ value. (●) 2.5 mg/mL, (○) 2.5 mg/mL, (◆) 5 mg/mL (◇) 5 mg/mL. All the hydrogels maintain the SF250 ratio and were obtained from a SFS 61 mg/mL (6.1%). ....	45
Figure 26. Frequency sweep of the fibroin hydrogels with different content of fibroin. Closed symbols represent the $G'$ value and open symbols the $G''$ value. (●) 10 mg/ml, (○) 10 mg/ml, (■) 7.5mg/ml, (□) 7.5mg/ml, (◇) 6.2 mg/mL, (◆) 6.2 mg/mL. ....	46
Figure 27. Frequency sweep of the fibroin hydrogels with different content of fibroin. Closed symbols represent the $G'$ value and open symbols the $G''$ value. (●) 15.2 mg/ml, (○) 15.2 mg/ml, (■) 15 mg/mL, (□) 15 mg/mL, (◇) 12.5mg/mL, (◆) 12.5mg/mL.....	46
Figure 28. Flow rheograms of the hydrogels composed of Fibroin 2.5 mg/mL. The arrows point the direction of the curve, upstream and downstream.....	49
Figure 29. Flow rheograms of the hydrogels composed of Fibroin 7.5 mg/mL. The arrows point the direction of the curve, upstream and downstream.....	50
Figure 30. Flow rheograms of the hydrogels composed of Fibroin 10 mg/mL. The arrows point the direction of the curve, upstream and downstream.....	51
Figure 31. Flow rheograms of the hydrogels composed of Fibroin 12.5mg/ mL. The arrows point the direction of the curve, upstream and downstream.....	51
Figure 32. Flow rheograms of the hydrogels composed of Fibroin 15.2 mg/mL . The arrows point the direction of the flow curve, upstream and downstream. ....	52
Figure 33. Viscosity vs. Shear rate curve of the hydrogels composed of 2.5 ,7.5 ,12.25 and 15.2 mg/ml of fibroin.....	53
Figure 34. Frequency sweep of the fibroin hydrogels (7.5 mg/mL of fibroin) with different content of Porphyrin. Closed symbols represent the $G'$ value and open symbols the $G''$ value. (●) 0.05 mg/ml, (○) 0.05 mg/ml, (■) 0.025 mg/ml, (□) 0.025 mg/ml and (◆) Fibroin 7.5mg/ml, (◇) Fibroin 7.5 for comparison.....	54
Figure 35. Frequency sweep of the fibroin hydrogels (7.5 mg/mL of fibroin) with different content of Porphyrin. Closed symbols represent the $G'$ value and open symbols the $G''$ value. (●) 1 mg/ml, (○) 1 mg/ml, (■) 0.5 mg/ml, (□) 0.5 mg/ml, (▲) 0.25 mg/ml, (▲) 0.25 mg/ml, (◆) 0.1 mg/ml, (◇) 0.1 mg/mL of porphyrin. ....	55
Figure 36. Viscosity vs. Shear rate curve of the hydrogels composed of Fibroin 7.5 mg/mL and 1, 0.25, 0.1 and 0.025 mg/mL of porphyrin. ....	57
Figure 37. Flow rheograms of the hydrogels composed of Fibroin 7.5mg/ml and Porphyrin 1mg/ml. The arrows point the direction of the flow curve, upstream and downstream.....	57
Figure 38. Flow rheograms of the hydrogels composed of Fibroin 7.5mg/ml and Porphyrin 0.25mg/ml. The arrows point the direction of the flow curve, upstream and downstream.....	58
Figure 39. Flow rheograms of the hydrogels composed of Fibroin 7.5mg/ml and Porphyrin 0.1mg/ml. The arrows point the direction of the flow curve, upstream and downstream.....	58
Figure 40. Flow rheograms of the hydrogels composed of Fibroin 7.5mg/ml and Porphyrin 0.0026mg/ml. The arrows point the direction of the flow curve, upstream and downstream. ....	59
Figure 41. UV-Vis spectrum from Fibroin solution 6.1% and Fibroin hydrogels with different ratios of fibroin solution and ethanol 50%. ....	61
Figure 42. UV-Vis spectrum from Porphyrin solutions in different concentrations. The UV-vis signal for 1mg/mL of porphyrin solution is not shown because it is higher than 2. ....	62
Figure 43. UV-Vis spectrum from Fibroin 7.5 mg/ml with different concentrations of Porphyrin. The UV-vis signal for 1mg/mL of porphyrin hydrogel is not shown because it is higher than 2. ....	63
Figure 44. Fluorescence spectra from Fibroin 7.5 mg/mL with different concentrations of Porphyrin (solid lines) and porphyrin solutions (dots). ....	65
Figure 45. CD spectra for Fibroin hydrogels at different concentrations and Fibroin solution 6.1% m/v (61 mg/mL), recorded at 25 °C with a 10-s accumulation time at the rate of 200 nm/min.....	67
Figure 46. CD spectra for Fibroin- Porphyrin hydrogels in different concentrations and 1mg/mL of porphyrin solution as a control recorded at 25 °C with a 10-s accumulation time at the rate of 200 nm/min.....	68
Figure 47. FTIR spectrum of fibroin films with different porphyrin concentrations (0.025, 0.05, 0.1, 0.25, 0.5 and 1mg/mL). It is potable to observe the typical absorption peaks of the amide I,II and III.....	69

Figure 48. SEM Images of dry films form from Silk Fibroin hydrogels with different concentrations of fibroin at 1 $\mu\text{m}$ : a) 7.5 mg/mL, b) 12.25 mg/mL and c) 15.2 mg/mL. ....	70
Figure 49. SEM Images of dry films form from silk fibroin hydrogels with different concentrations of porphyrins at 1 $\mu\text{m}$ : a) 1 mg/mL , b) 0.1mg/mL and c) 0.025 mg/mL. ....	71
Figure 50. SEM cross section Images of dry films form from 7.5 mg/mL of Silk Fibroin. ....	72
Figure 51. Scattering curve (log-log scale) of the concentration effect of porphyrin concentration in fibroin hydrogels. . 0 mg/mL (only fibroin 7mg/mL), 0.025 mg/mL, 0.25 mg/mL and 1mg/mL of porphyrin. ....	73
Figure 52. Guiner plot of the concentration effect of porphyrin concentration in fibroin hydrogels. 0 mg/mL (only fibroin 7mg/mL), 0.025 mg/mL, 0.25 mg/mL and 1mg/mL of porphyrin. ....	74
Figure 53. SAXS study of the concentration effect of porphyrin on fibroin hydrogel. SAXS curve linear fit performed on the lowest q region of the SAXS curves at 25°C. 0 mg/mL (only fibroin 7mg/mL), 0.025 mg/mL, 0.25 mg/mL and 1mg/mL of porphyrin. ....	75
Figure 54. SAXS study of the concentration effect of Porphyrin concentration in fibroin hydrogels. Change of Fractals Dimensions. ....	76
Figure 55. Fibroin – porphyrin hydrogel frequency sweep analysis with different concentration of porphyrin, storage modulus ( $G'$ ) plot against frequency. ....	77
Figure 56. Fluorescence spectrum of the hydrogels with SOSG for singlet oxygen detection a) Generation of reactive Oxygen species in a 7.2 mg/mL fibroin hydrogel with different times of exposure, b) Generation of reactive Oxygen species in a 7.2 mg/mL fibroin hydrogel (0 mg/mL porphyrin) with different concentrations of porphyrin 1mg/mL, 0.5mg/mL, 0.2mg/mL, 0.1 mg/mL, 0.05 mg/mL, 0.025 mg/mL and a blank with only fibroin, after a 80 exposure to red light. With 50 $\mu\text{L}$ of SOSG in each test. ....	80
Figure 57. Kinetic curve of Fibroin /Porphyrin hydrogel (•) and porphyrin solution (•) after being expose to red light from 0s to 80s. ....	81
Figure 58. Porphyrin release curves from a fibroin hydrogel matrix containing a) 1mg/mL, b) 0.1 mg/mL and c) 0.025 mg/mL of porphyrin, obtained by Uv-vis spectrometry. ....	82
Figure 59. Porphyrin permeation across a skin alike membrane, after 24 h, with different concentrations of fibroin a) 7.5 mg/mL, b) 12.5 mg/mL and c) 15.2 mg/mL. All the hydrogels contend 1mg/mL (0.09 mmol/mL) of porphyrin. ....	85

## Table Index

Table 1. Amino acid composition of different varieties of silk (mole %) (BABU, 2013) .....	4
Table 2. Silk fibroin dispersion in in four different solvents solutions, time needed to dissolve and characteristics of each dispersion obtained. ....	37
Table 3. Composition and Nomenclature of the fibroin hydrogels obtained at different fibroin solution and ethanol 50% ratios at 37 °C in a hot bath. ....	39
Table 4. Coefficient of determination for linear regression ( $R^2$ ), storage modulus ( $G'$ ), gel strength (S) and viscoelastic exponent (n) of the hydrogels obtained. ....	44
Table 5. Coefficient of determination for linear regression ( $R^2$ ), storage modulus ( $G'$ ), gel strength (S) and viscoelastic exponent (n) of the hydrogels obtained. ....	48
Table 6. Coefficient of determination flow index (n) and consistency index (k) of the hydrogels obtained. ....	53
Table 7. Coefficient of determination for linear regression ( $R^2$ ), storage modulus ( $G'$ ), gel strength (S) and viscoelastic exponent (n) of the hydrogels obtained with different concentrations of porphyrin. ....	56
Table 8. Coefficient of determination flow index (n) and consistency index (k) of the hydrogels obtained with different concentration of porphyrin. ....	60
Table 9. Fractal dimension, $G'$ value and gel strength (S) and viscoelastic exponent (n) of fibroin hydrogels (7.5 mg/mL) with various concentration of porphyrin: 1mg/mL, 0.1 mg/mL and 0.025 mg/mL. ....	77
Table 10. Porphyrin release kinetic data obtained from fitting experimental release data to Ritger-Peppas equation where “n” is the diffusion exponent and $R^2$ is the correlation coefficient. ....	83

# Table of Contents

1. Introduction.....	1
2. Literature review .....	3
2.1. Fibroin .....	3
2.4. Silk Fibroin Materials and Applications .....	8
2.5. Silk Fibroin Hydrogels.....	11
3. General Objective.....	23
3.1. Specifics Objectives.....	23
4. Materials and methods .....	24
4.1. Preparation of the hydrogels .....	24
4.1.1. Silk Fibroin degumming.....	24
4.1.2. Preparation of the Silk Fibroin Solution (SFS) .....	25
4.1.3. Hydrogel Formation.....	26
4.1.4. Fibroin – Porphyrin Hydrogels Preparation .....	28
4.2. Hydrogels Characterization .....	29
4.2.1. Rheology.....	29
4.2.2. UV-Visible spectra.....	30
4.2.3. Fluorescence.....	31
4.2.4. Circular Dichroism .....	31
4.2.5. Infrared spectroscopic analysis (FTIR) .....	31
4.2.6. Scanning electron microscopy .....	32
4.2.7. Small-angle X-ray scattering (SASX) .....	32
4.2.8. Generation of Reactive Oxygen Species (ROS) .....	32
4.2.9. In vitro porphyrin release studies.....	33
4.2.10. Porphyrin permeability studies .....	33
5. Results and Discussion .....	35
5.1. Silk dissolving methods .....	35
5.2. Preparation of the Fibroin Hydrogels .....	38
5.3. Fibroin – Porphyrin Hydrogels Formation.....	40
5.4. Rheology.....	42
5.4.1. Fibroin Hydrogels LVER.....	42



5.4.2.	Fibroin Hydrogels Oscillatory analysis .....	43
5.4.3.	Fibroin Hydrogels Continuous flow and Viscosity Profiling.....	48
5.4.4.	Fibroin-Porphyrin Hydrogels Oscillatory analysis.....	54
5.4.5.	Fibroin-Porphyrin Continuous flow and Viscosity Profiling .....	56
5.5.	UV–visible absorption spectra analysis .....	60
5.6.	Fluorescence spectrum .....	64
5.7.	Circular Dichroism.....	66
5.8.	FTIR analysis .....	68
5.9.	Scanning electron microscopy .....	70
5.10.	SAXS (Small-angle X-ray scattering) .....	73
5.11.	Generation of Reactive Oxygen Species (ROS) .....	78
5.12.	In vitro Porphyrin release studies .....	81
5.13.	Permeability studies.....	83
6.	Conclusions.....	86
7.	References .....	88

## 1. Introduction

Nowadays, the research into natural polymers has notably increased due to the opportunity of combining biocompatibility with exceptional physical, mechanical, and chemical properties, which would be arduous to obtain following a synthetic route, (GALEOTTI *et al.*, 2012). Among these natural polymers, silk fibroin is attractive because of its optical transparency, outstanding mechanical robustness and compatibility with living systems, with the formation of non-inflammatory degradation products (VEPARI; KAPLAN, 2007). The most extensively characterized silks fibroins are the ones obtained from the domesticated silkworm, *Bombyx mori*, and from spiders (*Nephila clavipes* and *Araneus diadematus*) (ALTMAN *et al.*, 2003; VEPARI; KAPLAN, 2007), being *Bombyx mori* silkworms the main producer of silk worldwide (KOH *et al.*, 2015).

Silk from *B.mori* has been highly explored to understand the processing mechanisms of this material and to exploit the properties of these proteins as biomaterials (VEPARI; KAPLAN, 2007). For example the silk fibroin (SF) extracted from *B.mori* cocoons has been mainly used commercially for biomedical sutures for decades, and in textile production for centuries and it can be processed into several forms of biomaterials such as nanofibers, microspheres, powders, hydrogels, and films (DE MORAES *et al.*, 2015) .

Biomaterials for biomedical applications must incorporate the following properties: excellent biocompatibility in vivo; optimized physical properties, especially mechanical properties; ability for construction of topographic and morphological cues; degradability with safe by-products; and diffusivity control. SF can be arranged to hold a broad range of forms, such as solution, powder, fibers, films, hydrogels, and sponges; this allows the use of SF for constructing many different scale structures ranging across the nano, micro, and macro with unique biological functions (BAILEY, 2013). SF is currently emerging as an important protein biomaterial of broad biomedical applicability due to the favorable interactions with biological systems without inducing adverse immunological responses, demonstrating its good biocompatibility with various cell types by promoting their adhesion, proliferation, growth and functionality. There is a growing interest to introduce diverse functionalities into silk fibroin while preserving its advantageous intrinsic

properties. The most recent research on materials from silk fibroin have mainly focused on the preparation and properties of silk fibroin hydrogel. Hydrogels are three-dimensional, hydrophilic, polymeric networks capable of absorbing large amounts of water or biological fluids. Due to their high-water content, porosity and soft consistency, they mimic natural living tissue, more so than any other class of synthetic biomaterials (UQI *et al.*, 2017) . For this reason they have been widely used and studied as matrices for cell culture and drug release as well as in many other areas .The molecular weights, mechanical properties, secondary structures, and morphological characteristics of silk fibroin hydrogel are different from those of silk fibroin and may vary depending on the methodology used for its preparation (UQI *et al.*, 2017).

Hydrogels made from silk proteins have shown a potential in overcoming limitations of hydrogels prepared from conventional polymers as unfavorable mechanical and thermal properties, unreacted monomers and the use of toxic cross linkers (ULLAH *et al.*, 2015). In addition to being used for cell culture and the formation of different biomedical devices, hydrogels can also act as biocompatible and biodegradable matrices for the transport and selective release of drugs or other compounds that can give greater functionality to the material and expand the number of possible applications. An example of this is the addition of porphyrins to a fibroin hydrogel matrix for use in photodynamic therapy (PDT). Photodynamic therapy is a clinically approved, minimally invasive therapeutic procedure that can exert a selective cytotoxic activity toward malignant cells.

The procedure involves administration of a photosensitizing agent followed by irradiation at a wavelength corresponding to an absorbance band of the sensitizer which results in the generation of reactive oxygen species (ROS) and eventually induces malignant cell death (AGOSTINIS *et al.*, 2011; CHEN; GAO; LIU, 2016). PDT has numerous advantages over typical cancer treatment including surgery, chemotherapy and radiotherapy, PDT is relatively non-invasive, simply requiring illumination of the tumor site, and therefore inducing minimal injury to the adjacent normal tissues ; PDT does not induce systemic immunosuppressive effects that may be translated into clinical opportunistic infection and PDT can be repeated without detrimental consequences to the patient (CHEN; GAO; LIU, 2016; MOREIRA *et al.*, 2008). Porphyrins are well known

agents to treat cancer via PDT owing to their adverse properties such as skin phototoxicity and low absorption in the visible spectrum (KUMARI; GAUTAM; MILHOTRA, 2016). Despite the many positive features of PDT on cancer therapy, PDT is still not fully adapted in the clinical settings because of some inherent properties of PS drugs. Most existing PS drugs are hydrophobic with poor solubility in water this is the reason why numerous nano-platforms using a variety of organic and inorganic nanomaterials have been investigated for efficient and targeted PS delivery. For effective and targeted PDT, functionalized nanomaterials are required to efficiently incorporate and deliver hydrophobic photosensitizer (PS) drugs only into target tissues/cells and to activate them to produce ROS. In addition, functionalized nanomaterials need to be biocompatible and to have sufficient PS-loading capacity. The main objective of this work is to extract pure fibroin from raw silk fibers to synthesize and characterize transparent fibroin hydrogels, and to use such hydrogel as scaffold and a matrix to incorporate porphyrins as photosensitizer for its future application in photodynamic therapy.

## **2. Literature review**

### **2.1. Fibroin**

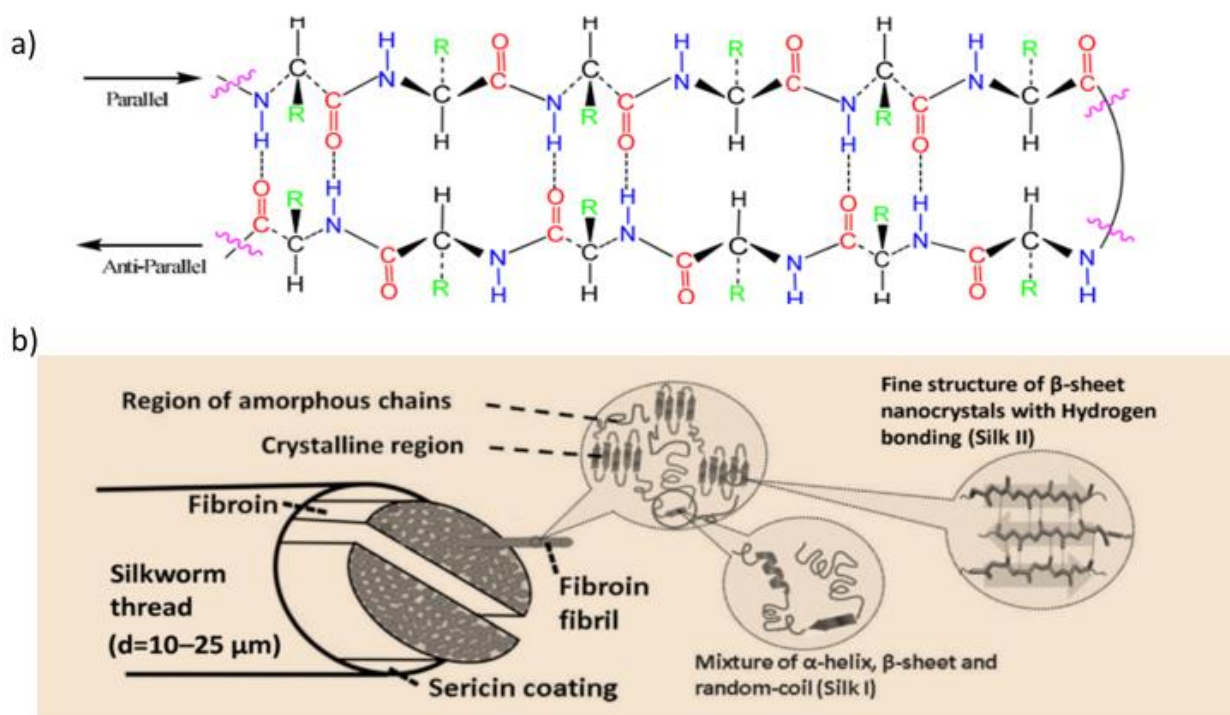
The silk, secreted by the silkworm *Bombyx mori*, a member of *Bombycidae* family is composed of a filament core of fibroin proteins cemented together with glue-like sericin proteins. It is a continuous strand composed of two proteins of very different nature and composition: fibroin and sericin. Fibroin constitutes 70% of the fiber strand weight and functions as a structural component. It is composed of two equimolar protein subunits of 370 (heavy chain) and light chain 25 kDa covalently linked by disulfide bonds (MYUNG *et al.*, 2008). Silk fibroin (SF) is secreted as a complex of three distinct proteins: the heavy chain, light chain and P25. The light chain is linked to the heavy chain by a single disulfide bond near the C-terminus (KHAN; TSUKADA, 2014).

SF is mainly composed by amino acids with different properties and characteristic like glycine, alanine, and serine (KUNDU *et al.*, 2012), the amino acid composition (Table 1) of silk proteins can vary from species to species, resulting in a wide range of mechanical properties, for example, depending on the silk worm species used for the extraction of the fibroin some solvents regularly used to dissolve the material could not work effectively (KUNDU *et al.*, 2014) . The light chain has a non-repetitive sequence and only plays a marginal role in the fiber. The heavy chain is highly periodic. The highly repetitive sections are composed of glycine (45%), alanine (30%), and serine (12%) in an approximately 3:2:1 ratio and dominated by [Gly-Ala-Gly-Ala-Gly- Ser]<sub>n</sub> sequences. SF presents two main conformational states, a glandular state prior to crystallization called Silk I (random coils and  $\alpha$ -helix) and a spun silk state which consists of the  $\beta$  -sheet secondary structure Silk II (Figure 1). A third silk polymorphism has been reported, this third state is an air/ water assembled interfacial silk called Silk III (KOH *et al.*, 2015). The silk I structure can be easily converted to silk II via methanol or potassium phosphate treatment.

**Table 1.** Amino acid composition of different varieties of silk (mole %) (BABU, 2013)

Amino acid	<i>B. mori</i> (mulberry)		<i>A. mylitta</i> (tasar)		<i>P. cynthia</i> (eri)		<i>A. assama</i> (muga)	
	1	2	1	2	1	2	1	2
Glycine	43.74	43.75	23.5	24.24	31.40	26.42	–	25.55
Alanine	28.78	29.05	36.0	39.0	47.90	35.35	–	34.34
Valine	2.16	1.85	0.80	0.67	0.57	0.54	–	0.53
Leucine	0.52	0.42	0.90	0.35	0.23	0.38	–	0.40
Isoleucine	0.65	0.53	–	0.36	0.34	0.52	–	0.39
Serine	11.88	11.17	9.80	8.82	5.10	4.96	–	7.88
Threonine	0.89	0.90	0.90	0.32	0.57	0.36	–	0.80
Aspartic acid	1.28	1.51	5.70	5.53	3.53	3.52	–	4.82
Glutamic acid	1.00	1.07	0.90	0.78	0.79	0.66	–	1.17
Phenylalanine	0.62	0.50	0.30	0.43	0.11	0.64	–	0.56
Tyrosine	5.07	5.42	4.80	4.71	5.56	5.37	–	4.61
Histidine	0.53	0.36	–	1.68	1.40	1.53	–	1.06
Arginine	1.83	1.90	13.3	11.84	1.87	6.95	–	12.25
Proline	0.35	0.50	–	0.70	0.34	0.52	–	0.47
Tryptophan	0.33	0.39	3.10	2.04	–	0.52	–	2.80
Methionine	–	–	–	–	–	0.30	–	–
Lysine	0.63	0.60	–	0.05	0.34	–	–	0.29
Cystine	–	0.08	–	0.29	–	–	–	–

**Figure 1** .Silk fibroin structure diagrams a) Silk fibroin  $\beta$ -sheet crystal secondary structure, b) Silk fibroin fibers structures (JOANA; VASCONCELOS, 2010).



## 2.2. Silk fibroin Properties

Silk fibers have an enhanced environmental stability in comparison to globular proteins due to the extensive hydrogen bonding, the hydrophobic nature of much of the protein, and the significant crystallinity. Silks usually are insoluble in most solvents, including water, dilute acid and alkali and different process involving high temperatures and great concentrations of salts are needed in order to obtain silk fibroin solutions. Silk fibers exhibit high tensile strength, flexibility and resistance to compressive forces, the excellent mechanical properties of silk fibroin make it well-suited for load-bearing biomedical applications (KUNDU *et al.*, 2014). Fibroin is a natural block copolymer that contains hydrophobic and hydrophilic blocks. The hydrophobic blocks create the  $\beta$ -sheet conformation of the fiber through hydrogen bonding between the blocks, and these regions are responsible for the high fiber strength, insolubility, and thermal stability of



fibroin (BAILEY, 2013; GREABU; VIRLAN, 2015). One of the most fascinating and remarkable properties of the SF is its biocompatibility and biodegradability *in vivo* through enzymatic degradation which processes the silk into harmless products that can be metabolized by the cell without causing any unwanted reaction due to the low foreign body response and inflammatory cell adhesion to fibroin (BAILEY, 2013; MEINEL *et al.*, 2005; PANILAITIS *et al.*, 2003; THURBER; OMENETTO; KAPLAN, 2015).

### **2.3. Silk Fibroin Solution Preparation**

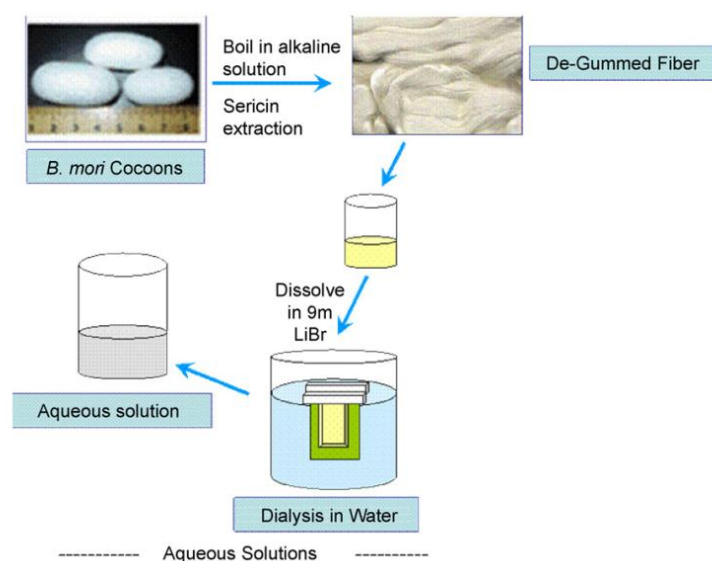
The silk fiber from domestic *Bombyx mori* silkworm, consists primarily of two components, silk fibroin and sericin (Ochi, Hossain, Magoshi, & Nemoto, 2002). These proteins are present in glands of silk-producing arthropods such as silkworms and spun into fibers during their metamorphosis (KUNDU *et al.*, 2013). For its use, the silk fibroin must first be separated from sericin by a process called degumming (Figure 2). This step is routinely carried out using a simple alkali like  $\text{Na}_2\text{CO}_3$  or an enzyme-based degumming procedure, which yields the starting material for sericin-free silk-based biomaterials. The degumming process is a critical step in the production of biocompatible silk for biomaterials because adverse effects experienced in the historical use of silk as suture thread have been attributed to inflammatory reactions promoted by sericin residues in the material (ZAHARIA *et al.*, 2012). The final molecular weight, mechanical properties and cell function of the pure protein depends on this process, as shown by Wray *et al.*, 2011 after exposed silk cocoons to different degumming times.

After being degummed, the fibroin is ready for use in the biomedical field as a suture, but if the objective is to elaborate other biomaterials like films, hydrogels and sponges, the fibroin must be dissolved in water or organic solvents (WENK; MERKLE; MEINEL, 2011). This is carried out by dissolving the silk fibroin in water using a high concentration of salts in a process denominated salting in (WRAY *et al.*, 2011). A variety of silk fiber dissolving methods using electrolyte solutions that are able to disrupt the hydrogen bonds that stabilize  $\beta$ -sheets have been reported, including the use of LiBr, LiCl,  $\text{CaCl}_2$ :ethanol: water solutions and organic solvents (RAQUEL; ACIARI, 2013). The

salting in of the silk fibroin with LiBr is the most commonly used method to dissolve the protein in water, because it has proven to be the most efficient and reliable method for this process. After solubilization, dialysis against water or buffers is performed to remove the electrolyte, then the solution can be store at 4°C for short periods of time or freeze-dried for longer periods of storage and to avoid eventual reprecipitation into its water insoluble state of the solution (WENK; MERKLE; MEINEL, 2011; ZHENG *et al.*, 2016).

After the solubilization of fibroin in water the protein is ready to be made in different biomaterial formats like hydrogels, silk tubes, silk spoons, silk films, patterned silk films, electro elated gels, silk sponges, silk microspheres and for electrospinning (ROCKWOOD *et al.*, 2011). Silk fibroin is capable to form hydrogels in a water solution to be used as cell culture scaffolds and wound healing agents. But the lack of transparency has been an obstacle to fully capitalize on this material format. Some, biological entities (cells), light sensitive molecules (e.g. fluorescent, bioluminescent, photoactive macromolecules) and ontogenetic tools can be incorporated into hydrogels for sensing and diagnostic applications, to generate biomimetic biological systems or to build optical interfaces with living tissues (MITROPOULOS *et al.*, 2015).

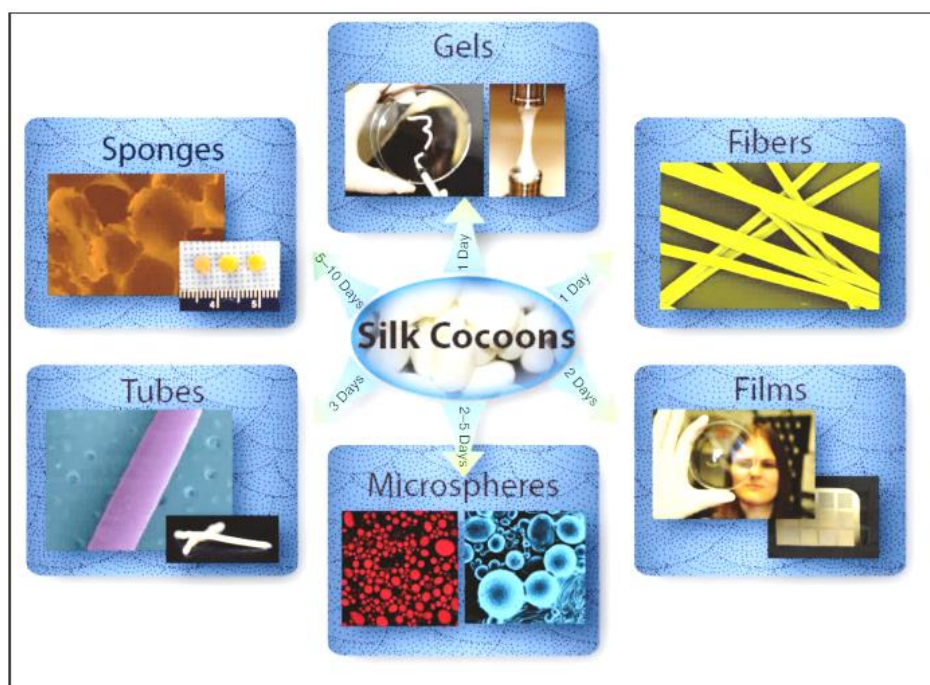
**Figure 2.** Silk Fibroin is purified from silk sericin and dissolved whit inorganic salts as LiBr to form silk fibroin solutions (HARDY; LEAL-EGAÑA; SCHEIBEL, 2013).



## 2.4. Silk Fibroin Materials and Applications

Silk obtained from silkworm has been used commercially in textile production and in biomedical sutures in the medical field. The uniformity of the protein content and the silk thread from this specific species makes it an ideal option for the non-absorbable sutures that are used in such a wide range of wound closures. Fibroin can be processed into many different forms, including films, sponges, hydrogels, microparticles and many more due to its remarkable properties (Figure 3) (KEARNS *et al.*, 2008; MOTTA *et al.*, 2004).

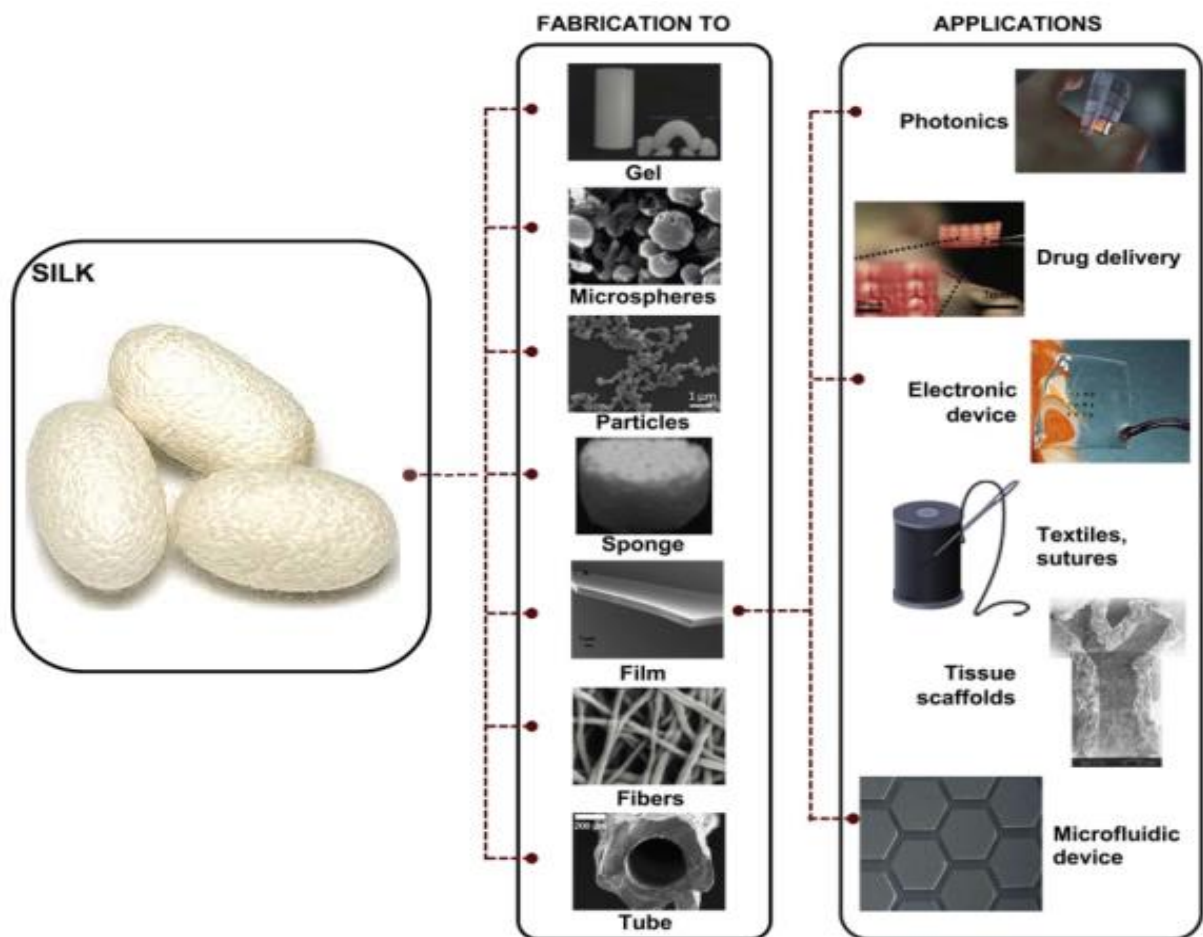
**Figure 3.** Schematic of material forms fabricated from silk fibroin (ROCKWOOD *et al.*, 2011).



Each of these materials have different applications in a large number of areas like textile industry, surgical suture, tissue engineering, therapeutic agent delivery and optical sensing. Fibroin films have been used to coat surfaces, resulting in improved cell adhesion for anchorage dependent cells comparable to collagen substrates. Fibroin films have also been shown to induce bone tissue growth *in vitro* when seeded with osteoblasts and also

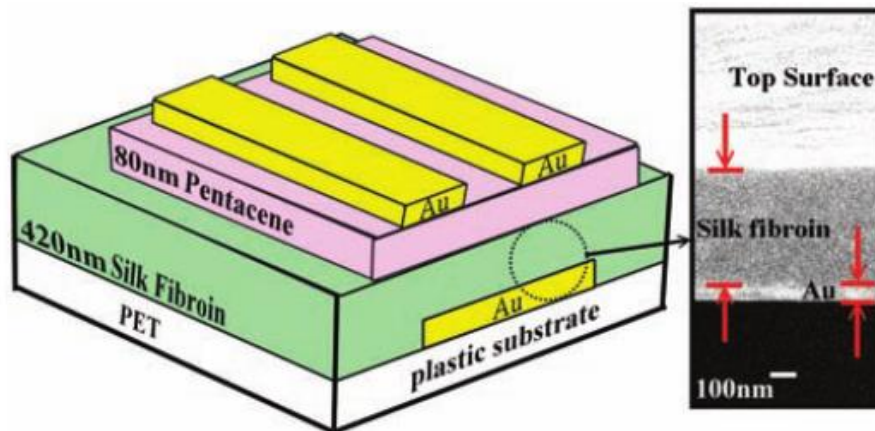
small fragments of silk fibroin are able to increase the expression of osteoblastogenic genes and DNA microarray results showed (ZAHARIA *et al.*, 2012). The SF extracted from *Bombyx mori* has been used for wound healing process, matrix for tissue cells growth, ligament tissue engineering applications, dental applications, nerves regeneration techniques, etc.. SF hydrogels and films have been widely used as the substrate for the culture of animal cells in place of collagen, for example the attachment and growth of L-929 cells by using silk proteins has been studied by a cell culture method. Films of pure component proteins were found to exhibit a high cell attachment and growth as in collagen (JOSEPH; RAJ, 2012).

**Figure 4.** Applications of different silk material formats in photonics, drug delivery, electronic devices, textiles and tissue scaffolds. (LIU; ZHANG, 2014)



Besides the applications of silk fibroin solution (SFS) in biomedicine regenerative medicine recent work demonstrates the ability of silk films to serve as a platform for transistors and various classes of electronic and photonic devices (KIM *et al.*, 2010). Silk fibroin has been reinvented as a sustainable material for optics, photonics and electronics applications has been predicated on the numerous material formats already mentioned (e.g. fibers, foams, particles, films, hydrogels) (Figure 4). The use of fibroin in optics and biosensing is particularly appealing for its biocompatibility and biostability. Fibroin has been imbued with dyes/probes or patterned to generate various optical and sensing dispositive, most notably fibroin has been developed as optical fibers, diffraction gratings, lens arrays, electrical sensors, oxygen sensors, pH sensors, glucose sensors, food sensors, etc. (FRANCIS; SAKTHI, 2013; KOH *et al.*, 2015). SF films have a promising future for the elaboration of electronic dispositive Organic thin-film transistors (OTFTs. For example, Chung-Hwa Wang, Chao-Ying Hsieh, and Jenn-Chang Hwang (2011) presented a pentacene OTFT made on a flexible poly (ethylene terephthalate) (PET) plastic substrate with a very high  $\mu\text{FE}$  value of  $23.2 \text{ cm}^2 \text{ V}^{-1} \text{ s}^{-1}$  in the saturation regime and a low operating voltage of minus 3 V (Figure 5), they chose Silk fibroin as the gate dielectric and fabricated in thin film form by a low-cost of fibroin processing to form solutions at room temperature.

**Figure 5.** Schematic of the pentacene OTFT with silk fibroin as the gate dielectric developed by Wang et al. 2011



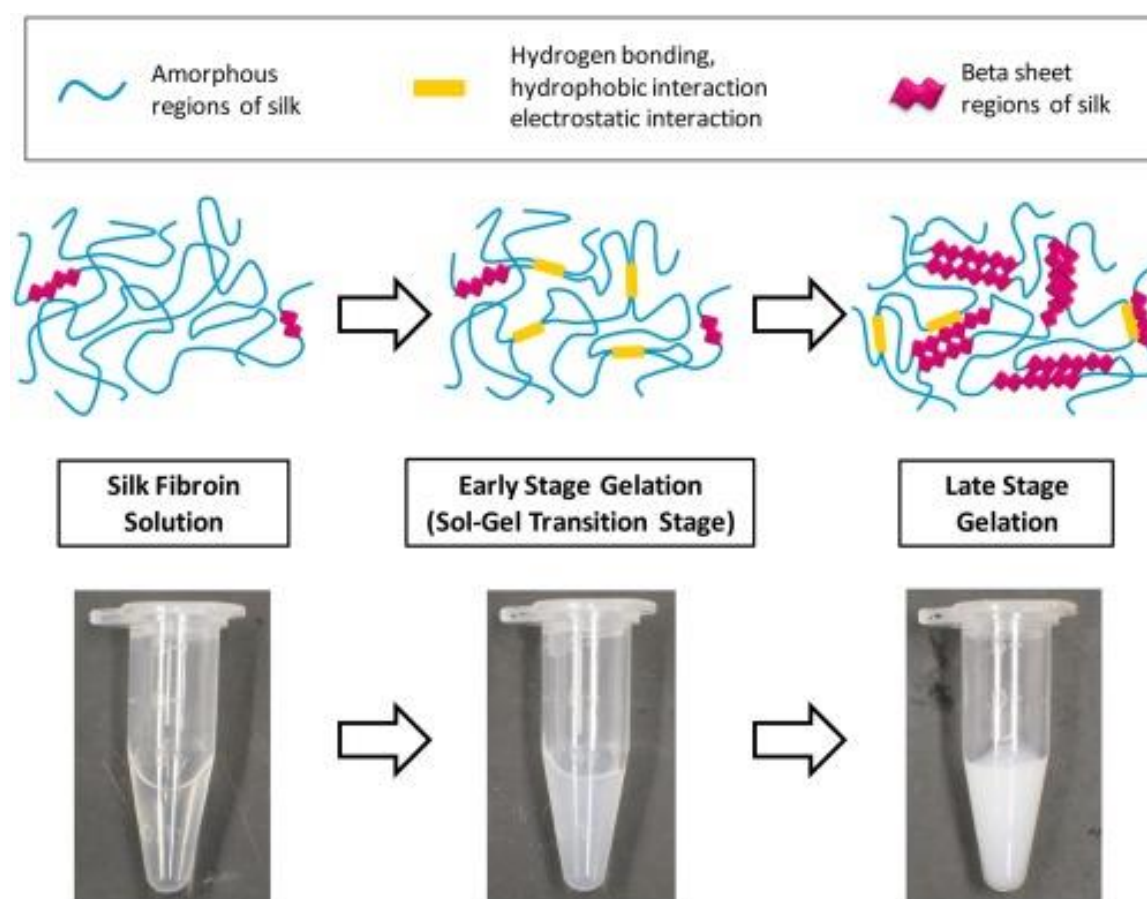
## 2.5. Silk Fibroin Hydrogels

SF dissolved in water is capable of forming hydrogels when is exposed to right conditions. The sol-gel transition occurs mainly by the formation of hydrogen bonds and hydrophobic interactions among protein chains, which fold from amorphous to thermodynamically stable beta-sheets, driven by exposure of silk solutions to shear forces, electric fields, pH near or below the isoelectric point ( $pI=3.8-3.9$ ), polar solvents, heat and water removal (MITROPOULOS *et al.*, 2015). Hydrogels are obtained by physical or chemical cross-linking of the polymeric chains in silk fibroin. Predominance of hydrophobic amino acid groups (glycine, serine and alanine) in fibroin makes gelation possible without the addition of any gelling agent but this is time consuming. This slow rate of gelation of fibroin has been one of the major challenges in preparing silk hydrogels. This limitation can be overcome by stimulating gel formation in fibroin by changing temperature, pH or by the addition of dehydrating agents like ethanol, methanol and acetone (KAPOOR; KUNDU, 2016).

The gelation process can be also induced by changes in the pH and the temperature, sonication, removal of bulk water by osmotic stresses, vortexing, heating and exposure to solvents, during this process structural changes of the SF occur from a disordered state to a  $\beta$ -sheet conformation (Figure 6) which physically cross-links and stabilizes the gel (LAWRENCE, 2014). When the gelification is induced by Electro gelation it leads to random structures and  $\alpha$ -helices rather than  $\beta$ -sheets and its temperature is reversible (MELKE *et al.*, 2015).



**Figure 6.** Modulation of silk fibroin properties through protein secondary structure formation using methanol (PRITCHARD et al., 2014)



## 2.6. Rheology and Hydrogels Characterization

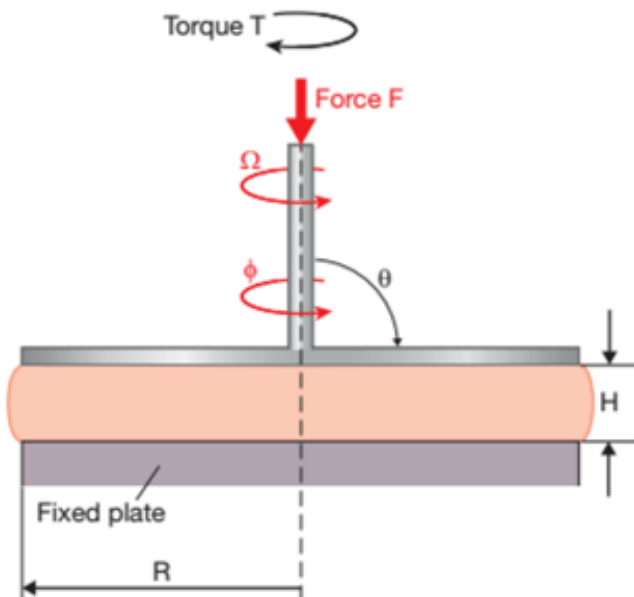
. Rheology is the study of the flow of matter; mainly liquids, but also soft solids, gels, pastes and even sold materials that exhibit some level of flow (i.e. do not just deform elastically). In 1920 the study of materials prompted a chemistry professor at Lehigh University, Eugene Bingham, to coin a new word, rheology. It comes from the Greek verb pt., to flow. Thus, rheology means the study of flow and deformation (MACOSKO, 1994).

The objective of rheology is to determine the fluid flow resulting from applied forces. Viscosity is a measure of the 'fluid friction' or the 'resistance to flow' , viscosity is the simplest rheometric measurement of material (BOISLY *et al.*, 2014).

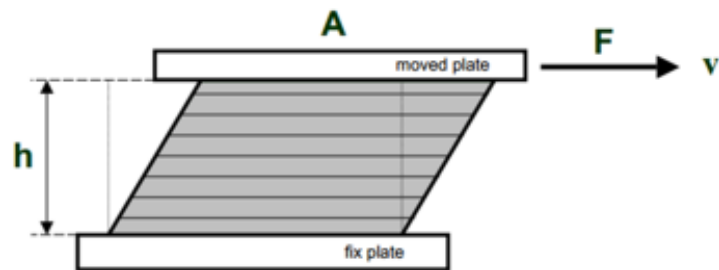
This is best illustrated by considering the parallel plate model a setting in which a gap between two parallel plates, of area  $A$  and separation  $L$ , is filled with a fluid (liquid or gas). One of the plates is moved with a velocity  $U$  relative to the second stationary plate, causing thinnest layers of the liquid to be displaced between the plates (SCHARAMM, 1998). This laminar flow is of fundamental importance for rheological investigations. It is of interest to determine the force required to move the upper plate at this constant velocity, as a function of the area, the velocity and the separation of the two plates. Some materials as hydrogels does not do not obey a simple linear relationship between applied stress and flow (Figure 7) (JANMEY; SCHLIWA, 2010).

**Figure 7.** a) Schematic diagram of a parallel-plate rheometer, one of the plates is moved with a velocity  $U$  relative to the second stationary plate, causing thinnest layers of the liquid to be displaced between the plates, b) Parallel plate model (OSSWALD, 2015).

a)



b)



Shear rate	$\dot{\gamma} = v / h$	in $s^{-1}$
Shear stress	$\tau = F / A$	in Pa
Viscosity	$\eta = \tau / \dot{\gamma}$	in Pas
Strain	$\gamma = dx / h$	dimensionless

A rheometric measurement normally consists of a strain (deformation) or a stress analysis at a constant frequency (normally 1 Hz) combined with a frequency analysis, e.g. between 0.1 and 100 Hz. The strain sweep gives information of the storage modulus  $G'$ , the loss modulus  $G''$  and the phase angle. The strain refers to the deformation or movement that occurs in a material, expressed as the amount of movement that occurs in a given sample dimension. This makes it dimensionless. A large value of  $G'$  in comparison of  $G''$  indicates pronounced elastic (gel) properties of the product being analyzed. The frequency sweep gives information about the gel strength where a large slope of the  $G'$  curve indicates low strength and a small slope indicates high strength (MURATA, 2012; OSSWALD, 2015).

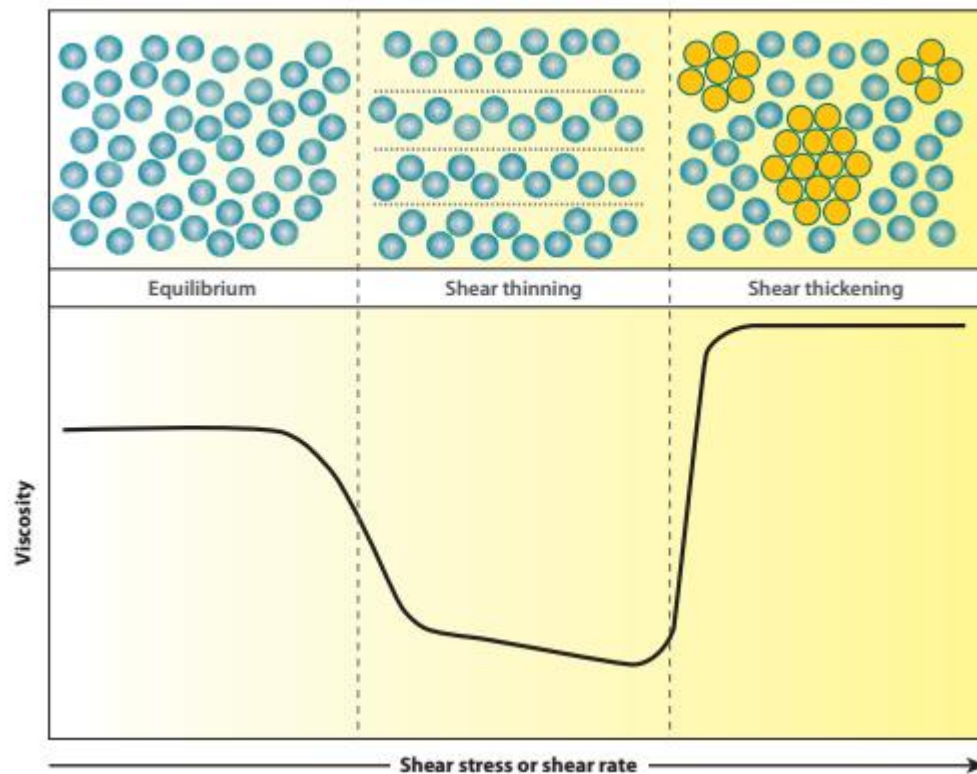
Stress is the force applied to a sample expressed as force units per unit area, commonly dynes/cm<sup>2</sup> or N/m<sup>2</sup>. The shear rate is the sliding deformation that occurs when there is movement between layers in a sample, and the viscosity is the ratio of shear stress/shear strain rate, or in other words, how resistant a liquid is to flow. Depending on their rheological characteristics materials can be classified in elastic materials, viscous materials and viscoelastic materials. Elastic materials follow Hooke's law, according to which the stress is directly proportional to strain in deformations and is not dependent of the rate of strain.

Elastic materials always have stress and strain when tested in a dynamic test. This is because the material transfers the applied stress with storage of the energy. On the other hand, hydrodynamics treats the viscous liquid that follow Newton's law: in this case the stress is directly proportional to the rate of strain and is not dependent on the strain. This means that the viscosity of the liquid or material does not depends on the shear applied to the sample, and the fluids are this are called Newtonian (MURATA, 2012). Viscous materials, like water or thin oils, will always have stress and strain shifted 90° from each other. This is because the main resistance to movement occurs when the rate of the movement is the greatest (GRILLET; WYATT; GLOE, 2012). A viscoelastic material presents both elastic and viscosity behaviors when a shear force is applied.

Depending on the behavior of the viscosity of a material when a shear stress is applied, the material can present a shear thinning behavior, this occurs when increasing

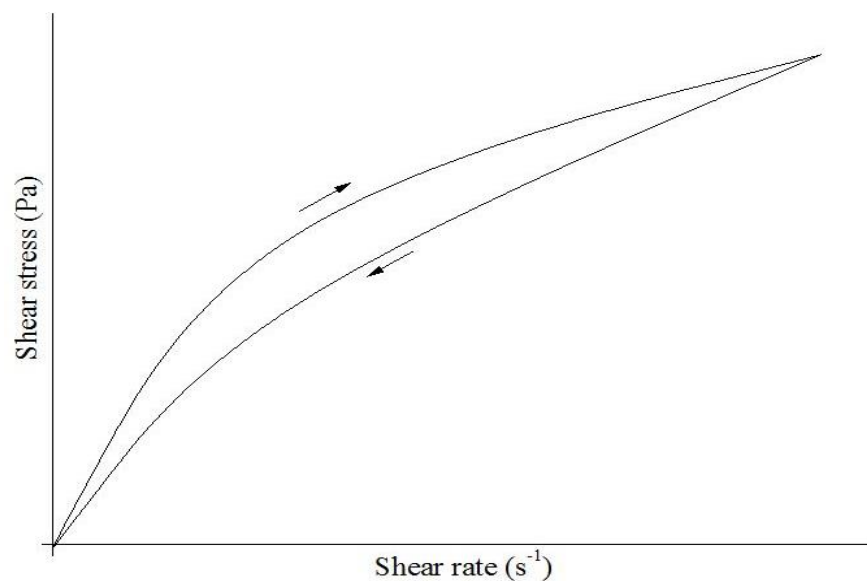
the shear rate applied to the material results in a viscosity decrease. This means that the resistance to flow of the material is lower when the deformation rate is increased. On the other hand, when the viscosity of a material increases after applying a shear stress on the sample it is classified as a shear thickening material (CHEN et al., 2010) (Figure 8).

**Figure 8.** Relationship between microstructure and viscosity of shear thinning-shear thickening transition in hard-sphere colloidal suspensions.



The majority of shear thinning samples can also experiment a phenomenon called thixotropy. Thixotropy is a property exhibited by non-Newtonian liquids, this phenomenon occurs when the viscosity of a sample under shear is reduced as a function of time (structure breakdown). Thixotropy also describes the increase of the viscosity as a function of time when the sample is not sheared anymore. Unlike "shear thinning", thixotropy is the change of viscosity as a function of time and not with changing shear rate (structure recovery) (Figure 9) (MALKIN,ALEXANDERYA.;ISAYEV,2012; TRIANTAFILLOPOULOS, 2000).

**Figure 9 .** Hysteresis loop of a thixotropic material (CHIARI et al., 2012) .



The viscoelastic properties of hydrogels correlate strongly with their microstructures and could provide useful information for modulating their performance characteristics. This rheological characteristic can be tested using oscillatory tests to determine the microstructure of material in other words to know how strong the material is. During oscillatory tests the measuring geometry oscillates around the rotation axis instead of moving constantly in one direction. Therefore, the measured values show not only the viscous behavior but also the stiffness (elasticity) of the sample. The viscoelastic properties of material systems undergoing gelation could be monitored by rheometry by frequency sweep and the amplitude sweep test.

During an amplitude sweep the amplitude of the deformation or alternatively the amplitude of the shear stress is varied while the frequency is kept constant. The amplitude is the maximum of the oscillatory motion. For the analysis, the storage modulus  $G'$  (Solid like behavior) and the loss modulus  $G''$  (viscous response) are plotted against the deformation (LIHUI WENG; CHEN, 2008; VIOLETA GHICA *et al.*, 2016). The main objective of these tests is to obtain information about the microstructure of the material. A microstructure means that there are forces between the molecules or particles in the

material. To break the microstructure is necessary to apply a force larger than the ones holding it. When the applied force is smaller than the molecular or inter particle forces, then  $G'$  (storage modulus) is larger than  $G''$  (loss modulus); the material has some capacity to store energy and should be able to return, to some extent, to its initial structure configuration before a mechanical force was applied. The material behaves as an elastic solid, although not an ideal one because some of the mechanical energy is dissipated. But when the applied force is higher, the microstructure collapses and the mechanical energy given to the material is dissipated, meaning that the material flows and when this happens  $G''$  is greater than  $G'$ .

By performing an amplitude sweep on the sample we can also obtain information about the Linear Viscoelastic Region (LVER), which this is the region of a  $G'$  and  $G''$  vs. shear stress plot where the values of  $G'$  and  $G''$  remain constant. The length of the LVER of the elastic modulus ( $G'$ ) can be used as a measurement of the stability of a sample's structure, since structural properties are best related to elasticity. A sample that has a long LVER is indicative of a well-dispersed and stable system (MALKIN, ALEXANDER YA.; ISAYEV, 2012; WYSS, 2007).

After the fluid's linear viscoelastic region has been defined by a strain sweep, its structure can be further characterized using a frequency sweep at a strain below the critical strain. During the frequency sweep the frequency is varied while the amplitude of the deformation or alternatively the amplitude of the shear stress is kept constant. For the analysis, the storage and loss modulus are plotted against the frequency. The data at low frequencies describe the behavior of the samples at slow changes of stress. Below the critical strain, the elastic modulus  $G'$  is often nearly independent of frequency, as would be expected from a structured or solid-like material. The more frequency dependent the elastic modulus is, the more fluid-like is the material (CHEN *et al.*, 2010).

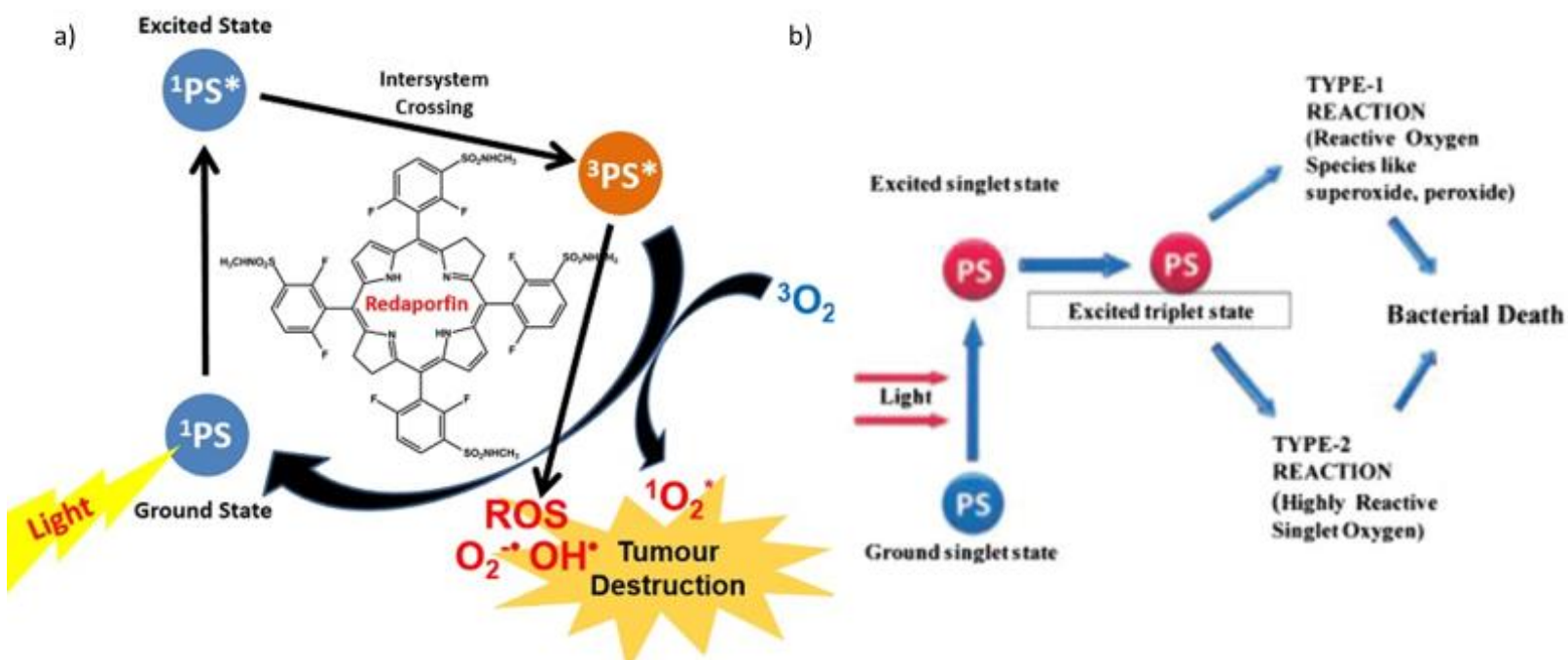


## 2.7. Photodynamic Therapy

Photodynamic therapy (PDT) is a promising therapeutic approach, which has been applied worldwide for cancer treatment. PDT has several advantages over conventional therapies due to its minimally invasive nature, selectivity, the ability to treat patients with repeated doses without initiating resistance or exceeding total dose limitations (KUMARI; GAUTAM; MILHOTRA, 2016). PDT combines the effects of visible light, molecular oxygen and a photosensitizing drug to achieve therapeutic effect, crucially, neither the light nor the drug alone have any biological effect.

Most of the photosensitizers used in cancer therapy are based on a tetrapyrrole structure, similar to that of the protoporphyrin contained in hemoglobin. An ideal photosensitizing agent should be a single pure compound to allow quality control analysis with low manufacturing costs and good stability in storage (AGOSTINIS *et al.*, 2011). When the photosensitizer is exposed to specific wavelengths of light, it becomes activated from a “ground state” to an “excited state”. As it returns to the ground state, the released energy from photosensitizer may cause the death of the target cell by two different mechanisms. First, it can react with the substrate to form radicals, which further interact with oxygen to produce oxygen free radicals such as superoxide and hydroxyl radicals (type I reaction). Or the energy can be directly transferred to oxygen to form singlet oxygen which then oxidizes various substrates (type II reaction) and thus mediates selective cell killing (HONG; CHOI; SHIM, 2016; LEE; BARON, 2011). The formed ROS may induce oxidative damage to cellular proteins, lipids, and nucleic acids, leading to direct tumor and vascular cell death, inside the treated tumor, which further leads to an activation of an immune response (BALDEA *et al.*, 2015). Tumor destruction from PDT can occur by both programmed (apoptotic) pathways and non-programmed (necrosis) pathways. This is advantageous, as some tumors have developed genetic mutations eliminating or minimizing apoptosis (ALLISON; MOGHISSI, 2013).

**Figure 10 .** a) Descriptive outline about the general PDT mechanism a) Type I reaction and Type II reaction PDT mechanism. (SINGH et al., 2014).

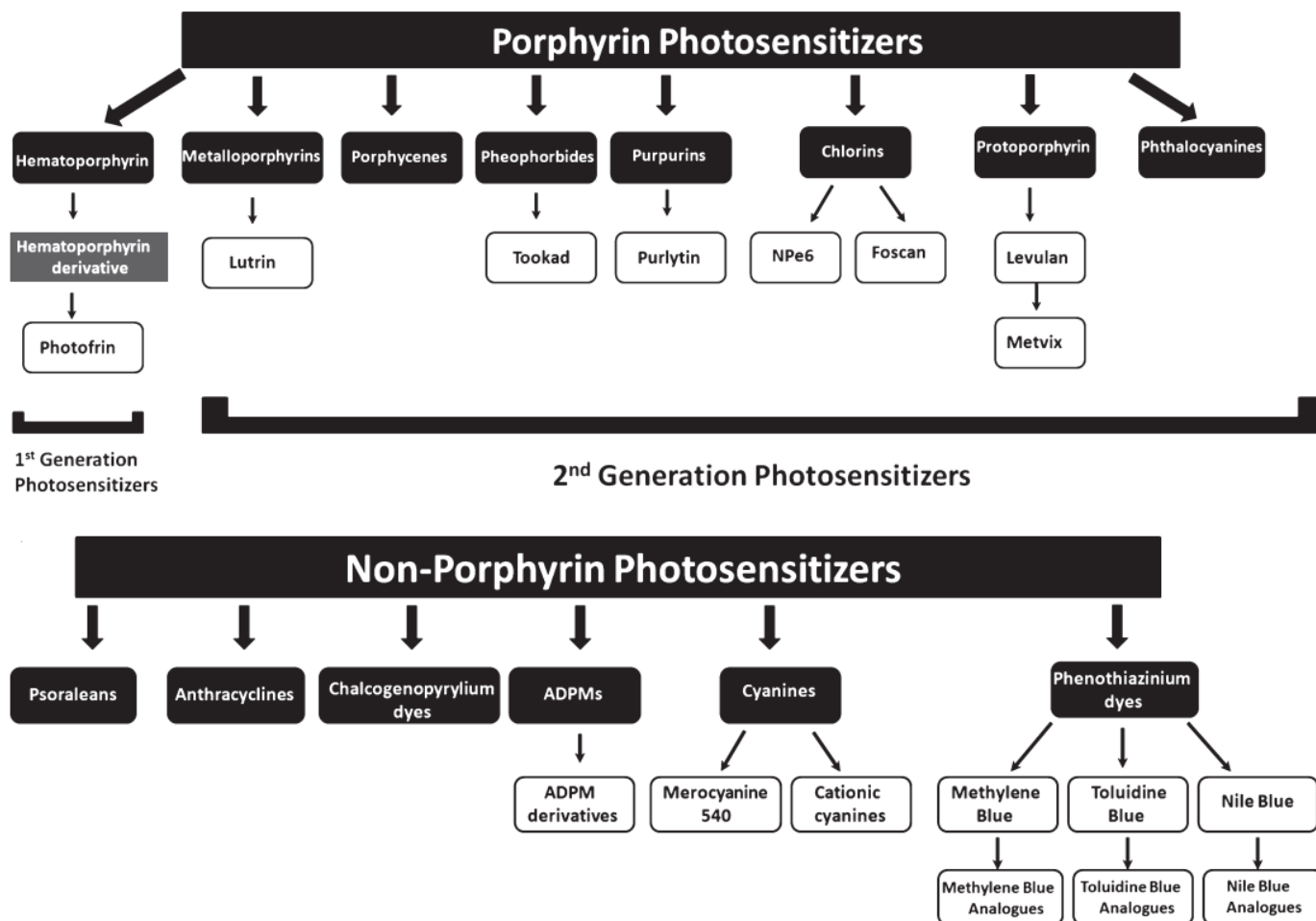


There are many types of photosensitizers available and several routes (topical, oral, or intravenous) by which they can be delivered to the patient depending on the desired application. Currently, the only photosensitizers approved by the US Food and Drug Administration for dermatologic indications are aminolaevulinic acid (ALA) and methyl aminolaevulinate (MAL). Both drugs are prodrugs that require conversion to porphyrin, this happens by the action of cells in the human body that can metabolize ALA or MAL into photoactivatable porphyrins (LEE; BARON, 2011).

## 2.8. Photosensitizers (PS)

The first observation of chemical sensitization of tissue by light was reported in 1900 by Raab *et al.* However, it was not until early 1980 when the first-generation photosensitizer an active component of hematoporphyrin derivative (HpD) was isolated and partially identified. This first-generation photosensitizer consist of a mixture of porphyrin dimers and higher oligomers. Though it proves to be a very effective photosensitizer for the treatment of various types of cancers it suffers from several limitations, especially, skin photosensitivity and relatively weak long wavelength absorption which affords less than optimal light penetration depth (ETHIRAJAN *et al.*, 2011). To overcome this limitation a set of second generation photosensitizers were developed. An ideal PS should be able to produce singlet oxygen efficiently, have a high absorption coefficient in the long wavelength region, have no dark toxicity, be stable, selectively accumulate in target tissue, have a short time interval between administration and maximum accumulation in the tissue and be rapidly cleared from the body after therapy and easy to dissolve in injectable solvents and chemically pure, the second generation of PS usually meet *a*ll the this requirements (ETHIRAJAN *et al.*, 2011; GRZYCZYN, 2015). Photosensitizers are generally classified as porphyrins or non-porphyrins (O'CONNOR; GALLAGHER; BYRNE, 2009) (Figure 11).

**Figure 11 .** Classification of photosensitizers as porphyrin-based or nonporphyrin-based molecules. post-treatment. (O'CONNOR; GALLAGHER; BYRNE, 2009)

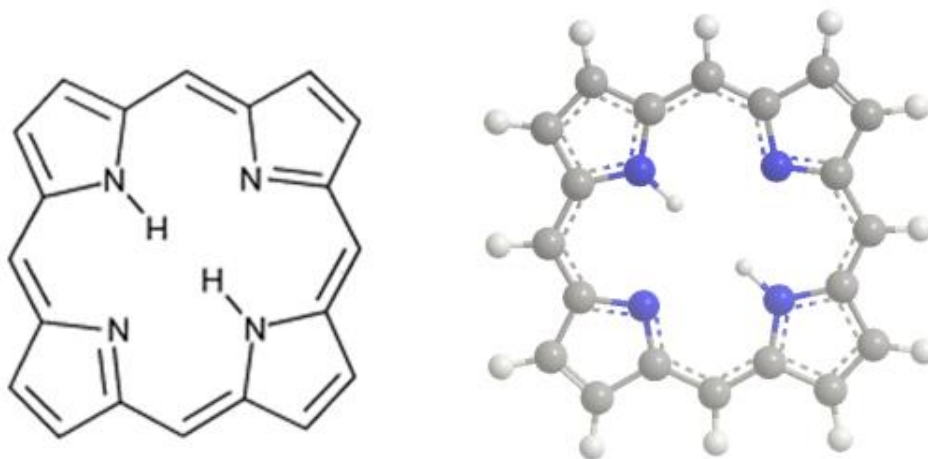


## 2.9. Porphyrins

Porphyrins are naturally occurring organic compounds that belong to the class of tetrapyrroles which comprises species such as hemoglobin and myoglobin and chlorophyll, essential for the biological activity of all living organisms (O'CONNOR; GALLAGHER; BYRNE, 2009). The main feature of their chemical structure is the porphyrin ring formed from four pyrrole molecules connected by methene bridges, this

porphyrin ring is a very stable system and exhibits aromatic character (GRYCZYN, 2015). A distinguishing feature of porphyrins is their ability to chelate a central metal atom. The porphyrin nucleus is a tetradentate ligand which makes it possible to form coordination complex with metals. When coordination occurs, two protons are removed from the pyrrole nitrogen atoms, leaving two negative charges (BIESAGA; PYRZYNSKA; TROJANOWICZ, 2000). The simplest porphyrin is porphin, also known as porphine, which consists of four pyrrole rings linked via four meso carbon atoms to produce a macrocycle consisting of 20 carbon atoms (Figure 12). This arrangement supports a network of alternating double bonds which permits a  $\pi$ -electron cloud to delocalize throughout the porphyrin macrocycle. Metallated porphyrins perform a variety of roles in biological system.

**Figure 12** . Porphin basic structure formed by a porphyrin ring of twenty carbon atoms composed by four pyrrole molecules connected by methane bridges.



Some methodologies have used to synthesized different types of porphyrins, the first reported thienyl substituted porphyrin, mesotetra (thien-2-yl) porphyrin was synthesized by Triebs *et al.* in 1968. Owing to numerous advantageous properties such as structural robustness, attractive absorption and emission properties, strong

aromaticity and rich metal coordination chemistry, porphyrins have been successfully utilized across a wide range of applications (OSUKA, 2014). For example, porphyrins have proven to play an important role in photodynamic antimicrobial chemotherapy (PACT) and photodynamic therapy as they are powerful photosensitizers, which potentiate the inactivation of cells by light.

### **3. General Objective**

The principal objective of this work is the preparation and physico-chemical characterization of translucent and stable silk fibroin hydrogels, embedded with porphyrin, that have photo responsive properties on epithelial cells, aiming at application in photodynamic therapy.

#### **3.1. Specifics Objectives**

- Extract the silk fibroin from raw silk.
- Form fibroin solutions in water.
- Form translucent and stable fibroin hydrogels.
- Prepare fibroin-porphyrin hydrogels aiming at application in photodynamic therapy, capable of generating singlet oxygen and allowing the release and permeation of the porphyrin through the skin.
- Characterize the obtained hydrogels by different spectroscopy and mechanical analysis.

#### 4. Materials and methods

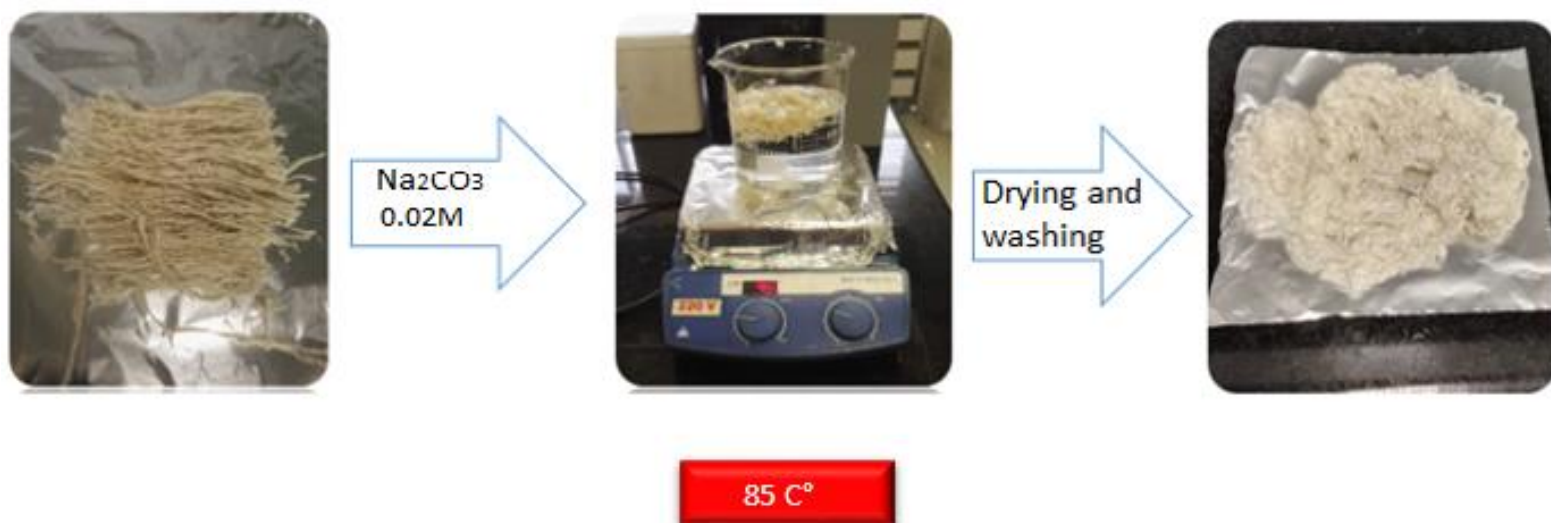
All reagents used in this work were of analytical grade. The silk fibroin was extracted from two different silk material: Maeda 21 (Process silk) and Frisson extra (residues from the silk processing), both provided by Bractac (Brazil, Londrina), previously extracted from *B.mori* cocoons. LiBr was purchased from Sigma and all the others reagents from Synth (Brazil).

##### 4.1. Preparation of the hydrogels

###### 4.1.1. Silk Fibroin degumming

The Fibroin Silk was degummed three times by soaking in a solution 0.02 M (2g/L) of  $\text{Na}_2\text{CO}_3$  solution at 85 °C for 30 min to remove the sericin of the cocoons, and then rinsing in deionized water 3 times for 20 min after each wash with the salt solution (MICHELLE NOGUEIRA *et al.*, 2011; ROCKWOOD *et al.*, 2011) .The fibers were dried for 24 h at 72 °C.

**Figure 13.** Frisson Silk degumming process in a 0.02 M (2g/L) of  $\text{Na}_2\text{CO}_3$  solution at 85 °C for 30 min for three times.



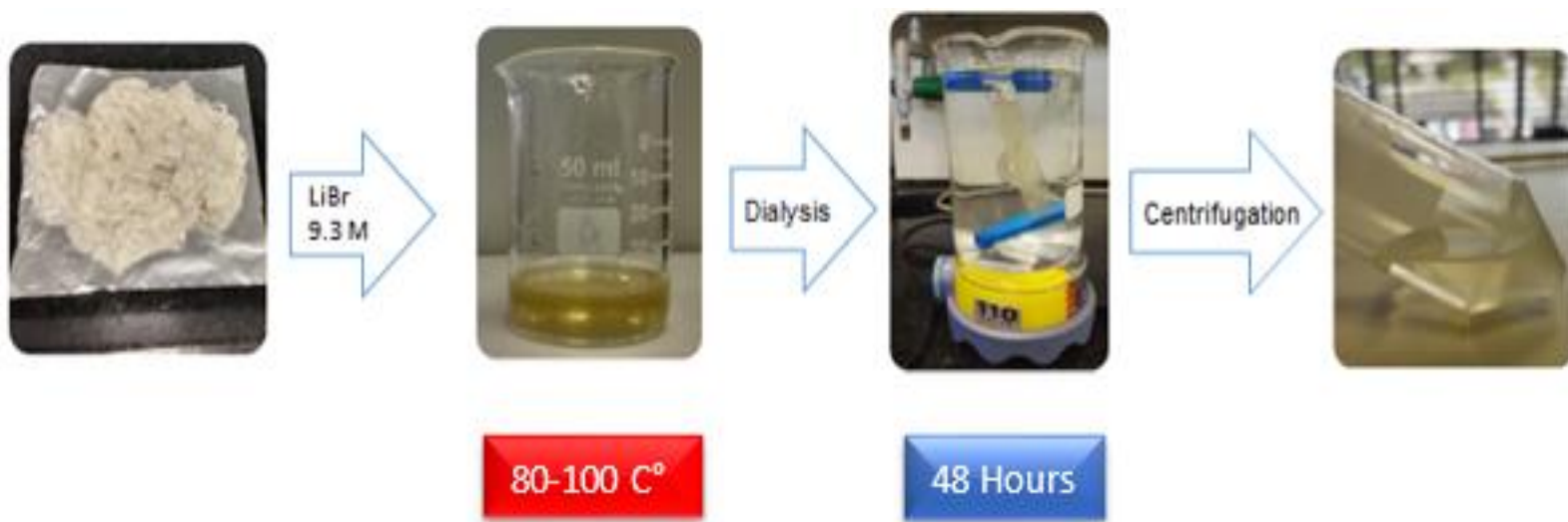
#### 4.1.2. Preparation of the Silk Fibroin Solution (SFS)

To dissolve the extracted fibroin in water several methods were tested. For each test 1g of silk was weighted and packed tightly in a beaker. To each beaker with silk was added one of the following solutions used in previous experiments:

- Ajisawa's reagent:  $\text{CaCl}_2\text{-EtOH-H}_2\text{O}$ , 1:2:8 (molar) (ZHENG et al., 2016).
- $\text{LiCl-H}_2\text{O}$  9.5 M (BEXIGA, 2014).
- $\text{LiCl-EtOH-H}_2\text{O}$ , 10:18:72 (w/w) (BEXIGA, 2014).
- $\text{LiBr}$  9.3 M (MARELLI et al., 2016).

The obtained suspensions were heated from 80 to 100 ° C on a hot plate with constant stirring to aid in the dispersion process of the fibroin. The obtained solutions were purified by dialysis against water for 48 hours, to eliminate the salts contained in the solutions. For this process was used a cellulose dialysis bag with a molecular cut off of 17.000 KDa. The solutions obtained from the treatment with  $\text{LiBr}$  were dialyzed in an ice bath to avoid the early gelation of the solution (NOGUEIRA *et al.*, 2010).

**Figure 14** .General degummed Frisson fibroin dissolving process with  $\text{LiBr}$  9.5M





After dialysis, the solution was centrifuged twice at 12,000g, 4 °C for 20 min to remove the impurities. The concentration of silk fibroin solution (SFS) was calculated using the equation (1):

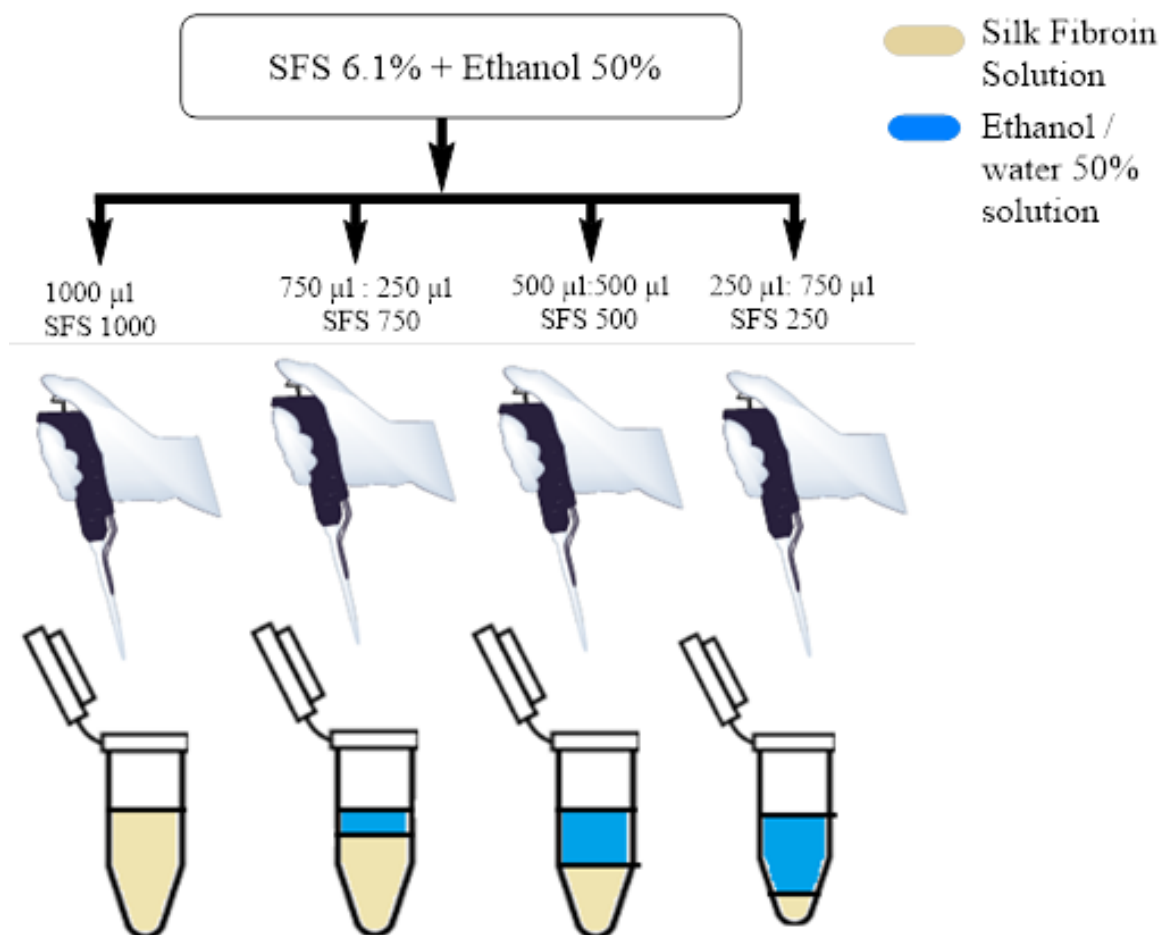
$$(1) \quad \text{SFS concentration (\%)} = \frac{W_2 - W}{W_1 - W} \times 100$$

Where  $W$  and  $W_1$  represent the plate mass before and after adding of 1 mL silk fibroin solution;  $W_2$  means the plate weight after the solution dried at 60 °C for 4 h.

#### **4.1.3. Hydrogel Formation**

For the formation of silk fibroin hydrogel, we chose the Frisson extra SFS (Silk Fibroin Solution) dissolved by LiBr. First, we tested the right proportion of 50 vol % ethanol solution needed to form fibroin hydrogels. For this test a 50 vol % ethanol solution was added in the SF solution in several volume ratios: 1000:0, 750:250, 500:500 and 250:750 fibroin/ethanol  $\mu\text{L}$  (DE MORAES *et al.*, 2015). The mixed solutions were placed on a thermostatted bath at 37 °C until gelation occurred. After choosing the optimal SFS/ethanol ratio, we formed hydrogels of varying SF concentration but with the same SFS-ethanol (50%) proportions.

**Figure 15.** Methodology used for the Preparation of fibroin - ethanol-water Hydrogels from a 61 mg/mL fibroin solution (6.1% m/v).



From the ratio 250SFS we prepared translucent fibroin hydrogels changing the fibroin concentration without changing the SF/Ethanol (50%) solution ratio. We prepared hydrogels with 15.2, 15, 12.5, 10, 7.5, 6.2, 5 and 2.5 mg/mL with the objective of obtaining more translucent hydrogels to incorporate the desired porphyrin. These hydrogels were prepared from the initial solution with 6.1% (61 mg/mL) of fibroin.

#### 4.1.4. Fibroin – Porphyrin Hydrogels Preparation

The porphyrin sodium (4,4',4''-(20-(4-(3-carboxypropanamido) phenyl) porphyrin-5,10,15-triyl) tribenzenesulfonate) added to the hydrogel matrix was provided by professor Francesca Giuntini from the School of Pharmacy and Biomolecular Sciences at Liverpool John Moores University (UK). We chose this porphyrin to prepare the hydrogels due to its excellent solubility in water and ethanol (GIUNTINI *et al.*, 2014).

To form fibroin – porphyrin hydrogels the fibroin solution 6.1% (61 mg/ml) was diluted to a concentration of 7.5 mg/mL . We also made a stock solution of porphyrin 5mg/ml, diluting the pure porphyrin (Figure 17) in a solution of ethanol (50%) to ensure that the SFS-Ethanol (50%) proportion will be always the same. To obtain the fibroin - porphyrin hydrogel we first mixed 123  $\mu$ L of the stock fibroin solution with distilled water to obtain a final volume of 250  $\mu$ L, and then we mixed this solution with the porphyrin solutions in 50% ethanol with the following porphyrin–concentrations: 1 mg/mL, 0.5 mg/mL, 0.25 mg/mL, 0.1 mg/mL, 0.05 mg/mL and 0.025 mg/mL. Ethanol was then added to the mixture to a total volume of 1 ml of solution.

**Figure 16** .Structure, formula and molecular weight of the water-soluble porphyrin added to the fibroin hydrogel matrix.

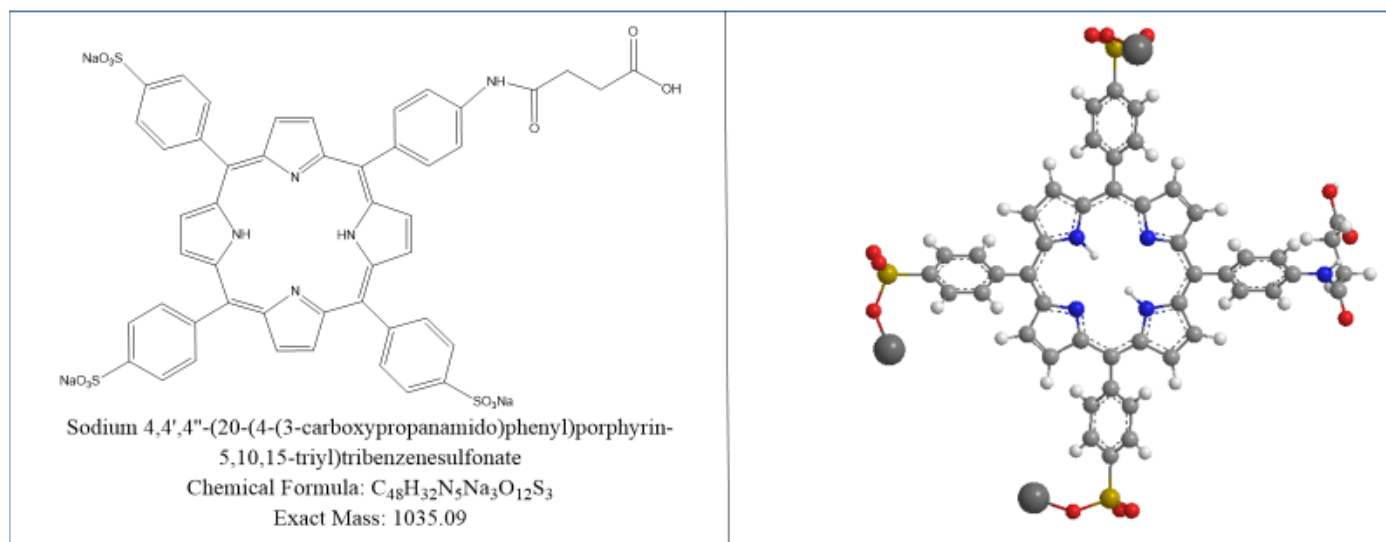
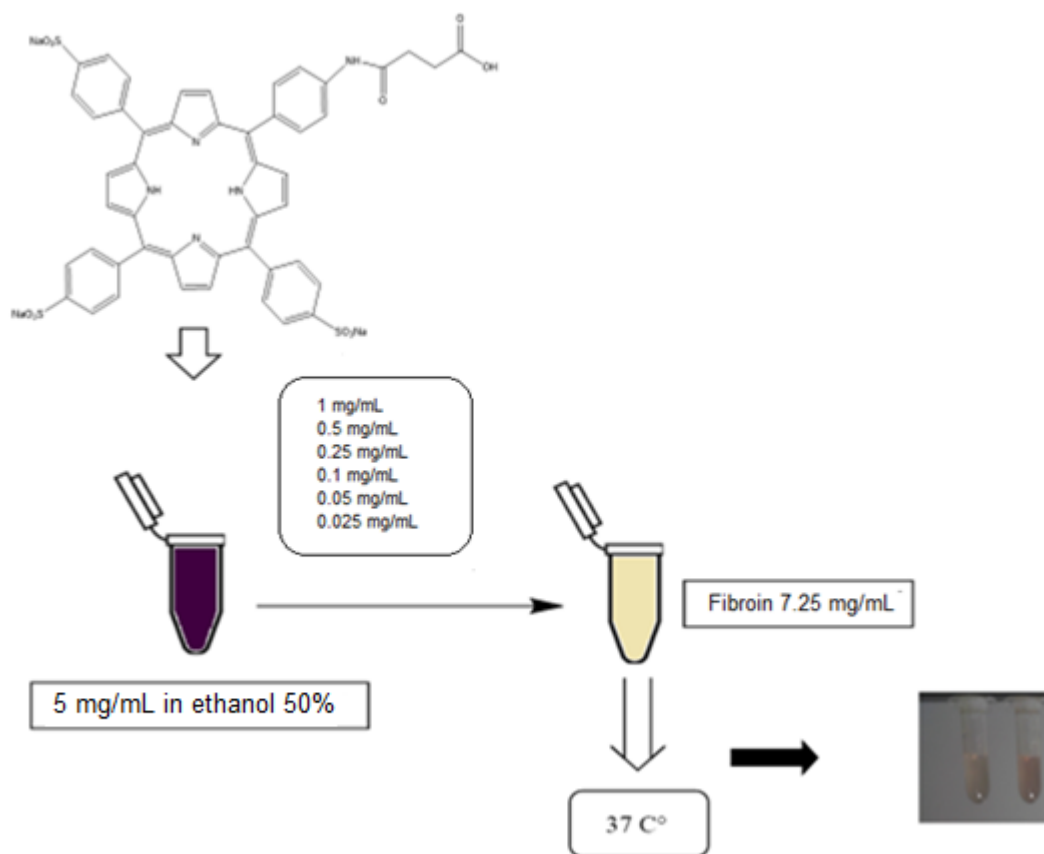


**Figure 17.** Preparation of SF and porphyrin hydrogels at different concentration of porphyrin.



## 4.2. Hydrogels Characterization

### 4.2.1. Rheology

Viscoelastic properties of all hydrogels were analyzed on a controlled-stress Malvern rheometer (Ki nexus Lab +) equipped with 25 mm parallel plate geometry and sample gap of 0.1 mm, at  $25 \pm 0.1^\circ\text{C}$ , in triplicate. Oscillatory analyses were started by the conduction of a stress vs weep, in order to determine the viscoelastic region of the sample. The analysis was carried out at a constant frequency of 1 Hz and a stress sweep from 0.1 to 10 Pa. A constant shear stress of 1 Pa was then selected to perform the frequency sweep from 0.1 to 20 Hz, which was within the previously determined linear viscoelastic

region for all samples and the storage ( $G'$ ) and loss ( $G''$ ) moduli were recorded. Continual testing to analyze the thixotropy of the materials was performed using a controlled shear rate procedure in the range from 0.1 to 100  $\text{s}^{-1}$  and back, each stage lasting 2 minutes.

For the determination of the gels strength ( $k$ ) and viscoelastic exponent ( $n$ ) also called relaxation exponent, we used the power law model (Equation 2). The variation of storage modulus ( $G'$ ) at low frequencies in a log–log plot of  $G'$  versus frequency follows the Power law equation:

(2)

$$G' = S \cdot \omega^n$$

$G'$ : Storage Modulus  
 $S$ : Hydrogel Strength  
 $\omega$ : Angular Frequency  
 $n$ : Viscoelastic exponent

The  $n$  and  $S$  values allow a quantitative estimation of strength of hydrogel structures that can be related with the crosslinking density within the polymer network. The consistency index and flow index were determined from the Power law described in Equation (3) for a quantitative analysis of flow behavior:

(3)

$$\tau = k \cdot \dot{\gamma}^n$$

$T$ : shear stress  
 $\dot{\gamma}$ : Shear rate  
 $n$ : Flow index  
 $K$ :Consistency index

#### 4.2.2. UV-Visible spectra

Absorbance spectra of porphyrin solutions at concentrations of 1,0.5,0.25,0.1,0.05 and 0.025 mg/mL and fibroin /porphyrin hydrogels at concentrations of 7.5 mg/mL of fibroin with the same concentrations of porphyrin used in the solutions. using a Varian Carry 50 Bio UV-Vis spectrophotometer. The absorbance was measure over a range of 200–1000 nm for all the samples. The freshly prepared hydrogels were measured with a

sandwich cell with a 0.1mm optic path for the more concentrate samples. At least three measurements were performed for each sample for consistency

#### **4.2.3. Fluorescence**

Fluorescence spectra of porphyrin solutions at concentrations of 1,0.5,0.25,0.1,0.05 and 0.025 mg/mL and fibroin /porphyrin hydrogels at concentrations of 7.5 mg/mL of fibroin with the same concentrations of porphyrin were performed on a Varian Cary Eclipse Fluorescence Spectrophotometer. We used an excitation of  $\lambda_{exc.}=400$  nm and a scanning from 450 to 790 nm. A slow scan speed was used with excitation and emission slits set to yield a 5-nm resolution in all the porphyrin-fibroin hydrogels. We also measured the fluorescence of the porphyrin solutions to use them as control samples.

#### **4.2.4. Circular Dichroism**

Circular dichroism (CD) spectra were recorded with a 0.1 mm path length (Hellma Analytics), sandwich cell, at different concentrations on a Jasco-815 CD spectrophotometer (Jasco Co). All samples were scanned at 25 °C with a 10-s accumulation time at the rate of 200 nm/min.

#### **4.2.5. Infrared spectroscopic analysis (FTIR)**

The hydrogels were dried for 2 hours at 52 °C to eliminate the water and ethanol from the sample. Infrared spectra of hydrogels were obtained using Spectrum 1000 (PerkinElmer) spectrometer in the range of 400-4000  $\text{cm}^{-1}$ .

#### **4.2.6. Scanning electron microscopy**

The image acquisition was performed using a scanning electron microscope, FEI Inspect F50 at LNNano, Brazilian Nanotechnology National Laboratory (CNPEM, Campinas, Brazil). The images were made by secondary electrons, 5 kV voltage, 3-3.5 mm spot size, 10-12 mm working distance and gold coating. For the metallization, 60 seconds of deposition and 40 mA current were used. The images were analyzed using the ImageJ program to measure fiber diameters

#### **4.2.7. Small-angle X-ray scattering (SAXS)**

SAXS data were collected using the SAXS1 beamline at LNLS, Brazilian Synchrotron Light Laboratory (CNPEM, Campinas, Brazil). Hydrogel samples were loaded into 1.5 mm quartz capillaries and analyzed using the XEUSS-Xenocs instrument operating at photon energy of 8 keV. Detection was performed using a Pilatus 300k detector, and the sample-to-detector distance was set at 0.77 m, leading to a q-range from 0.11 to 4 nm<sup>-1</sup> at 25°C. Four frames of 30 minutes each were recorded and averaged before background subtraction.

#### **4.2.8. Generation of Reactive Oxygen Species (ROS)**

For the determination of the generation of reactive oxygen species (ROS) by the Fibroin/Porphyrin hydrogel, we used Singlet Oxygen Sensor Green (SOSG, ThermoFisher Scientific) as detection reagent that is highly selective for singlet oxygen. Singlet Oxygen Sensor Green does not show any appreciable response to hydroxyl radical or superoxide. This indicator initially exhibits weak blue fluorescence, but in the presence of singlet oxygen, it emits a green fluorescence (excitation/emission maxima ~504/525 nm) similar to that of fluorescein. The samples were exposed to red light from 0 to 80s for determinate the effect of the of the exposed time and fibroin in the singlet oxygen generation by the porphyrin. We used a hydrogel formed only by 7.5 mg/mL of fibroin as a blank to confirm that all the singlet oxygen was only generated by the

porphyrins. After the irradiation of the sample, the fluorescence of the SOSG was measured using a Varian Cary Eclipse Fluorescence Spectrophotometer. We used an excitation of 400 nm and a scanning from 450 to 790 nm. A slow scan speed was used with excitation and emission slits set to yield a 5-nm resolution in all the porphyrin-fibroin hydrogels.

#### **4.2.9. In vitro porphyrin release studies**

The evaluation of in vitro drug release was performed by incubating the fibroin hydrogels with different concentrations of porphyrin (1mg/mL, 0.1 mg/mL and 0.025 mg/mL) with 15 mL of a 1X PBS buffer, pH 7.4 at 37 °C, to determine the release profile of the porphyrin and the best concentration to perform future permeability analysis. An aliquot of each sample (1 mL) was removed from the receptor compartment at times T=0.5, 1, 3, 5, 7, 9 and 24 hours

The release behavior of compounds from polymeric systems can be determined by fitting the release data to the empirical relationship given by Ritger-Peppas equation (4) .  $M_t/M_\infty$  is the fractional drug release at time t; “t” is the release time; “k” is the kinetic constant that measures the drug release rate and, “n” is the diffusion exponent that depends on the release mechanism and on the geometry of the matrix.

(4)

$$\frac{M_t}{M_\infty} = kt^n$$

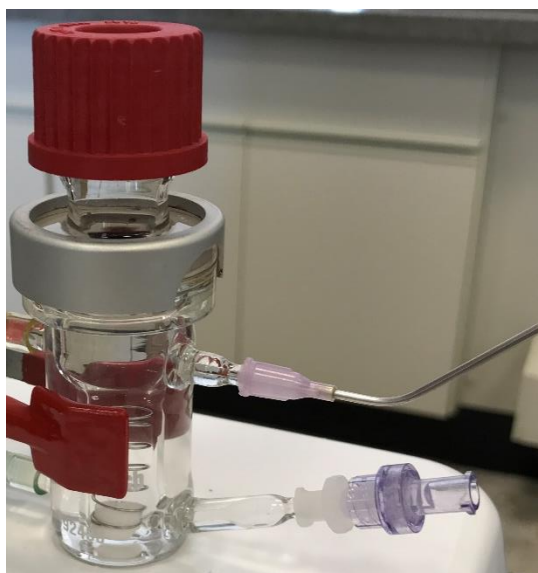
#### **4.2.10. Porphyrin permeability studies**

In vitro release of porphyrin from hydrogel was determined using Franz’s cell apparatus (Figure 17). We used a synthetic membrane (Strat-M® Membrane for Transdermal Diffusion Testing, 25 mm discs, Merck Millipore), a non-animal based model for transdermal diffusion testing that is predictive of diffusion in human skin, circulating



water baths were set to 37 °C. Compartments were clamped together, ensuring that the shiny side of the membrane was facing the donor compartment. The receptor compartment was filled with water. When the receptor solution reached 37 °C, 1 mL of the sample was added. An aliquot of each sample (500 µL) was removed from the receptor compartment at times  $T=0.5, 1, 2, 3, 4, 5, 6, 7, 8, 24$  hours.

**Figure 18.** Franz's cell apparatus used in the permeability test.



## 5. Results and Discussion

### 5.1. Silk dissolving methods

The silk fibroin is mainly insoluble in water, that is why we need to use different solvent compositions and salts to obtain SFS in water. We tested four different solvents systems to dissolve the extracted fibroin. The best solvent was chosen base on the time needed for dissolving the fibroin and the observable characteristics of the solution. The best dissolution times were observed in the treatments with LiBr 9.3M and with LiCl-H<sub>2</sub>O 9.5 M (Table 2). In the case of LiCl-H<sub>2</sub>O 9.5 M, we observed two phases in the solution due to the incomplete solubilization of the fibroin in water (Chen *et al.*, 2001.). This may have happened due to the salting out (precipitation) of the fibroin triggered by the excess of salt concentration. Salts exert specific effects on proteins which depend on the nature of the salt and its concentration, resulting in either the stabilization or denaturation of proteins, as well as in the salting in or salting out of the protein (ARAKAWA; TIMASHEFF, 1984) . Because a protein contains multiple charged groups, its solubility depends on the concentrations of dissolved salts and others parameters like the polarity of the solvent, the pH, and the temperature.

The solubility of a protein at low ion concentrations increases as salt is added as can be seen in treatments with LiBr. The additional ions shield the protein's multiple ionic charges, thereby weakening the attractive forces between individual protein molecules (such forces can lead to aggregation and precipitation). However, as more salt is added, the solubility of protein again decreases (ARAKAWA; TIMASHEFF, 1984; BEXIGA, 2014; FALLIS, 2013). This "salting out" effect is primarily a result of the competition between the added salt ions and the other dissolved solutes (protein molecules) for molecules of solvent (water). At very high salt concentrations, so many of the added ions are solvated that there is significantly less bulk solvent available to dissolve other substances, including proteins (FALLIS, 2013) .The high saline concentration of the LiBr 9.3M solution promotes the dispersion of the fibers by increasing the conductivity and ionic strength of the medium, leading to rupture of hydrogen bonds and the consequent dissolution of the polypeptides (BEXIGA, 2014).

The treatments that took more time to dissolve the fibroin were the ones with  $\text{CaCl}_2\text{-EtOH-H}_2\text{O}$ , 1:2:8 (molar) and  $\text{LiCl-EtOH-H}_2\text{O}$ , 10:18:72 (w/w) in comparison with the other two treatments. One possible explanation for this fact is related to the atomic radius of lithium, considerably smaller than calcium, which could facilitate the permeability of LiBr in the fibroin fibers. This could explain the substantial difference between the fibroin processing times (ARAKAWA; TIMASHEFF, 1984; BEXIGA, 2014; ZHENG *et al.*, 2016). We didn't expect the results obtained for the treatments with LiCl as the treatment with LiCl with EtOH took more time to dissolve the fibroin than the treatment without EtOH. Being the salt solution  $\text{LiCl-EtOH-H}_2\text{O}$  very similar to the Ajisawa reagent we expected to observe a lower dissolution time in the treatment with EtOH because the addition of a proper quantity of monohydric alcohol, such as  $\text{CH}_2\text{OH}$  and  $\text{C}_2\text{H}_5\text{OH}$  improves the solubility of silk fibroin in water (AJISAWA, 1968). From these results it is possible to conclude that the best salt to dissolve the extracted fibroin in water is the one with a 9.3 M concentration of LiBr in water, due the short dissolving time needed to completely dissolve the fibroin fibers and the appropriate characteristics of the obtained solution.

Another parameter we used to choose the treatment to dissolve the fibroin in water for the following experiments was the low tendency of the solutions obtained to form a hydrogel during the dialysis of the solutions. This happened with the solutions obtained with the Ajisawa reagent ( $\text{CaCl}_2\text{-EtOH-H}_2\text{O}$ ), because the ethanol in the solution helps to the breakdown of the metastable solution and the formation of the  $\beta$ -Sheets (AJISAWA, 1968; ZHENG *et al.*, 2016).

**Figure 19.** Fibroin solutions obtained by four different dispersion methods, A)  $\text{CaCl}_2$ -EtOH-  $\text{H}_2\text{O}$ , 1:2:8 (molar), B)  $\text{LiCl}$ - $\text{H}_2\text{O}$  9.5 M. C)  $\text{LiCl}$ -EtOH- $\text{H}_2\text{O}$ , 10:18:72 (w/w), D)  $\text{LiBr}$  9.3 M.

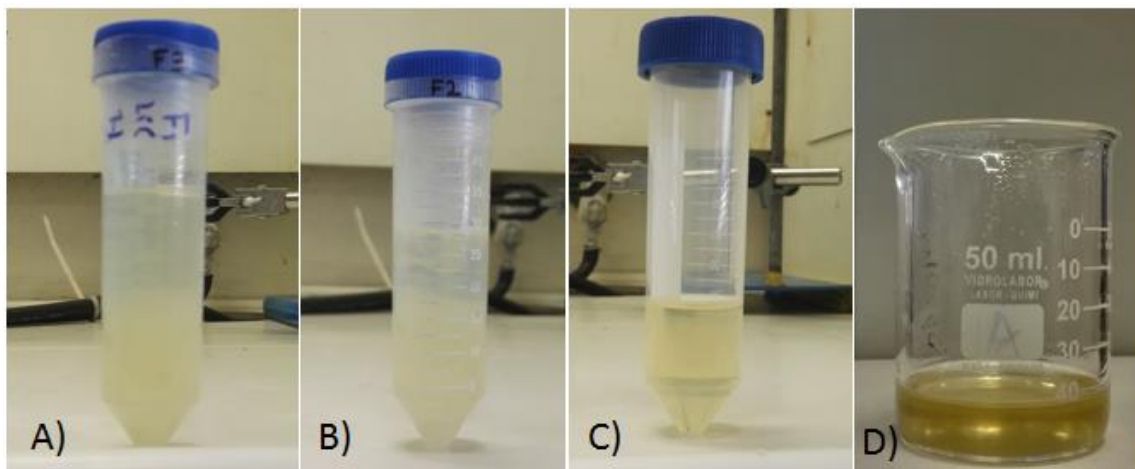


**Table 2.** Silk fibroin dispersion in in four different solvents solutions, time needed to dissolve and characteristics of each dispersion obtained.

Treatments	$\text{CaCl}_2$ -EtOH- $\text{H}_2\text{O}$ , 1:2:8 (molar)		$\text{LiCl}$ - $\text{H}_2\text{O}$ 9.5M		$\text{LiCl}$ -EtOH- $\text{H}_2\text{O}$ , 10:18:72(w/w)		$\text{LiBr}$ 9. 3M	
Silk Type	Dissolution time (min)	Observations (min)	Dissolution Time(min)	Observations	Dissolution time (min)	Observations	Dissolution time (min)	Observations
Frison Extra	109	Homogeneous, yellow and opaque	28	Two phases, yellow	58	Two phases, yellow	2	Yellow, One translucent
Meada 21	229	Viscus, yellow and opaque	18	Two phases, yellow	64	Two phases, yellow	4	Yellow, One translucent

## 5.2. Preparation of the Fibroin Hydrogels

We investigated the formation of fibroin hydrogels by varying the SF/ ethanol ratio of the solution with different concentrations of fibroin. For that, we monitor the gelation time by visual inspection of the samples. We observed that varying the content of ethanol of the solutions has an effect in the gelation time of the samples. At higher content of ethanol, the time needed to form a hydrogel decreases. The ethanol added to the solutions dehydrates SF molecules, increasing intra and intermolecular bonds, providing the formation of silk II structures, which stabilizes the hydrogel (DE MORAES *et al.*, 2015).

The silk II structure consists in a crystalline  $\beta$ -sheets embedded in an amorphous matrix, this structure makes the fibroin predominantly hydrophobic. In aqueous solution, the fibroin is metastable (this means that the molecules will start to aggregate and hydrophobic and hydrogen interactions may occur eventually) (ASAKURA; OKUSHITA; WILLIAMSON, 2015), and there are always two opposite interactions: hydrophobic hydration and hydrophobic interaction. The formation of a hydrophobic hydration structure will enhance the solubility of the nonpolar species and disfavor their aggregation because of the decrease in entropy.

The stabilization of the protein in an aqueous solution is also due to the hydrophobic interaction that arises from the unique three-dimensional structure of water (ASAKURA; NAKAZAWA, 2008; YANG *et al.*, 2004). The gelation process of fibroin is a natural process, but can be accelerated by factors such as pH, temperature, salt concentration and the addition of alcohol that attenuated these hydrophobic interactions. Because the hydrophobicity of ethanol might match that of the interior of regenerated silk fibroin (RSF), the direct interaction between the hydrophobic groups of fibroin and ethanol molecules becomes increasingly favorable with adding ethanol, and ethanol gradually occupies the accessible site and replaces the water molecules (CALANDRINI *et al.*,

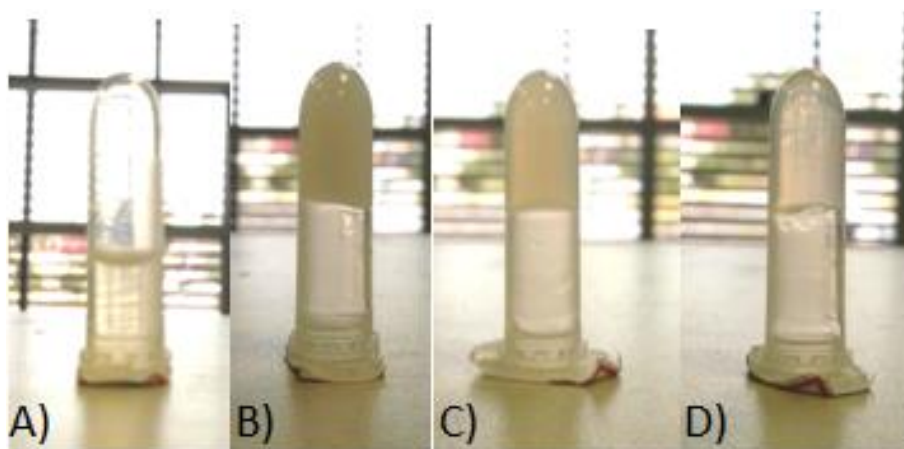
2000). This progressive replacement of the ethanol molecules destabilizes the hydrophobic interaction and promotes the movement of the molecular chain of RSF, which will then lead to the structure altering from the high energy random coil to the lower energy  $\beta$ -sheet. The collapse of the hydrophobic core might initiate the conformational transition of regenerated *Bombyx mori* silk fibroin hydrogels (YANG *et al.*, 2004).

**Table 3.** Composition and Nomenclature of the fibroin hydrogels obtained at different fibroin solution and ethanol 50% ratios at 37 °C in a hot bath.

Nomenclature	Volume of Fibroin Solution (0,06 g/mL) ( $\mu$ L)	Volume of ethanol solution (50%)	SF-Ethanol ratio $\mu$ l	Gelation Time	Observations
SFS1000	1000	0	100/0	-----	-----
SFS750	750	250	75/25	24 h	Opaque
SFS500	500	500	50/50	2 h 14min.	Opaque
SFS250	250	750	25/75	20 min.	Translucent

The results obtained are very similar to the ones published by DE MORAES 2015 and collaborators, in his research he describes the same behavior of the fibroin solution after adding different amounts of ethanol 50%. We also note differences in the observable characteristics of the formed hydrogel, these depend on the amount of fibroin solution added to the final solution of the hydrogel. At higher concentration of fibroin, the hydrogel obtained was opaque and at lower concentrations the hydrogel was more translucent due to the change in the reflection index. Also, the SFS750 hydrogel is more rigid than the other hydrogels (Figure 20), and it is not uniform and crumbles easily. SFS250 hydrogel is the most fragile of the obtained hydrogels and most translucent hydrogel. The SF250 ethanol ratio was chosen for the preparation of the hydrogels used in the following analysis due to its desirable physical characteristics such as translucency and stability. Maintaining this ratio, we prepared hydrogels with 15.2,15,12.5,10,7.5,6.2,5 and 2.5 mg/mL of fibroin. This obtained hydrogel was translucid and stable, at higher concentrations (10 to 15.2 mg/mL) more opaque hydrogels were obtained.

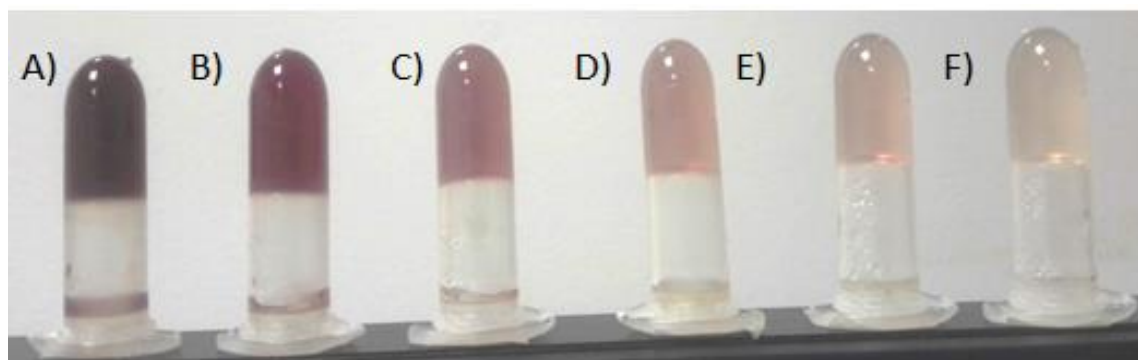
**Figure 20 .** Fibroin hydrogels obtained by adding different ratios of ethanol to the silk fibroin solutions: A) SFS1000, B) SFS750, C) SFS500 and D) SFS250.



### 5.3. Fibroin – Porphyrin Hydrogels Formation

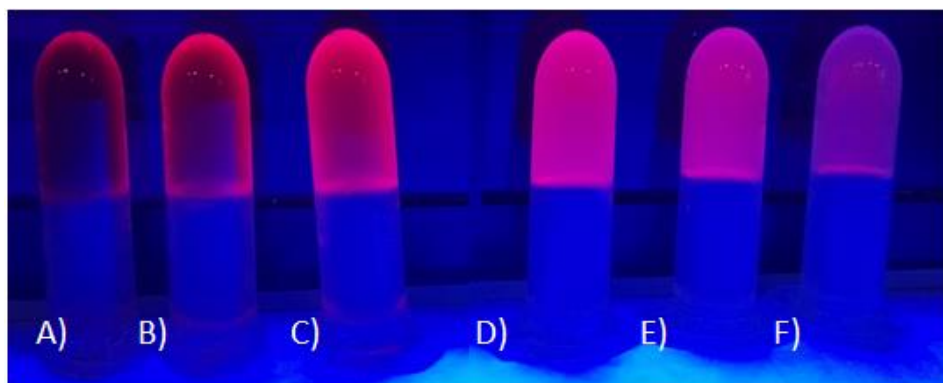
We also studied the effect of different concentrations of porphyrins in the formation of fibroin-porphyrin hydrogels. We used a single fibroin concentration for this experiment (7.5 mg/mL) due to its rheological properties and reproducibility. It was observed from a tube inversion test that all the solutions formed stable hydrogels independently of the porphyrin concentrations added to each hydrogel. We noticed differences in the physical characteristics of the obtained hydrogels. The ones with the higher porphyrin concentrations were opaque and darker and the hydrogels obtained with lower concentrations were more translucent and clearer (Figure 21).

**Figure 21** . Fibroin hydrogels with different porphyrin concentrations: A)1mg/ml, B)0,5mg/ml, C)0,25 mg/ml, D)0,1 mg/ml, E) 0,05 mg/ml and F) 0,025 mg/ml.



After exposing the hydrogels to UV light, we also observed differences in the intensity of the luminescence emitted from each hydrogel (Figure 22). At higher porphyrin concentration, the intensity of the emitted light decreases and at lower concentrations it increases, due to a quenching effect caused by the high concentrations of the porphyrin contained by the hydrogels. This is caused by scattering of the light by the internal chambers of the hydrogel (GUO et al., 2016; LOVELL et al., 2011a, 2011b).

**Figure 22** . Fibroin hydrogels(3,9mg/ml) with different porphyrin concentrations: A)1mg/ml, B)0,5mg/ml, C)0,25 mg/ml, D)0,1 mg/ml, E) 0,05 mg/ml and F) 0,025 mg/ml.



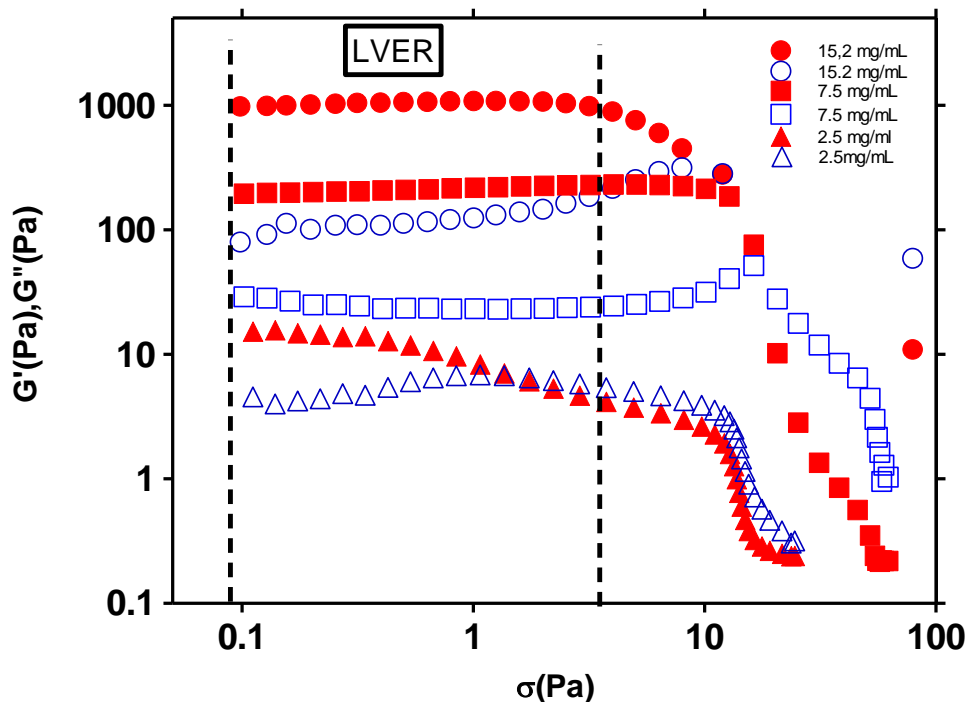


## 5.4. Rheology

### 5.4.1. Fibroin Hydrogels LVER

We used oscillatory rheology to determine the behavior of the obtained hydrogels, the basic principle of an oscillatory rheometer is to induce a sinusoidal shear deformation in the sample and measure the resulting stress response. The time scale probed is determined by the frequency of oscillation,  $\omega$ , of the shear deformation (WYSS, 2007). In order to determine the viscoelastic region of the sample we first elaborated an amplitude sweep to define the LVER (Linear Viscoelastic Region) of the hydrogel (Figure 12); we then performed the following analysis in a shear rate within this region, because when oscillatory shear measurements are performed in the linear viscoelastic regime, the storage modulus  $G'$  (elastic response) and loss modulus  $G''$  (viscous behavior) are independent of the strain amplitude. Observation of a dependence of  $G'$  and  $G''$  on strain amplitude signifies nonlinear viscoelastic response.

**Figure 23** . LVER curve of a Fibroin Hydrogel with different concentrations of fibroin solutions (●) 15.2 mg/mL, (○) 15.2 mg/mL, (■) 7.5 mg/mL, (□) 7.5 mg/mL, (▲) 2.5 mg/mL, (△) 2.5 mg/mL. . Closed symbols represent the  $G'$  value and open symbols the  $G''$  value.



#### 5.4.2. Fibroin Hydrogels Oscillatory analysis

Analysis of changes in the material's viscoelastic properties over time, as well as the material's final complex shear modulus, is often used to understand phase transitions associated with molecular rearrangement in aqueous environments (CALIXTO *et al.*, 2014). We used the frequency sweep test, which analyses the elastic response component  $G'$  (storage modulus) and the viscous response component  $G''$  (loss modulus) of hydrogels with different concentrations of fibroin but keeping the SFS/ethanol 50% solution ratio.  $G'$  gives us information about the deformation energy stored during shear process of a test material (i.e. the stiffness of the material) and  $G''$  measures the energy dissipated during shear (i.e. the flow or liquid-like response of the material). If  $G'' > G'$ , the sample behaves like a viscous liquid, but when  $G' > G''$ , the sample behaves like an elastic solid. We observed that the samples with the higher ratio of fibroin solution have higher  $G'$  and  $G''$  values than the samples with lower fibroin solution ratio.

The  $G'$  (storage modulus) values were higher than the  $G''$  (loss modulus) in all the samples. The elastic component prevailed over the viscous one, evidencing the elastic behavior of the hydrogel over the viscous behavior. This means that part of the mechanical energy used to produce deformation is stored in the material and recovered on release of stress. Higher values of  $G'$  indicate an increase of the crosslinking density in the polymer matrix. A hydrogel formed from a fibroin solution SF250 forms stronger hydrogels, due to the high concentration of fibroin in the solution. We also observed that the concentration increases of the protein solution raised the  $G'$  values, increasing the elastic character of the hydrogels as we can notice from frequency sweep of the hydrogels SFS250, SFS500 and SFS750 (Figure 24).

**Figure 24 .** Frequency sweep of the fibroin hydrogels with different ratios of silk fibroin solution and ethanol 50% solution . Closed symbols represent the  $G'$  value and open symbols the  $G''$  value. (●) 750F-250EtOH 50%, (○) 750F-250EtOH 50%, (■) 500F-500EtOH 50%, (□) 500F-500EtOH 50%, (◆) 250F-750EtOH.

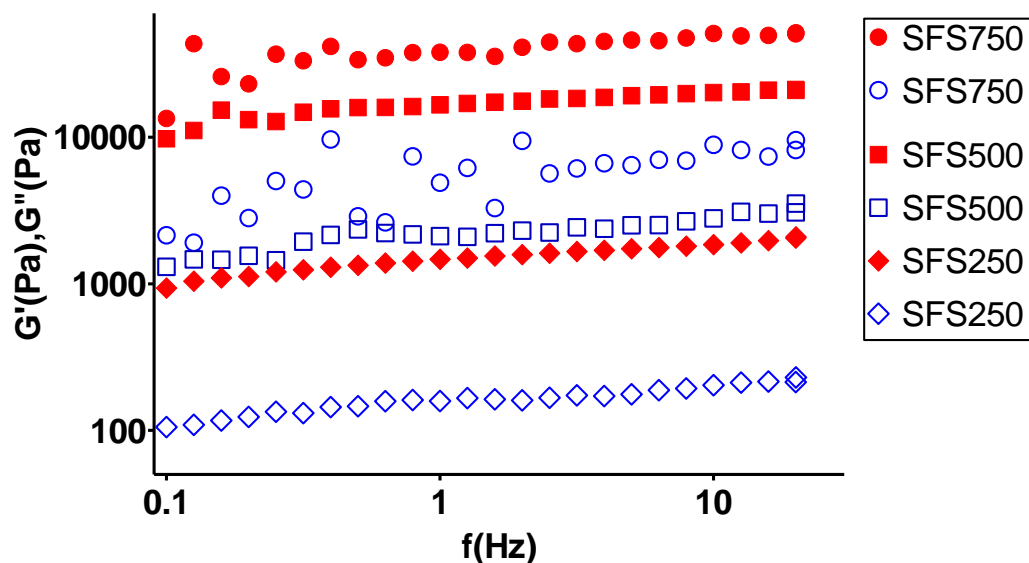


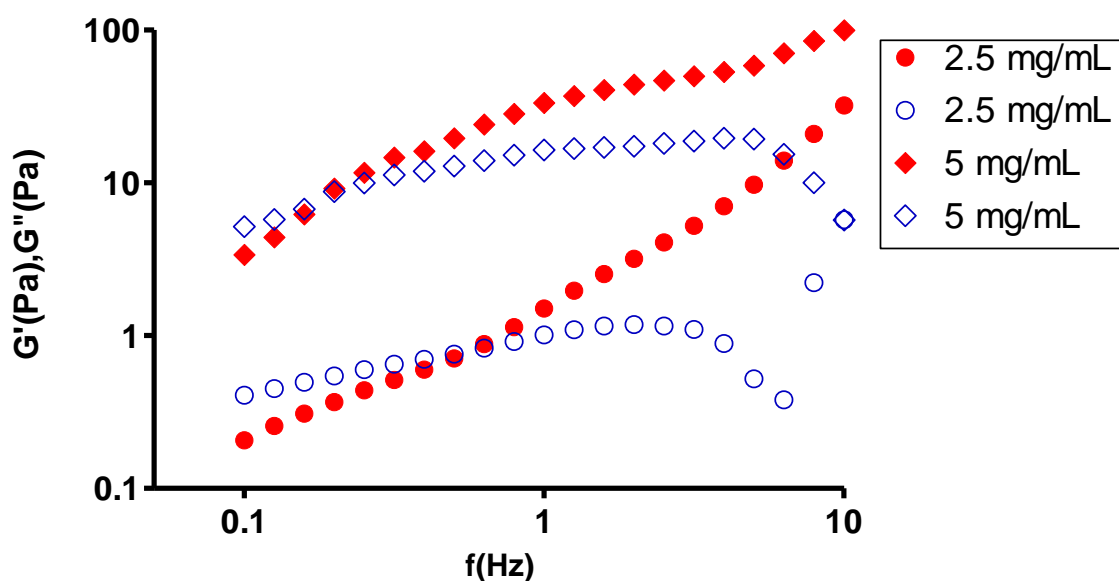
Table 4 presents the coefficients obtained with equation 1 adjusted for the  $G'$  results of each hydrogel. The values of  $n$  (viscoelastic exponent) and  $S$  (gel strength) allow for a quantitative estimation of the hydrogel's strength. The  $n$  and  $S$  values allow a quantitative estimation of strength of hydrogel structures that can be related with the crosslinking density within the polymer network. In this sense, higher  $S$  and  $G'$  values and low  $n$  exponent values indicate an increase of the crosslinking density, which is related to stronger gel structures. At higher concentration of SF, the polymer built stronger hydrogels.

**Table 4.** Coefficient of determination for linear regression ( $r^2$ ), storage modulus ( $G'$ ), gel strength ( $S$ ) and viscoelastic exponent ( $n$ ) of the hydrogels obtained.

Hydrogel	$r^2$	$G'$ (Pa)	$S$ (Pa)	$n$
SFS750	0.67654	$38013.33 \pm 15488.56$	$37405.36 \pm 1171.64$	$0.11443 \pm 0.016$
SFS500	0.89175	$16643.33 \pm 3281.23$	$16103.41 \pm 221.54$	$0.1005 \pm 0.007$
SFS250	0.98127	$1473.66 \pm 141.58$	$1422.79 \pm 9.84$	$0.12417 \pm 0.003$

We also observed the same behavior in the hydrogels with different concentration of fibroin but with the same ratio 250  $\mu$ l FS – 750  $\mu$ l ethanol (50%) solution (SFS250). At higher concentration of the fibroin in the hydrogels  $G'$  increases (Figure 25). This means that at higher concentrations of FS we obtained more stabilized and stronger hydrogels.

**Figure 25.** Frequency sweep of the fibroin hydrogels with different content of fibroin. Closed symbols represent the  $G'$  value and open symbols the  $G''$  value. (●) 2.5 mg/mL, (○) 2.5 mg/mL, (◆) 5 mg/mL (◇) 5 mg/mL. All the hydrogels maintain the SF250 ratio and were obtained from a SFS 61 mg/mL (6.1%).



The hydrogels with higher concentrations of fibroin have an almost independent response of frequency (Figure 26 and Figure 27) thus it infers that a stable gel was formed with all polymer concentrations except the ones with a low concentration of the protein (5 mg/mL and 2.5 mg/mL). This means that the fibroin hydrogels behave mainly like a solid and this is more pronounced in hydrogels with more fibroin in their structure. On the other hand the gel with 5 mg/mL and 2.5 mg/mL behave more like a viscoelastic liquid. This can

be observed from the behavior of the storage and loss moduli of the material. At lower frequency, the  $G''$  is higher than the  $G'$  but as we increase the frequency the  $G'$  has a tendency to increase too. As we mentioned before this means that, unlike at high concentrations, at low concentration of the protein, the storage and loss moduli of the material are frequency dependent (Figure 26 and Figure 27) forming less stable hydrogels that behave more like a liquid than a gel.

**Figure 26.** Frequency sweep of the fibroin hydrogels with different content of fibroin. Closed symbols represent the  $G'$  value and open symbols the  $G''$  value. (●) 10 mg/ml, (○) 10 mg/ml, (■) 7.5mg/ml, (□) 7.5mg/ml, (◇) 6.2 mg/mL, (◇) 6.2 mg/mL.

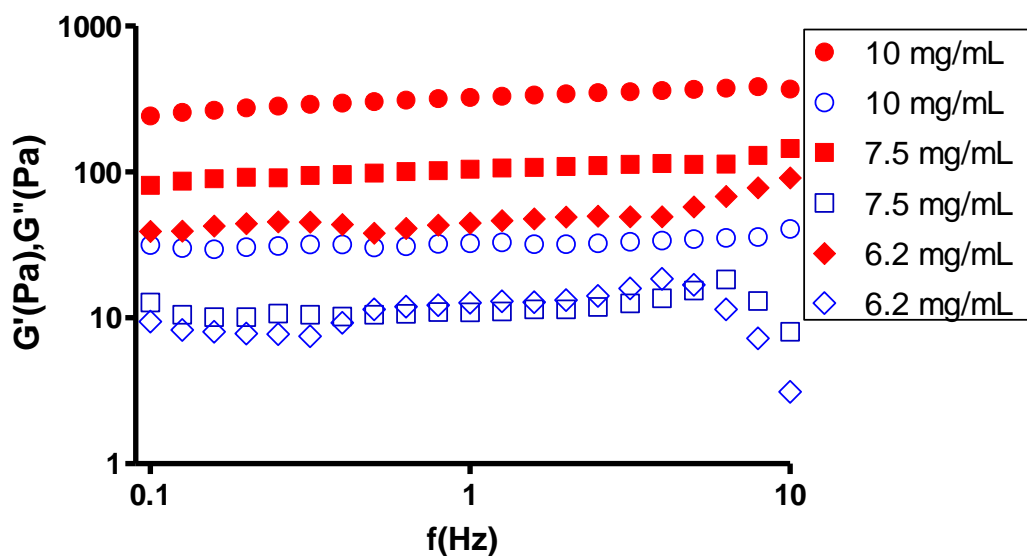
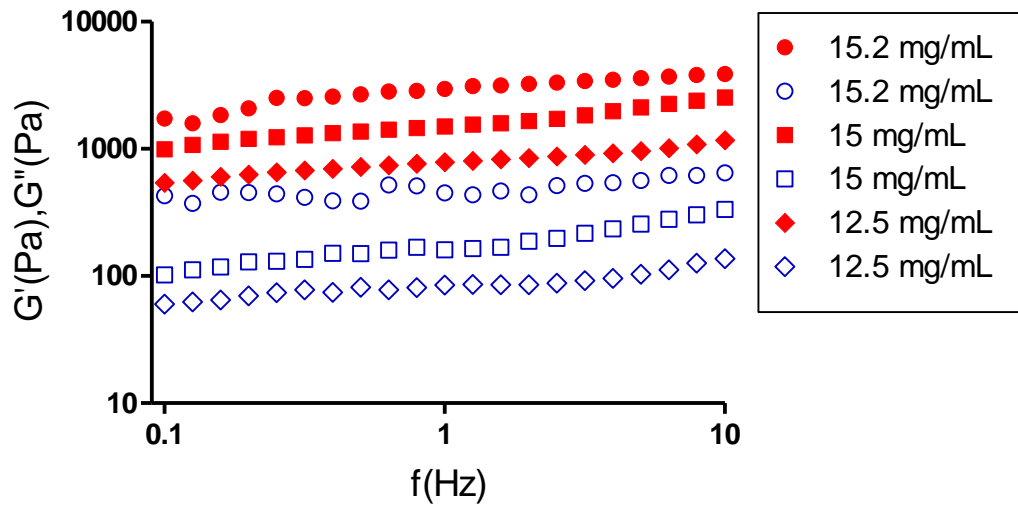


**Figure 27.** Frequency sweep of the fibroin hydrogels with different content of fibroin. Closed symbols represent the  $G'$  value and open symbols the  $G''$  value. (●) 15.2 mg/ml, (○) 15.2 mg/ml, (■) 15 mg/mL, (□) 15 mg/mL, (◇) 12.5mg/mL, (◇) 12.5mg/mL.



For these hydrogels, we also calculate the gel strength ( $S$ ) and viscoelastic exponent ( $n$ ), to perform comparative analysis of strength of different hydrogels. We can observe that they present the same behavior than the 750SF, 500SF and 250SF hydrogels. When higher concentration of SF is used to obtain the hydrogel the  $S$  values become higher. This is due to an increasing in the crosslinking density. This helps demonstrate that increase of the fibroin concentration raised the  $S$  and  $G'$  values, increasing the elastic character of the hydrogels. The coefficient of determination for linear regression ( $r^2$ ) of the hydrogels (Table 5) demonstrated that all hydrogels have response that is almost independent from of frequency, since the frequency was not dependent on the storage modulus. At lower concentrations, the data does not adjust properly to the power law model this means these hydrogels could behave more like a Newtonian liquid.

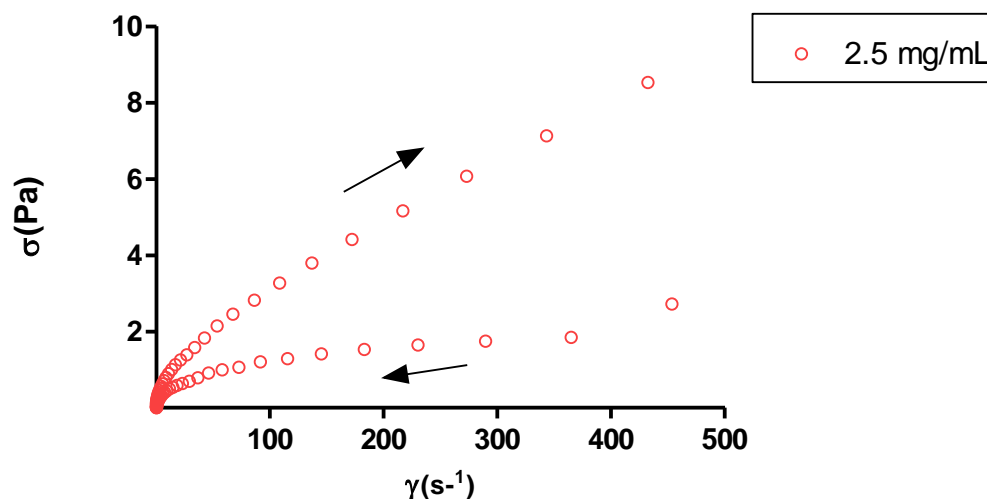
**Table 5.** Coefficient of determination for linear regression ( $r^2$ ), storage modulus ( $G'$ ), gel strength (S) and viscoelastic exponent (n) of the hydrogels obtained

Hydrogel	$r^2$	$G'$ (Pa)	S (Pa)	n
15.25mg/ml	0.982	2963.33 $\pm$ 1424.58	2173,556 $\pm$ 55.54	0,143 $\pm$ 0.007
15 mg/ml	0.983	1499.66 $\pm$ 95.82	1045.979 $\pm$ 22.44	0.211 $\pm$ 0.005
12.25mg/ml	0.962	785.50 $\pm$ 72.32	566.125 $\pm$ 14.74	0.178 $\pm$ 0.007
10 mg/ml	0.907	323.86 $\pm$ 26.21	260.637 $\pm$ 6.38	0.112 $\pm$ 0.007
7.5 mg/ml	0.715	104.44 $\pm$ 11.8	71.545 $\pm$ 6.78	0.205 $\pm$ 0.02
6.2 mg/ml	0.774	44.82 $\pm$ 11.2	17.356 $\pm$ 3.98	0.453 $\pm$ 0.05
5 mg/ml	0.970	33.33 $\pm$ 27.1	5.442 $\pm$ 0.93	0.735 $\pm$ 0.038
2.5 mg/ml	0.998	1.50 $\pm$ 0.08	0,00601 $\pm$ 0,01	2.079 $\pm$ 0.034

#### 5.4.3. Fibroin Hydrogels Continuous flow and Viscosity Profiling

The flow curves of the samples are presented in figure 28 through Figure 32 , in which the relation between the shear stress ( $1s^{-1}$ ) and shear rate (Pa) , evidenced that all hydrogels exhibited “shear thinning” pseudo- plastic flow behavior except the hydrogel with a concentration of 2.5 mg/mL of fibroin, it shows a Newtonian behavior because we can observe an almost linear conduct (Figure 28) but as the concentration of fibroin in the hydrogel increase the behavior of the material flow changes and adopts a non-Newtonian behavior.

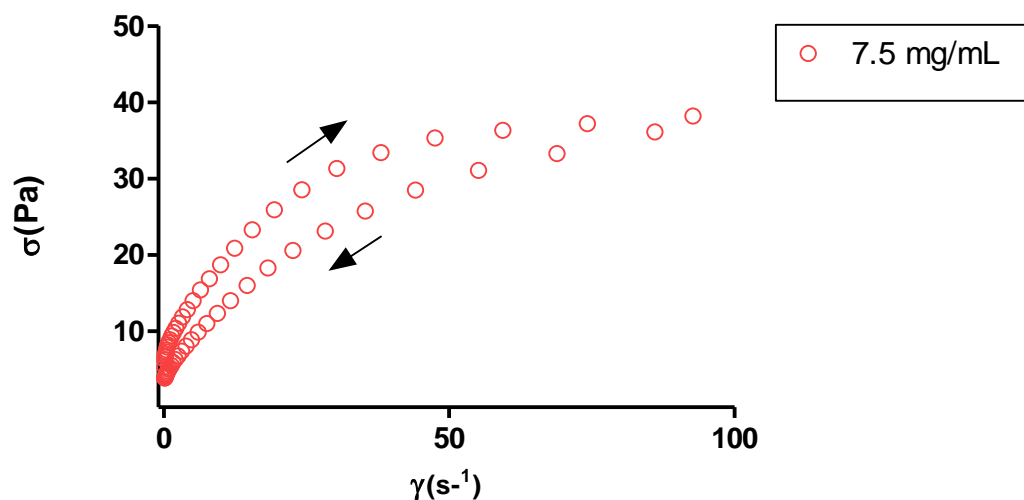
**Figure 28.** Flow rheograms of the hydrogels composed of Fibroin 2.5 mg/mL. The arrows point the direction of the curve, upstream and downstream.



In order to determine the general flow behavior of fibroin hydrogels the viscosity was measured as a function of the shear rate in a rotational rheometer. For the presentation of the data the shear stress is plotted against the shear rate, each time we increase the shear rate applied to the samples we observed a decrease in the viscosity. This means that the viscosity of the fibroin hydrogels is dependent on the shear rate applied to the samples. This is a shear-thinning behavior, which is characteristic of pseudo-plastic gels, and is observed when the viscosity decreases with increase in shear stress. The pseudo-plastic and shear-thinning behavior of the hydrogels shows to be concentration dependent because when the fibroin concentration increased, a higher stress was required to generate an significant deformation of the hydrogel as can be seen in Figures 29,30 and 31. This may be due to the higher entanglement of protein chains enabling a physical crosslinking when the concentration increases (CALIXTO *et al.*, 2014).



**Figure 29.** Flow rheograms of the hydrogels composed of Fibroin 7.5 mg/mL. The arrows point the direction of the curve, upstream and downstream



Interestingly, the fibroin hydrogels behave like thixotropic materials, as the descending curve does not overlap with the ascending one, and they show a strong ability to recover its structure when the shear stress is removed. This means that after applying a shear to the sample the viscosity decreases (structure breakdown) and increases after stopping the stresses applied to the sample (structure recovery). The bonds between the particles in these gels are very weak and can be broken down by mechanical stress. The resulting solution will revert back to the gel state by subsequent rest phase due to the clustering of the particles or by physical cross-linking. Agar gels, gelatin gels, iron oxide gels, and certain clays such as kaolin and bentonite, exhibit thixotropic property (FRANCIS; SAKTHI, 2013). This thixotropic behavior is desirable in pharmaceutical preparations, both in engineering design and consumer application, in order to deliver an initially thick product as a thinner, easily spreadable material (MOHAMED, 2004).

**Figure 30.** Flow rheograms of the hydrogels composed of Fibroin 10 mg/mL. The arrows point the direction of the curve, upstream and downstream.

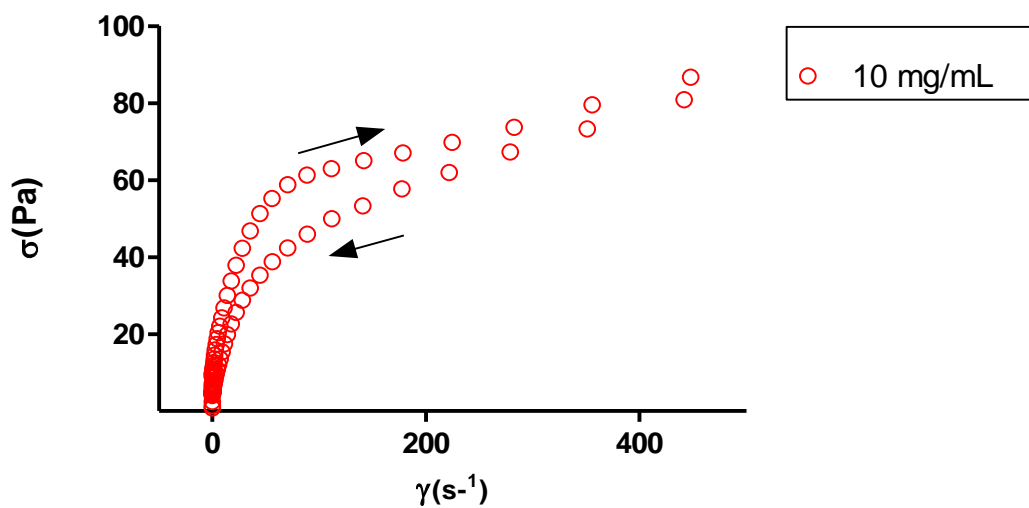


**Figure 31.** Flow rheograms of the hydrogels composed of Fibroin 12.5mg/ mL. The arrows point the direction of the curve, upstream and downstream.

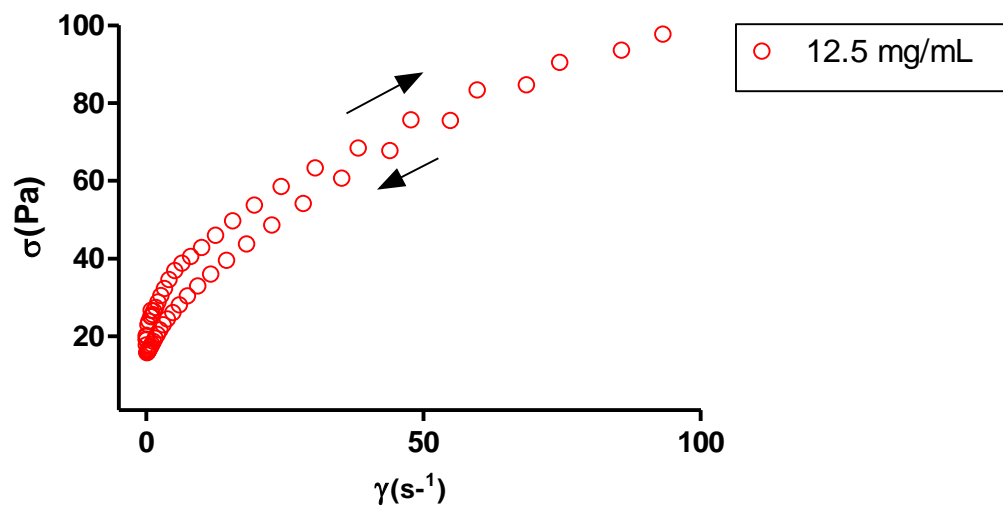
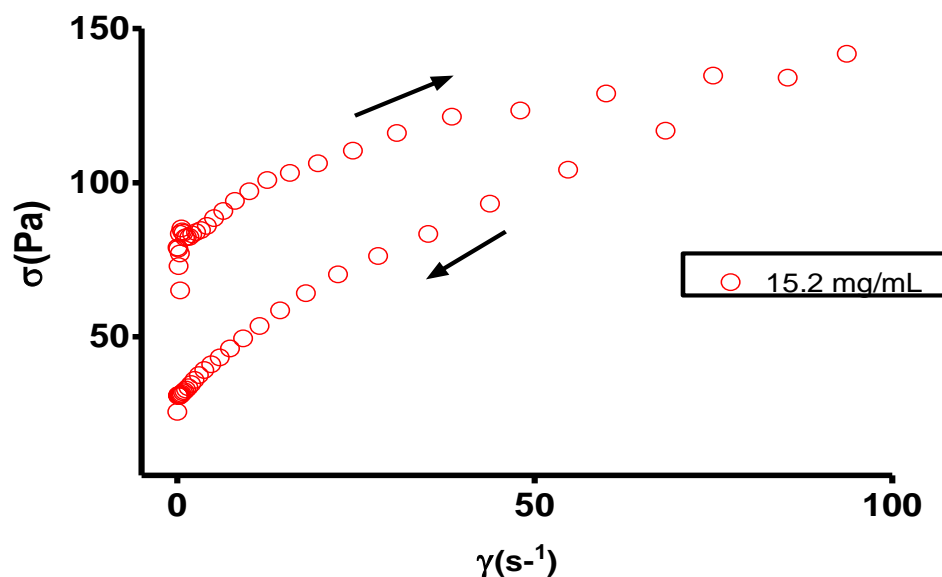


**Figure 32.** Flow rheograms of the hydrogels composed of Fibroin 15.2 mg/mL . The arrows point the direction of the flow curve, upstream and downstream.



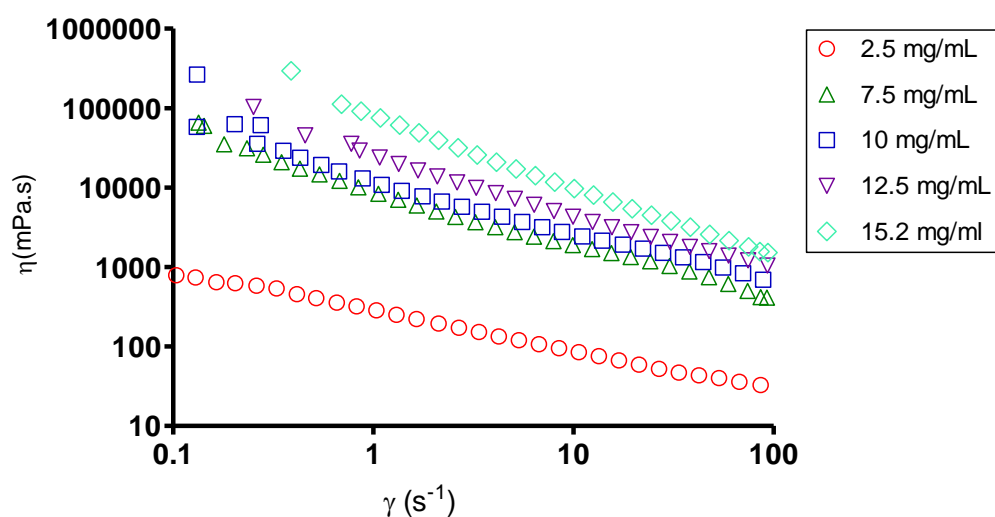
All the fibroin hydrogels exhibit shear thinning behavior ( $n < 1$ ) calculated from Equation 2. Thixotropy is a desired characteristic in materials for topical use because after administration of the stress application, the formulation starts to flow easily, leading to a good spreading during application enabling a formation of a uniform film on the skin surface. After withdrawal of the stress, the viscosity of formulation increases instantaneously avoiding its outflow (LIU et al., 2014).

**Table 6.** Coefficient of determination flow index (n) and consistency index (k) of the hydrogels obtained.

Hydrogel	<i>k</i>	<i>n</i>
15.25mg/mL	80.37 ± 1.85	0.107 ± 0.008
12.25mg/mL	24.51 ± 1.17	0.287 ± 0.015
10 mg/mL	12.73 ±0.56	0.349 ± 0.012
7.5 mg/mL	9.09 ± 0.31	0.333 ± 0.011
5 mg/mL	0.25 ±0.00	0.541 ±0.007

In the shear rate vs. viscosity curve, we can observe better the shear thinning behavior of the silk fibroin hydrogels. The viscosity decreases at higher shear rates in all the samples with different amounts of fibroin (Figure 33). As the shear stress is increased, the normally disarranged molecules of the hydrogel material are caused to align their long axes in the direction of flow. The change in the orientation of the molecules reduces the internal resistance of the material and hence decreases the viscosity (MOHAMED, 2004; VIOLETA GHICA *et al.*, 2016).

**Figure 33.** Viscosity vs. Shear rate curve of the hydrogels composed of 2.5 ,7.5 ,12.25 and 15.2 mg/ml of fibroin.



#### 5.4.4. Fibroin-Porphyrin Hydrogels Oscillatory analysis

To compare the response of Fibroin-Porphyrin hydrogels, we use a concentration of 7.5 mg/mL of fibroin to obtain the hydrogels and different concentrations of porphyrin. With low amounts of porphyrin, we obtain  $G'$  and  $G''$  similar to the ones of the pure fibroin hydrogel. In all the cases  $G'$  is higher than  $G''$  which confirms the results observed in the inversion test of this hydrogels (Figure 20). This means that all the fibroin/porphyrin hydrogels behave like an elastic solid, the storage modulus is in all the cases higher than the loss modulus as is represented in Figure 34 and 35.

**Figure 34.** Frequency sweep of the fibroin hydrogels (7.5 mg/mL of fibroin) with different content of Porphyrin. Closed symbols represent the  $G'$  value and open symbols the  $G''$  value. (●) 0.05 mg/mL, (○) 0.05 mg/mL, (■) 0.025 mg/mL, (□) 0.025 mg/mL and (◆) Fibroin 7.5mg/mL, (◇) Fibroin 7.5 for comparison.

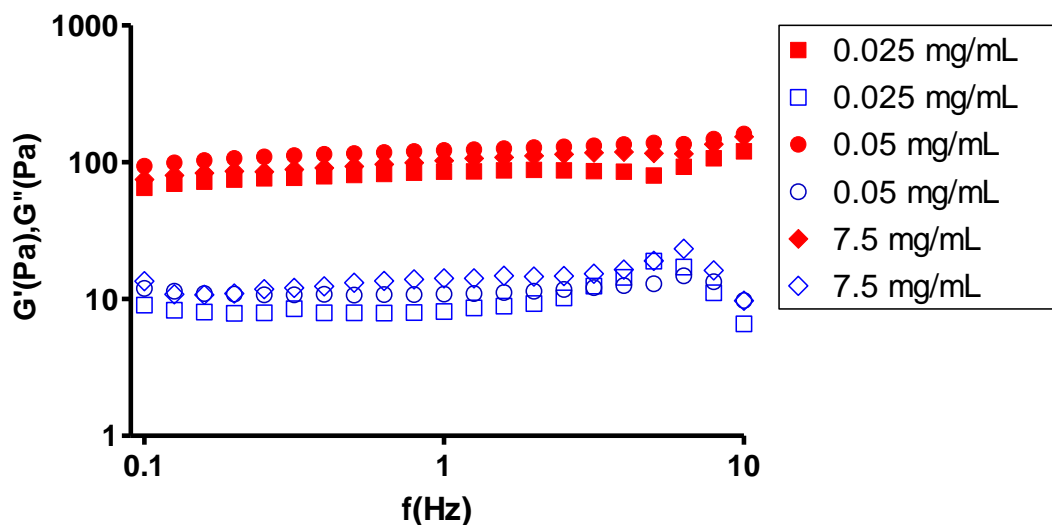
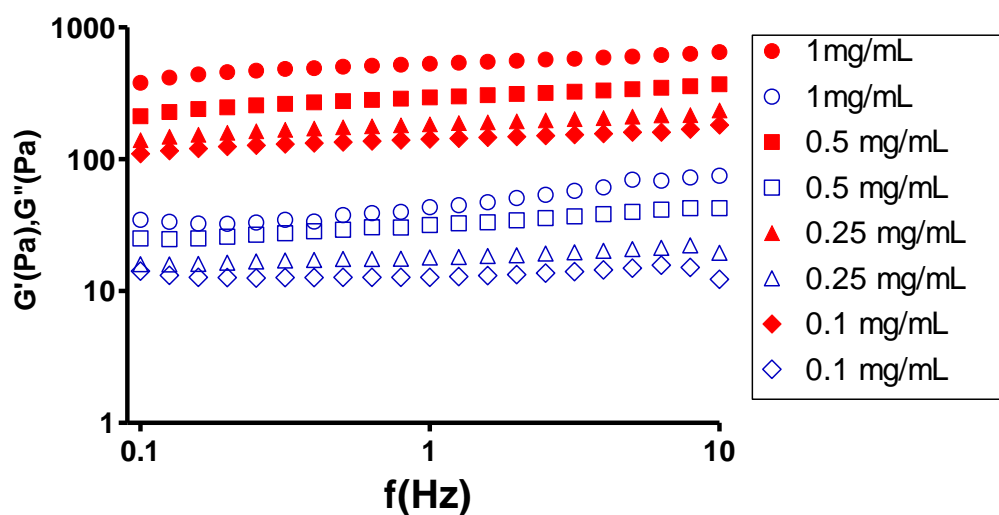


**Figure 35.** Frequency sweep of the fibroin hydrogels (7.5 mg/mL of fibroin) with different content of Porphyrin. Closed symbols represent the  $G'$  value and open symbols the  $G''$  value. (●) 1 mg/mL, (○) 1 mg/mL, (■) 0.5 mg/mL, (□) 0.5 mg/mL, (▲) 0.25 mg/mL, (△) 0.25 mg/mL, (◆) 0.1 mg/mL, (◇) 0.1 mg/mL of porphyrin.



After addition of porphyrin to the hydrogel matrix, the changes in the storage modulus ( $G'$ ), gel strength ( $S$ ) and viscoelastic exponent ( $n$ ), shows the rheological properties of the material are slightly modified. At higher concentration of porphyrin, the  $G'$  values of the samples also increase, this means that there is a relationship between the porphyrin concentration added to the matrix and the storage modulus of the hydrogels obtained. Also, the strength ( $S$ ) of the hydrogel increases increasing the elastic character of the hydrogels.

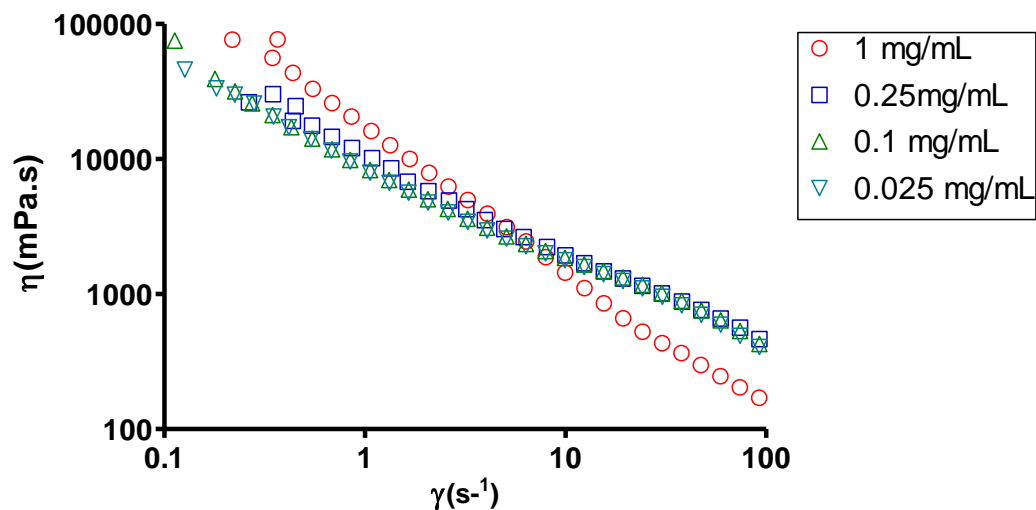
**Table 7.** Coefficient of determination for linear regression ( $R^2$ ), storage modulus ( $G'$ ), gel strength (S) and viscoelastic exponent (n) of the hydrogels obtained with different concentrations of porphyrin.

Hydrogel	$r^2$	$G'$ (Pa)	S (Pa)	n
1mg/ml	0.965	529.50 ± 70.71	434.20 ± 5.73	0.103± 0.004
0.5mg/ml	0.912	294.33 ± 121.15	230.16 ± 6.42	0.130 ± 0.008
0.25 mg/ml	0.829	184.16 ± 11.58	141.58 ± 6.55	0.146 ± 0.013
0.1 mg/ml	0.773	142.16 ± 7.18	107.60 ± 6.31	0.155 ± 0.017
0.05 mg/ml	0.745	122.23 ± 11.09	88.56 ± 6.59	0.178 ± 0.021
0.025 mg/ml	0.665	85.25 ± 2.54	54.19 ± 6.66	0.233 ± 0.033

#### 5.4.5. Fibroin-Porphyrin Continuous flow and Viscosity Profiling

In the case of fibroin-porphyrin hydrogels continuous flow and viscosity profiles show that is notable the shear thinning behavior of all the hydrogels, as the viscosity decreases every time we increase the shear rate applied to the sample until the structure of the material breaks. As the fibroin hydrogels, the hydrogels with Porphyrin incorporated in the matrix of fibroin also present a pseudo-plastic behavior almost Independently of the porphyrin concentration. Only the hydrogel with a 1mg/ml of Porphyrin shows significant differences in comparison with the other samples like is shown in figure 36.

**Figure 36.** Viscosity vs. Shear rate curve of the hydrogels composed of Fibroin 7.5 mg/mL and 1, 0.25, 0.1 and 0.025 mg/mL of porphyrin.



In regard to effects of the shear rate on the shear stress, we observed no overlap between the upstream and downstream curve of each sample, this mean that the sample with a fibroin hydrogel matrix of 7.5 mg/mL and different amounts of porphyrin also present a Thixotropic behavior.

**Figure 37.** Flow rheograms of the hydrogels composed of Fibroin 7.5mg/ml and Porphyrin 1mg/ml. The arrows point the direction of the flow curve, upstream and downstream

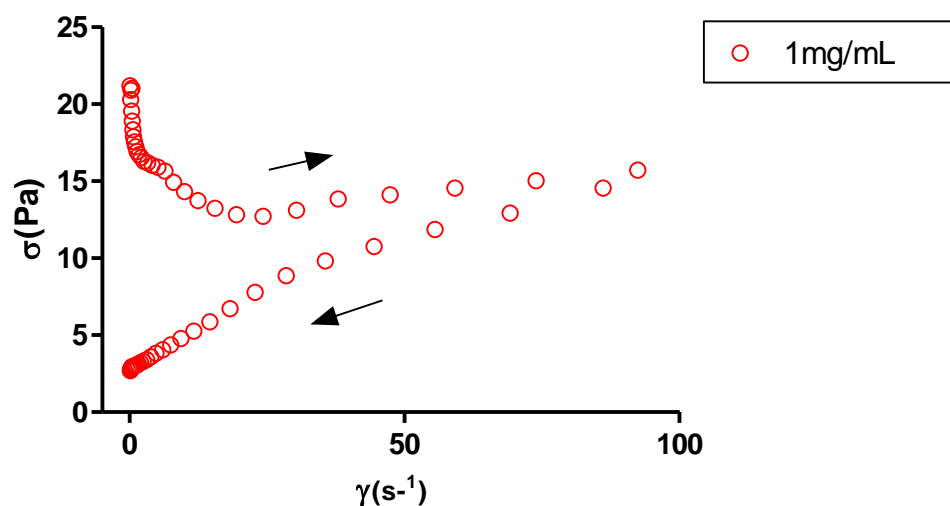




**Figure 38.** Flow rheograms of the hydrogels composed of Fibroin 7.5mg/ml and Porphyrin 0.25mg/ml. The arrows point the direction of the flow curve, upstream and downstream.

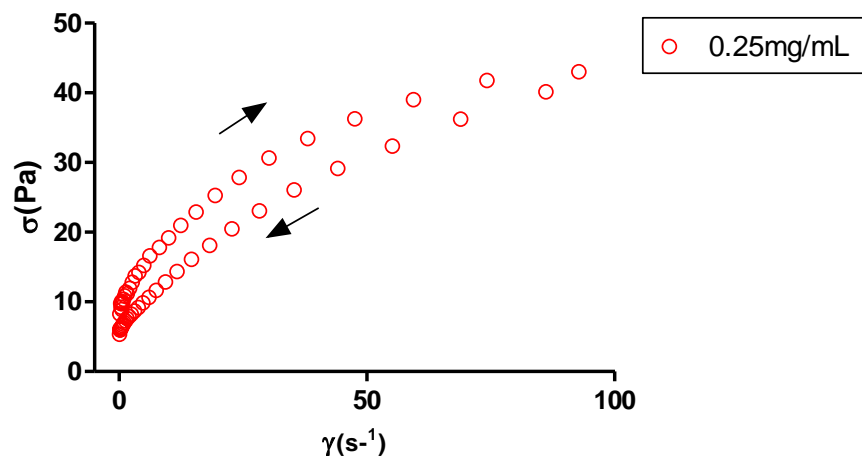


**Figure 39.** Flow rheograms of the hydrogels composed of Fibroin 7.5mg/ml and Porphyrin 0.1mg/ml. The arrows point the direction of the flow curve, upstream and downstream.

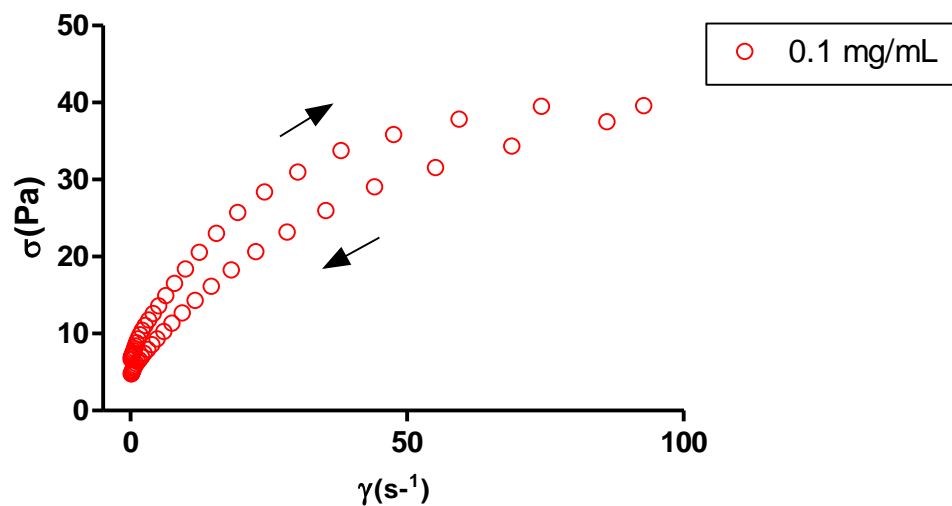
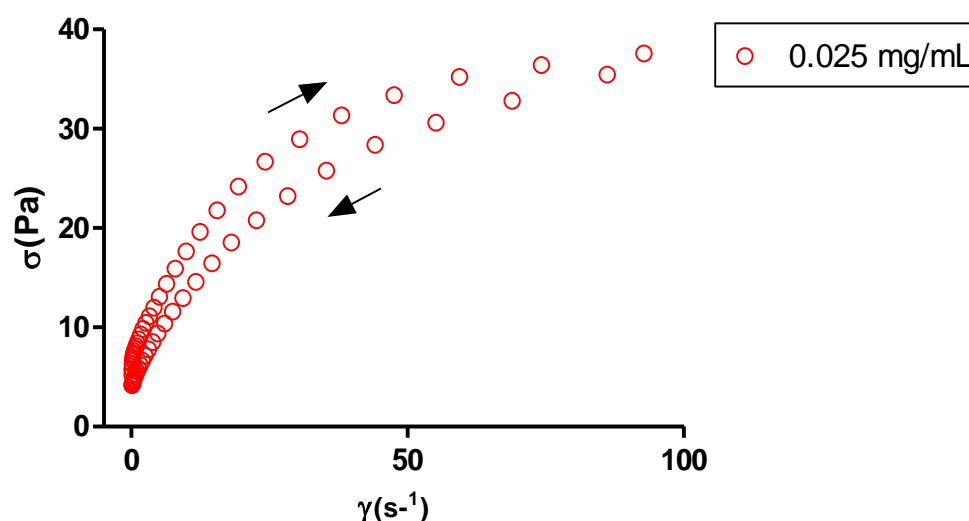


**Figure 40.** Flow rheograms of the hydrogels composed of Fibroin 7.5mg/ml and Porphyrin 0.0026mg/ml. The arrows point the direction of the flow curve, upstream and downstream.



The flow index ( $n$ ) and consistency index ( $k$ ) for the hydrogels with 7.5 mg/mL of fibroin with different concentrations of porphyrin show a similar behavior to the ones shown by the hydrogels containing only fibroin. All the hydrogels maintain a shear thinning behavior and can be classified as pseudo-plastic materials. This means that after the addition of the porphyrin the structure and rheological properties of the hydrogels are only slightly modified. At higher concentrations of porphyrin, the thixotropy of the hydrogels increases, which means that the addition of porphyrin in the fibroin hydrogel matrix has an effect in the structure recovery time of the material. At lower concentration of porphyrin added (0.1mg/mL and 0.025 mg/mL) the hydrogel behaves more like the hydrogels prepared with only fibroin. The consistency index also experiments an increase after addition of porphyrin to the hydrogels, indicating that the crosslinking of the hydrogels increase maybe due to an interaction between the porphyrin and the fibroin molecules or by the effect of the porphyrin  $\pi$ - $\pi$  stacking interactions.

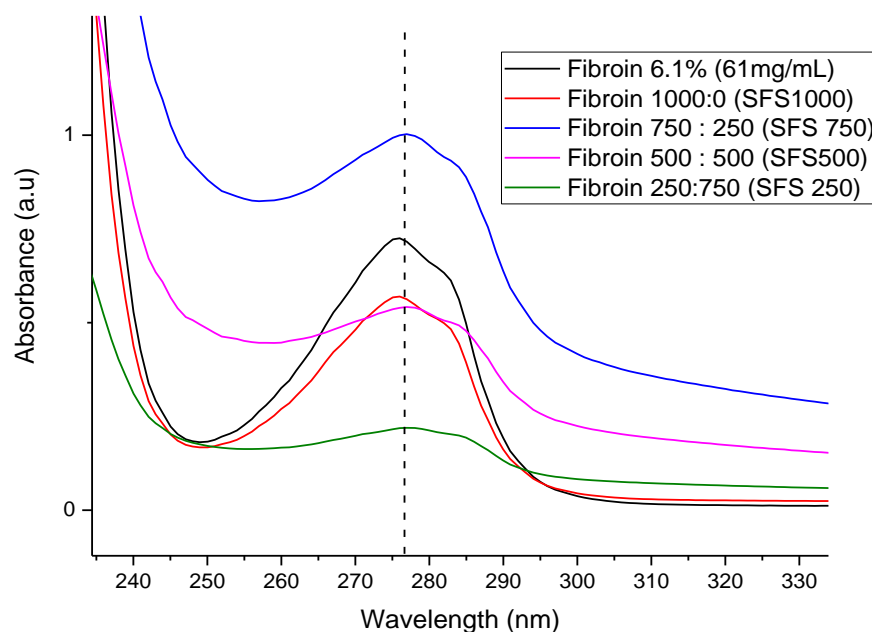
**Table 8** Determination of flow index (n) and consistency index (k) of the hydrogels obtained with different concentration of porphyrin.

Hydrogel	<i>k</i>	<i>n</i>
1mg/ml	16.926 ± 0.450	-0.045 ± 0.011
0.25 mg/ml	10.327 ±0.424	0.314 ± 0.011
0.1 mg/ml	8.935 ±0.382	0.345 ± 0.012
0.025	8.507 ±0.317	0.341 ± 0.011

## 5.5. UV–visible absorption spectra analysis

The UV–visible absorption spectra of the fibroin solution and the fibroin hydrogels at different concentrations showed as expected a signal around 274 nm, this common in proteins samples, as they usually show absorption maxima between 275 and 280 nm (Figure 41) which are caused by the absorbance of radiation in the near UV of the two aromatic amino acids tryptophan (Trp) and tyrosine (Tyr) and to a very small extent on the amount of phenylalanine (Phe) and disulfide bonds (of disulfide bonds) (SCHMID, 2001). Therefore this signal varies greatly between proteins, depending on the concentration of the solution and the aminoacidic composition of the analyzed protein (WALKER, 2009). The SF is mainly composed by glycine, serine and alanine in the highly repetitive sections but also contain others amino acids as tyrosine and tryptophan in the no repetitive sections of the protein (Table 1).

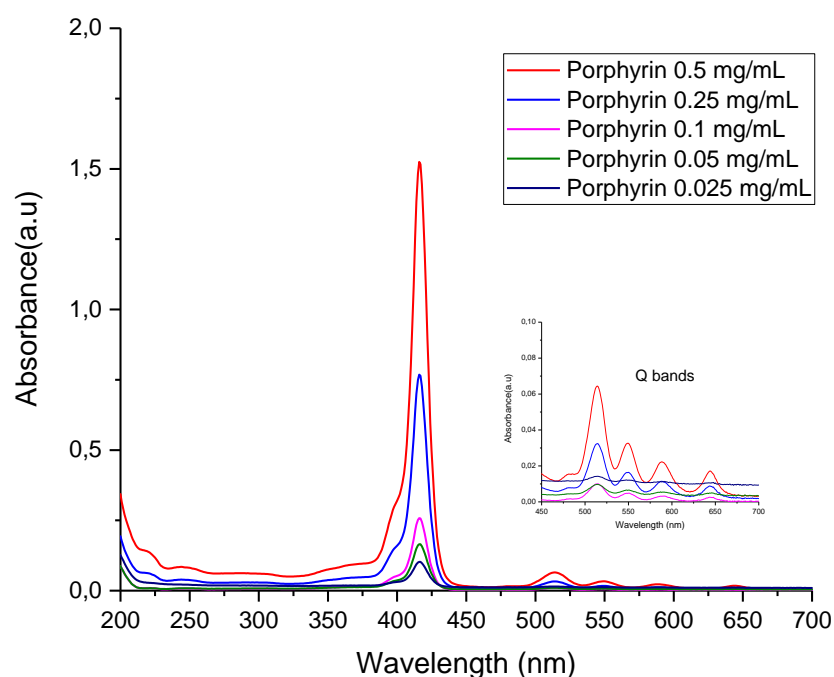
**Figure 41.** UV-Vis spectrum from Fibroin solution 6.1% and Fibroin hydrogels with different ratios of fibroin solution and ethanol 50%.



One of the most interesting features of porphyrins is their characteristic UV-visible spectrum, which consists of two distinct regions: in the near ultraviolet and in the visible region. For the UV-visible spectrum of the porphyrin solutions we can observe one signal with a high intensity around 420 nm and other four low intensity signals around 520, 540, 575 and 645 nm in all the porphyrin solutions samples. This extremely intense band around 350 to 500 nm, is known as the Soret band, while the bands at higher wavelengths with a relatively low intensity are denominated Q bands. The absorption bands in porphyrin systems arise from transitions between two HOMOs and two LUMOs, the transitions between these orbitals gave rise to two excited states and the orbital mixing splits these two states in energy, creating a higher energy state with greater oscillation strength, giving

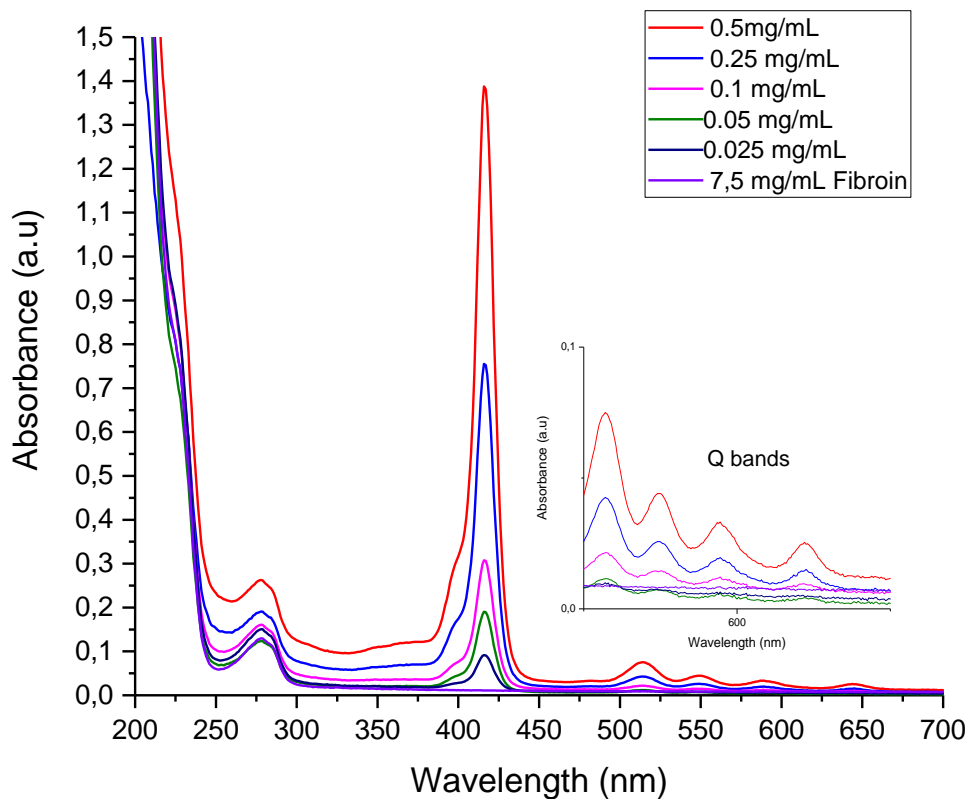
rise to the Soret band, and a lower energy state with less oscillation strength, giving rise to the Q-bands (PÉREZ-MORALES *et al.*, 2009; UDDIN, 2012).

**Figure 42.** UV-Vis spectrum from Porphyrin solutions in different concentrations. The UV-vis signal for 1mg/mL of porphyrin solution is not shown because it is higher than 2.



In the UV-visible spectrum of the different concentrations of Porphyrin in a fibroin (7.5 mg/mL) hydrogel matrix we can observe six different signals. There is one signal around 274 nm corresponding to the signal observed in the fibroin hydrogel spectrum. As we discussed before, this signal is due the absorption of the amino acids forming the protein tyrosine and tryptophan. We can also notice the five bands corresponding to the Soret band and Q bands IV (520nm), III (540 nm), II (575 nm) and I (675 nm) (Figure 43).

**Figure 43.** UV-Vis spectrum from Fibroin 7.5 mg/ml with different concentrations of Porphyrin. The UV-vis signal for 1mg/mL of porphyrin hydrogel is not shown because it is higher than 2.



There is no difference between the spectra of aqueous solutions of porphyrins and porphyrin-containing hydrogels, except for the signal caused by the fibroin. It is possible to classify the type of porphyrin based on the intensity of the four Q bands. The relative intensity of Q bands varies with different kind and the position of substituents on the macrocycle ring.

Porphyrins can be classified as *etio*, *rhodo*, *oxo-rhodo* and *phyllo* porphyrins. When the relative intensities of Q bands are such that  $IV > III > II > I$ , the spectrum is said *etio*-type and porphyrins called *etioporphyrins*. This kind of spectrum is found in all porphyrins

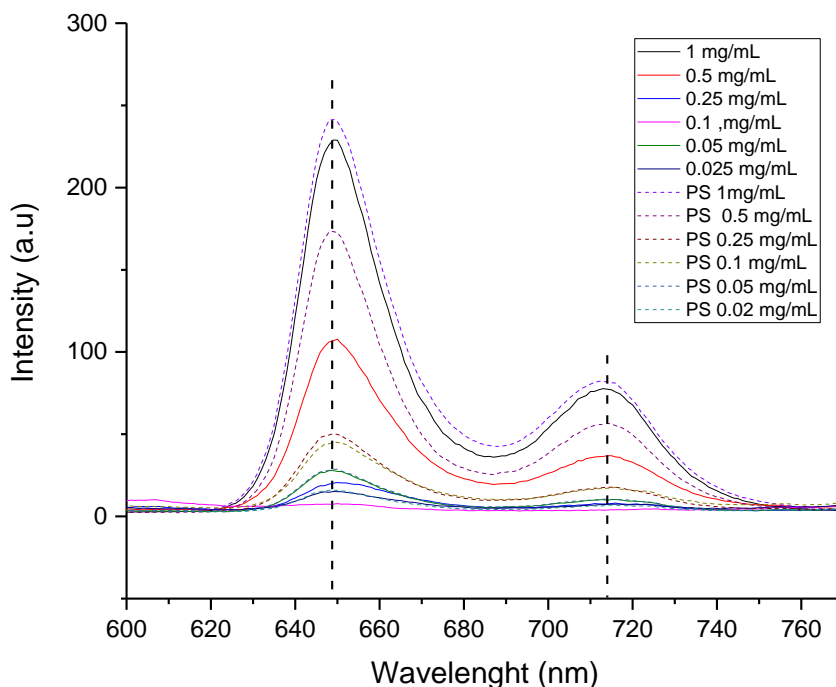
in which six or more of the  $\beta$ -positions are substituted with groups without  $\pi$ - electrons, e.g., alkyl groups (COSMA, 2007; KAROLCZAK *et al.*, 2004; UDDIN, 2012).

## 5.6. Fluorescence spectrum

In regards to the fluorescence spectra of Fibroin – Porphyrin hydrogels, we can observe two signals, one around 580 nm and the other one close to 640 nm, these signals are characteristics of the porphyrin ring (Figure 44) . The emission intensity decreases at lower concentrations of porphyrin inside the hydrogel matrix.

There is no evidence of quenching due to the concentration of porphyrin added as we observed that the intensity does not decrease at high concentration of the porphyrin. Even so it is not possible to rule out the existence of a quenching effect of the intensity due to a higher concentration than 1mg/ml of porphyrin. The peaks at 580 and 640 nm are due the transition from an excited electronic state to a ground electronic state (S1 to S0 transition) (BALA MURALI KRISHNA *et al.*, 2012).

**Figure 44.** Fluorescence spectra from Fibroin 7.5 mg/mL with different concentrations of Porphyrin (solid lines) and porphyrin solutions (dots).



When sample (fluorophores) molecules are exposed to light having an energy that matches a possible electronic transition within the molecule, some of the light energy will be absorbed as the electron is promoted to a higher energy orbital and energetically favored electron promotion will be from the highest occupied molecular orbital (HOMO), usually the singlet ground state,  $S_0$ , to the lowest unoccupied molecular orbital (LUMO), and the resulting species is called the singlet excited state  $S_1$  (SAUER; HOFKENS; ENDERLEIN, 2011). As the light radiation over the sample ceases, the excited molecules decays back to the ground state by emitting a photon from an excited singlet state. The relaxation between an excited vibrational state to the lowest energy vibrational state of the singlet state is responsible for the Stoke shift, which results in the difference between the band maxima of the absorption and emission spectra of the same electronic transition (Figure 44). After relaxation, the fluorophore remains in the lowest vibrational level of the excited electronic state for a period on the order of nanoseconds, corresponding to the fluorescence lifetime. Fluorescence emission occurs as the fluorophore decays from the



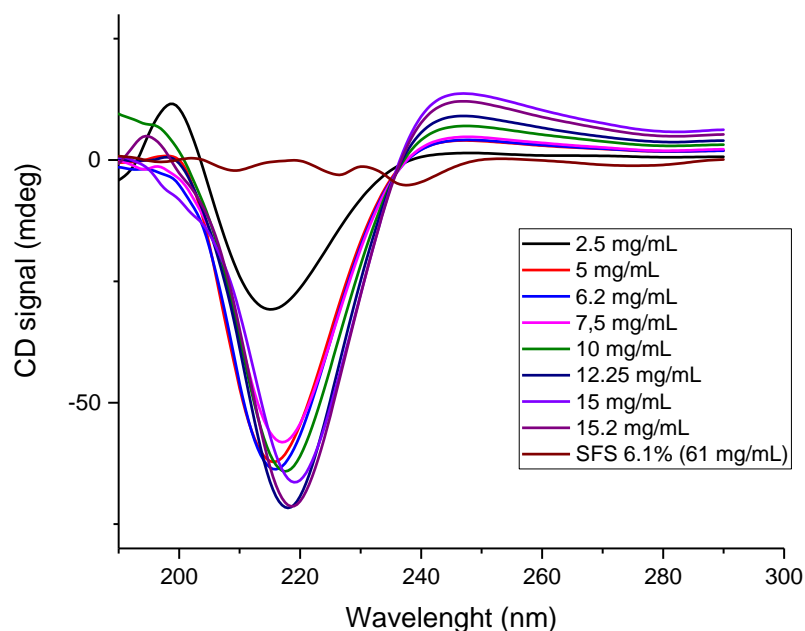
singlet electronic excited states to an allowable vibrational level in the electronic ground state emitting a photon (BALA MURALI KRISHNA *et al.*, 2012; LE *et al.*, 2013; SO; DONG, 2002).

### **5.7. Circular Dichroism**

Circular dichroism is a powerful tool to identify and study the secondary structure of proteins and how these are affected in different conditions. Figure 40 shows the CD spectra of Fibroin solutions at different concentration and Fibroin solution at 6,1% w/v (61 mg/mL). All the hydrogel samples presented a minimum around 220 nm and the intensity of the signal increased as the amount of fibroin in the hydrogels increase. When the silk fibroin form hydrogels it presents an ordered conformation of  $\beta$ -sheets that aggregates to form the hydrogel due to the tendency of the protein to return to the most stable conformation and form fibers.

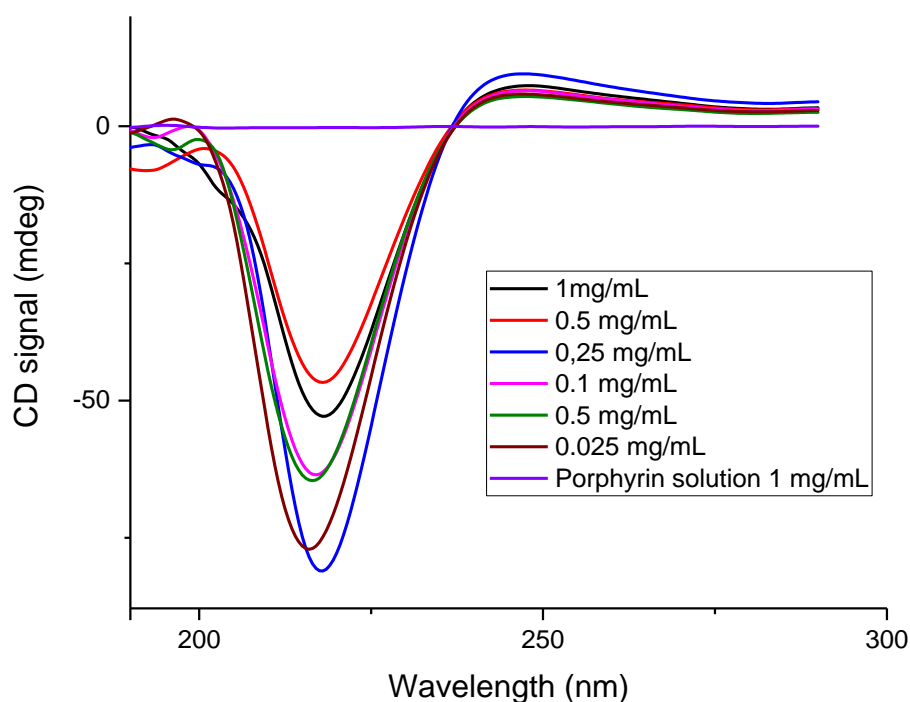
In all the hydrogel samples, we can observe the negative Cotton effect corresponding to  $\beta$ -sheets, indicated by a minimum around 220 nm: this confirms that the formation of fibroin in an ethanol solution with SFS250 ratio is due to the destabilizing effect of the Ethanol over the hydrophobic interactions and promotes the aggregation of the protein molecules and forms a more stable  $\beta$ - sheet structure (YANG *et al.*, 2004).

**Figure 45.** CD spectra for Fibroin hydrogels at different concentrations and Fibroin solution 6.1% m/v (61 mg/mL), recorded at 25 °C with a 10-s accumulation time at the rate of 200 nm/min.



In Figure 45 we can observe that there is not a significant change in the CD spectra of the Fibroin Hydrogel (7.5 mg/ml) after add different concentration of Porphyrin to the matrix. The negative Cotton effect can be observed with the characteristic  $\beta$ - sheet signal around 220 nm. With this data, we can confirm that the secondary structure responsible in the formation of the silk fibroin hydrogels is the  $\beta$  – sheet.

**Figure 46.** CD spectra for Fibroin- Porphyrin hydrogels in different concentrations and 1mg/mL of porphyrin solution as a control recorded at 25 °C with a 10-s accumulation time at the rate of 200 nm/min.



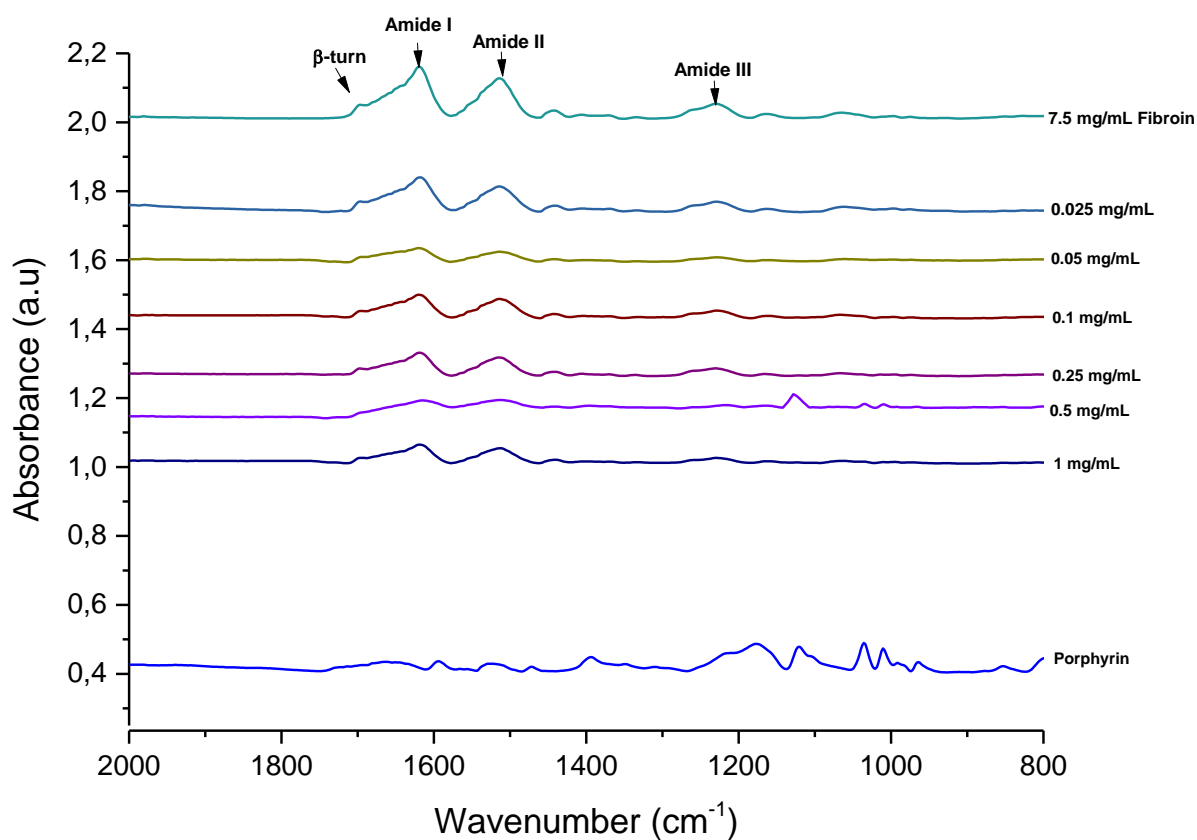
## 5.8. FTIR analysis

FTIR analysis shows that the molecular conformation of *B. mori* silk fibroin is characterized by  $\beta$ -sheet secondary structure. The typical absorption peaks of  $\beta$ -sheet are around 1630, 1530 and 1240  $\text{cm}^{-1}$ , and random coil conformation absorption peaks at 1650 or 1645, 1550 and 1230  $\text{cm}^{-1}$ , and an  $\alpha$ -helix absorption peak around 1655  $\text{cm}^{-1}$ . FTIR spectra of the regenerated silk fibroins showed intense absorption peaks around 1620  $\text{cm}^{-1}$  (shoulder peaks), 1514  $\text{cm}^{-1}$ , and 1230  $\text{cm}^{-1}$ , which are the characteristic absorption peaks of  $\beta$ -sheet. There is also a peak around 1700  $\text{cm}^{-1}$  close to the amide I

absorbance, which was associated with a  $\beta$ -turn or intermediate  $\beta$ -sheet structure (SWINERD et al., 2007).

The obtained absorption peaks correspond to the ones previously reported by Hang *et al.* (2012). The characteristic vibration bands around  $1620\text{ cm}^{-1}$  correspond to the absorption peak of the peptide backbone of amide I (C=O stretching), bands around  $1513\text{ cm}^{-1}$  to amide II (N-H bending), the bands around  $1230$  and  $1444\text{ cm}^{-1}$  to amide III (C-N stretching). All these characteristic signals indicate the existence of a hydrogen-bonded NH group. The presence of amide III (C–N stretching) peaks at  $1233\text{ cm}^{-1}$  indicates that the reconstituted silk matrix contained a mixture of disordered  $\alpha$ -helical and crystalline  $\beta$ -sheet domains (SWINERD et al., 2007).

**Figure 47.** FTIR spectrum of fibroin films with different porphyrin concentrations (0.025, 0.05, 0.1, 0.25, 0.5 and 1mg/mL). It is potable to observe the typical absorption peaks of the amide I,II and III.



## 5.9. Scanning electron microscopy

All different kinds of silk fibroin and SF-Porphyrin hydrogels did not show any marked difference in their structure. All the samples showed a very similar and homogenous structure. We did not find any difference between the morphology of fibroin hydrogels in different concentrations and fibroin hydrogels with different concentrations of porphyrin. It has been previously reported that four major classes, including particles, grains, nanofibrils, and an irregular morphology, exist in fibroin films (LV et al., 2004)

**Figure 48.** SEM Images of dry films form from Silk Fibroin hydrogels with different concentrations of fibroin at 1  $\mu\text{m}$  : a) 7.5 mg/mL, b) 12.25 mg/mL and c) 15.2 mg/mL.

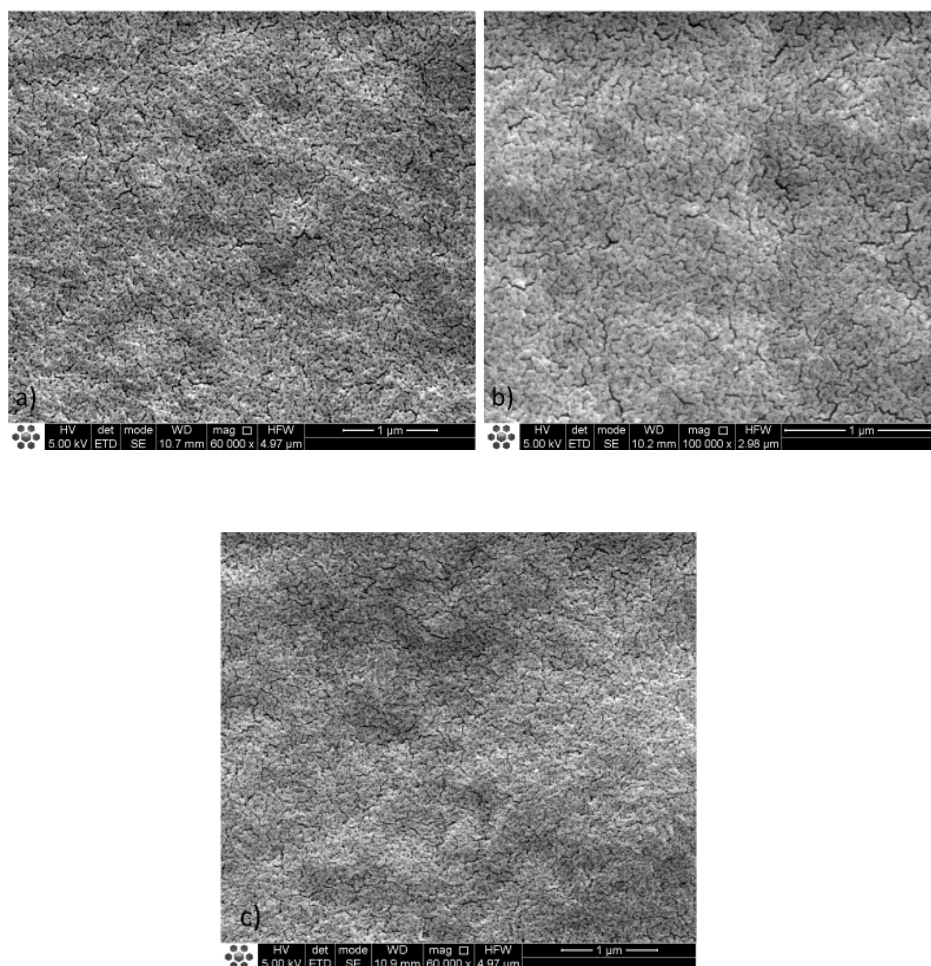
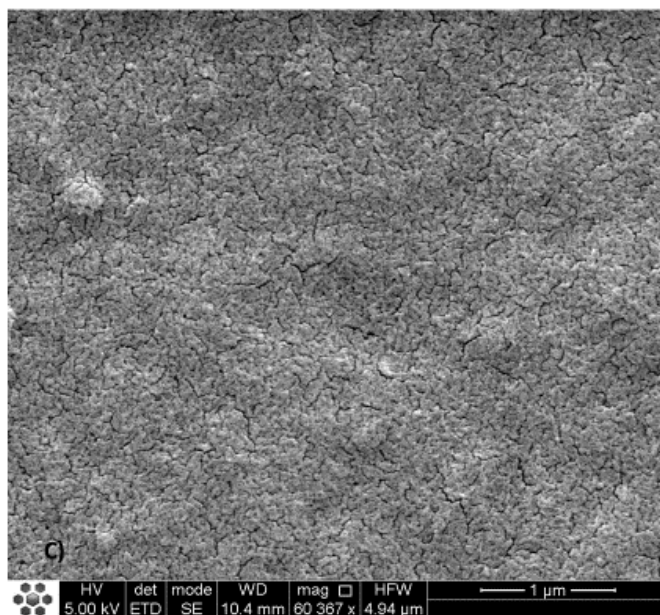
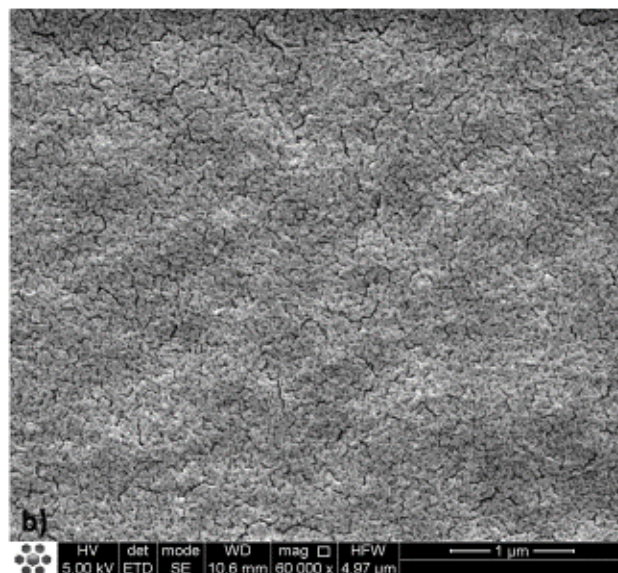
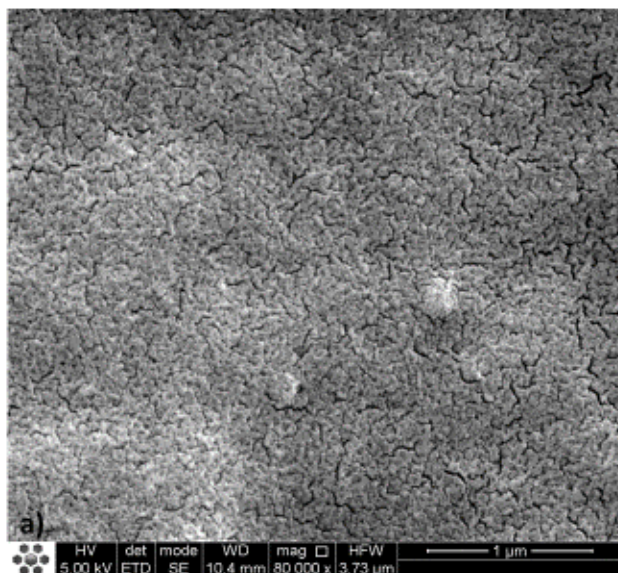


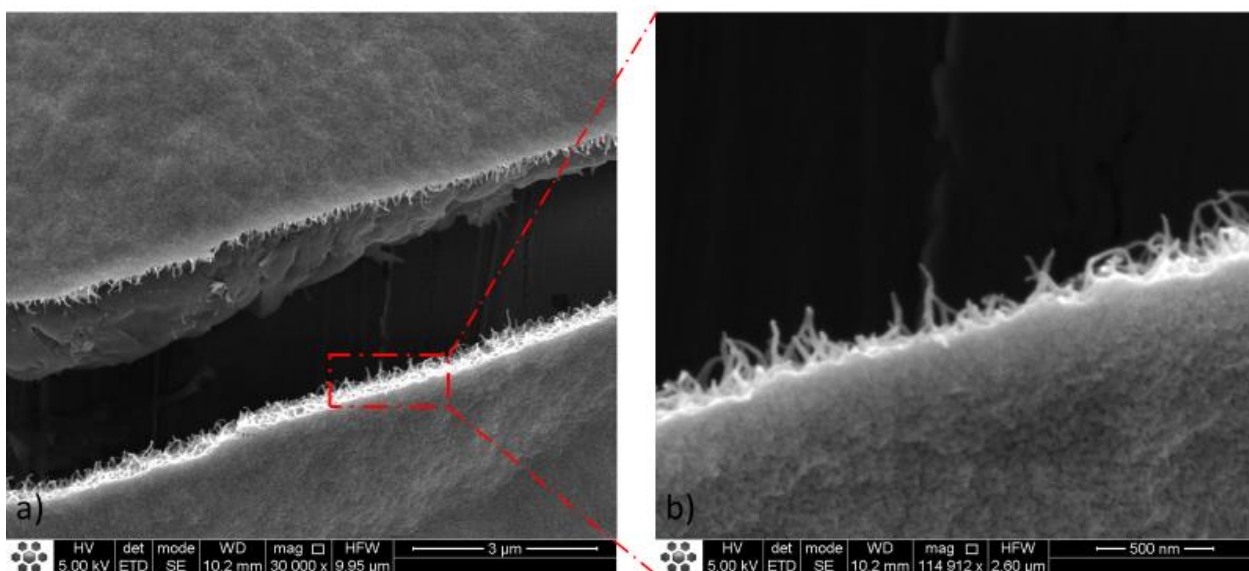


**Figure 49.** SEM Images of dry films form from silk fibroin hydrogels with different concentrations of porphyrins at 1  $\mu\text{m}$  : a) 1 mg/mL , b) 0.1mg/mL and c) 0.025 mg/mL.



The results of the SEM analysis showed the presence of interconnected fibers that form the structure of the Fibroin film and hydrogels (Figure 50). The diameter of the fibers was around 37 to 40 nm.

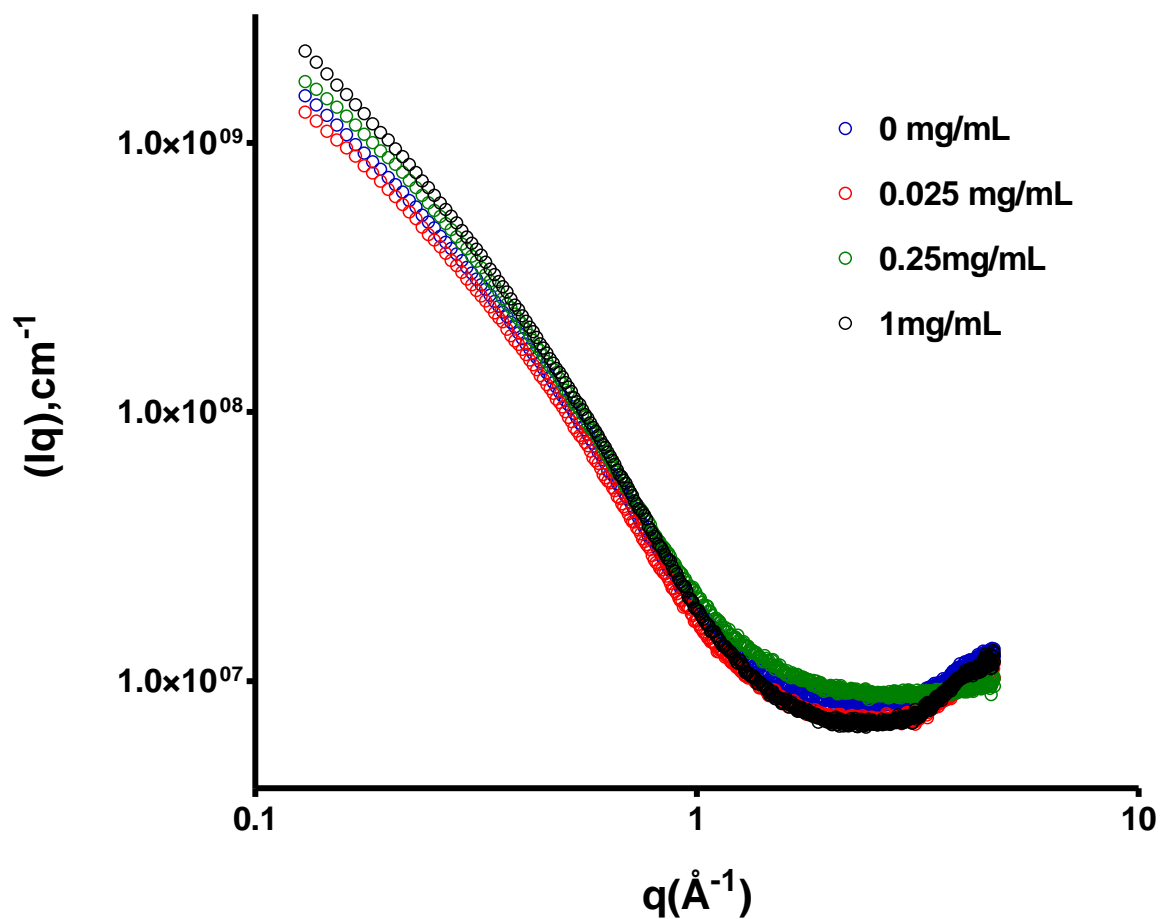
**Figure 50.** SEM cross section Images of dry films form from 7.5 mg/mL of Silk Fibroin.



### 5.10. SAXS (Small-angle X-ray scattering)

SAXS was used to further study the structural variation of fibroin/porphyrin hydrogels complexes (Figure 51).

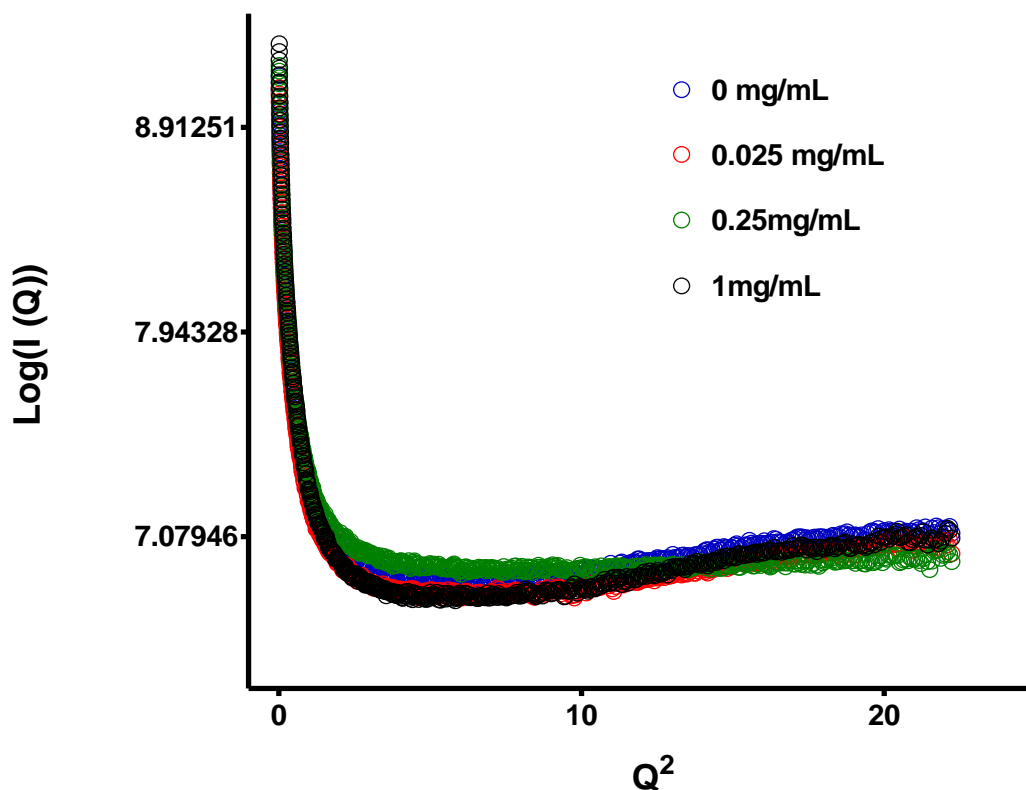
**Figure 51.** Scattering curve (log-log scale) of the concentration effect of porphyrin concentration in fibroin hydrogels. . 0 mg/mL (only fibroin 7mg/mL), 0.025 mg/mL, 0.25 mg/mL and 1mg/mL of porphyrin.





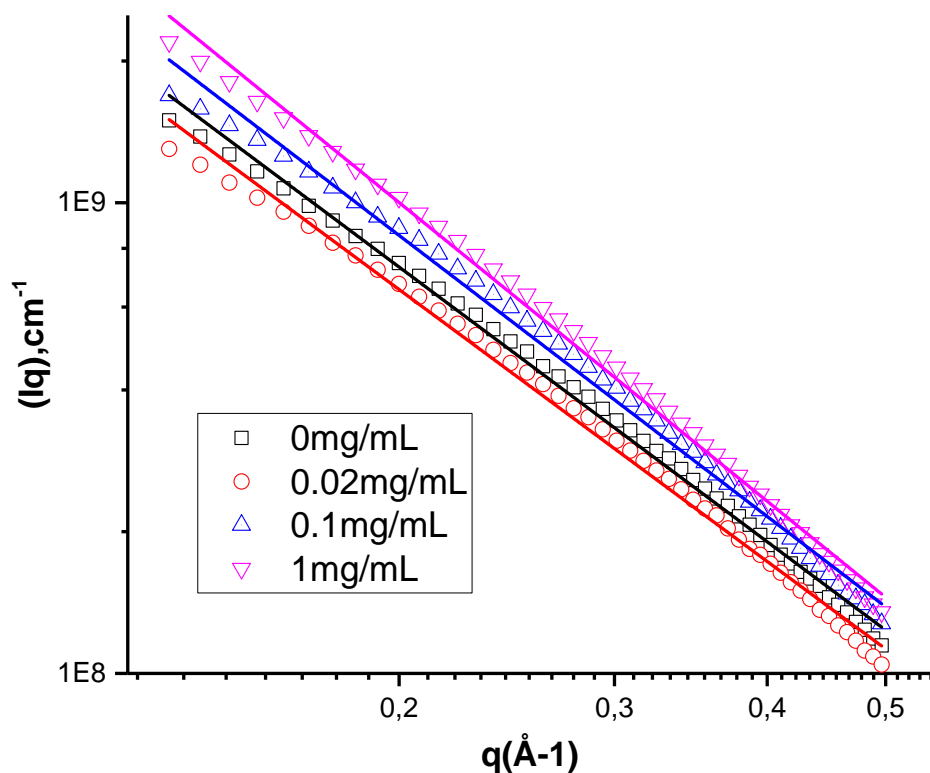
For monodispersed systems, where the particles are randomly distributed with uncorrelated positions and orientations,  $I(Q)$  can be related to the molecular weight and radius of gyration of the molecule by the Guinier equation. The Guinier plot exhibits a linear region for monodisperse systems. In contrast if the region of Guinier is not linear, this means that the material is formed by a polydisperse system of fibroin, in which the molecules have different sizes. This behavior of the curve also means that possible aggregation of the particles occurs

**Figure 52.** Guinier plot of the concentration effect of porphyrin concentration in fibroin hydrogels. 0 mg/mL (only fibroin 7mg/mL), 0.025 mg/mL, 0.25 mg/mL and 1mg/mL of porphyrin.



For a better understanding of the SAXS data we performed a fit of the curve using the low  $q$  data region and from the slope we calculated the Fractal Dimension ( $D$ ) to study any possible change in the structure of the hydrogel caused by the addition of porphyrin.

**Figure 53.** SAXS study of the concentration effect of porphyrin on fibroin hydrogel. SAXS curve linear fit performed on the lowest  $q$  region of the SAXS curves at 25°C. 0 mg/mL (only fibroin 7mg/mL), 0.025 mg/mL, 0.25 mg/mL and 1mg/mL of porphyrin.



Systems with structures that look similar over a range of length scales may be described as fractals and their behavior is reflected in their small-angle scattering curves, which may be described via a power law (REKAS et al., [s.d.]). The  $D$  values (fractals

dimensions) obtained from the slope of the low  $q$  data are summarized in Figure 54. We used the  $D$  values as a semi quantitative measure of the structural change of hydrogels with different concentrations of fibroin. We can observe that at higher  $D$  the  $G'$  increase too, this means that changes in the concentration of the porphyrin in the hydrogel means also a change in viscosity of the material.  $D$  values between one and two correspond to the ones presented by one-dimensional structures, such as fibers, and a two-dimensional structure, such as a membrane. In other words, a fractional dimensionality between 1 and 2 is consistent with a mesh of interwoven fibers as we can confirm in the scanning electron microscopy images. The  $D$  value for the porphyrin concentration is closer to the  $D$  value of the hydrogel with of porphyrin this mean that the concentration added to the hydrogel is not enough to cause any visible change in the structure like form crosslinking within the structure.

**Figure 54.** SAXS study of the concentration effect of Porphyrin concentration in fibroin hydrogels. Change of Fractals Dimensions.

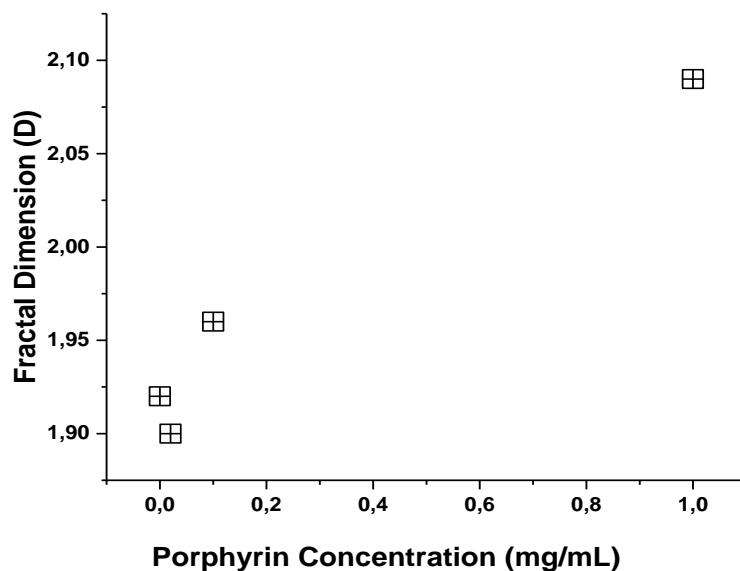
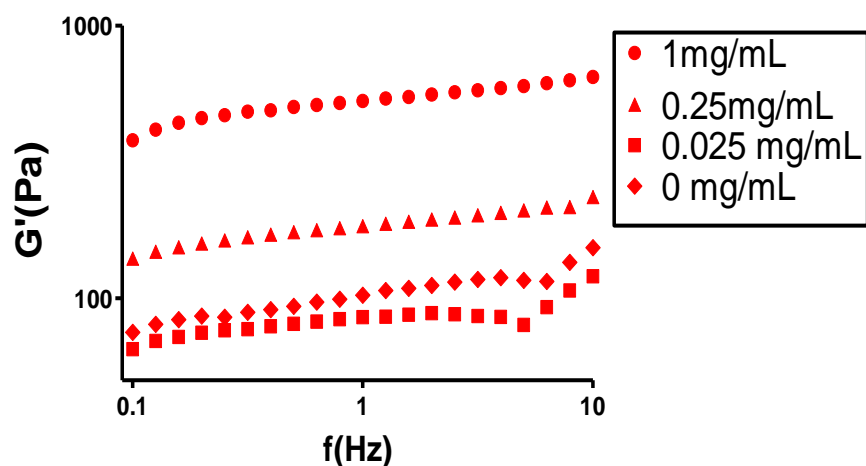


**Figure 55.** Fibroin – porphyrin hydrogel frequency sweep analysis with different concentration of porphyrin, storage modulus ( $G'$ ) plot against frequency.



We used the  $n$  (viscoelastic exponent) and  $S$  (gel strength) values for a better quantitative estimation of strength of hydrogel structures that can be related with the crosslinking density within the polymer network. In this sense, higher  $S$  and  $G'$  indicate an increase of the crosslinking density, which is related to stronger gel structures. This can be observed in the frequency sweep curve, with the increase of the porphyrin concentration in the fibroin hydrogel the storage modulus also increase resulting in a higher value of  $s$ , low values of  $n$  indicate a purely elastic gel behavior.

**Table 9.** Fractal dimension,  $G'$  value and gel strength ( $S$ ) and viscoelastic exponent ( $n$ ) of fibroin hydrogels (7.5 mg/mL) with various concentration of porphyrin: 1mg/mL, 0.1 mg/mL and 0.025 mg/mL.

Porphyrin mg/mL	Fractal Dimensions	$G'$ (Pa)	$S$ (Pa)	$n$
0	1.92	$86.01 \pm 11.50$	$66.05 \pm 6.11$	$0.234 \pm 0.025$
0,025	1.90	$85.30 \pm 2.54$	$54,20 \pm 6.66$	$0.233 \pm 0.033$
0,25	1.96	$184.16 \pm 11.58$	$141,59 \pm 6.55$	$0.146 \pm 0.013$
1	2.09	$529.50 \pm 70.71$	$434,21 \pm 5.73$	$0.104 \pm 0.004$

This increase of the crosslinking of the hydrogels is related by the addition of porphyrin to the fibroin hydrogel matrix. Adding cross-links between polymer chains affects the physical properties of the polymer depending upon the degree of cross linking and presence and absence of crystallinity (MAITRA; SHUKLA, 2014). It has been reported that when proteins are irradiated with UV or visible light in the presence of a sensitizer, both photooxidation of sensitive amino acid residues such as cysteine, histidine, tyrosine, methionine and tryptophan and covalent cross-linking of peptide chains can be observed, leading to the formation of molecular aggregates (AFONSO; ENRIQUEZ DE SALAMANCA; DEL, 1999; AKHTAR, 2016). This cross linking occurs as a secondary reaction between photooxidation products of susceptible amino acid residues and other groups in the protein, the oxygen singlet form by the porphyrin by a type II reaction interacts with triplet oxygen ( $^3\text{O}_2$ ) resulting in a highly reactive oxygen species that interacts with the protein. Silk Fibroin hydrogels due to the high content of tyrosines (~5%) in the protein are capable to form dityrosine Cross-linking hydrogels by the effect of photo-chemical crosslinking (PARTLOW et al., 2016). Applegate *et al.* demonstrated that it is possible to form transparent, elastic, silk fibroin hydrogels in which excited riboflavin form tyrosine residues radicals in the silk protein backbone, resulting in the formation of dityrosine complexes binding silk molecules together (APPLEGATE et al., 2016).

#### **5.11. Generation of Reactive Oxygen Species (ROS)**

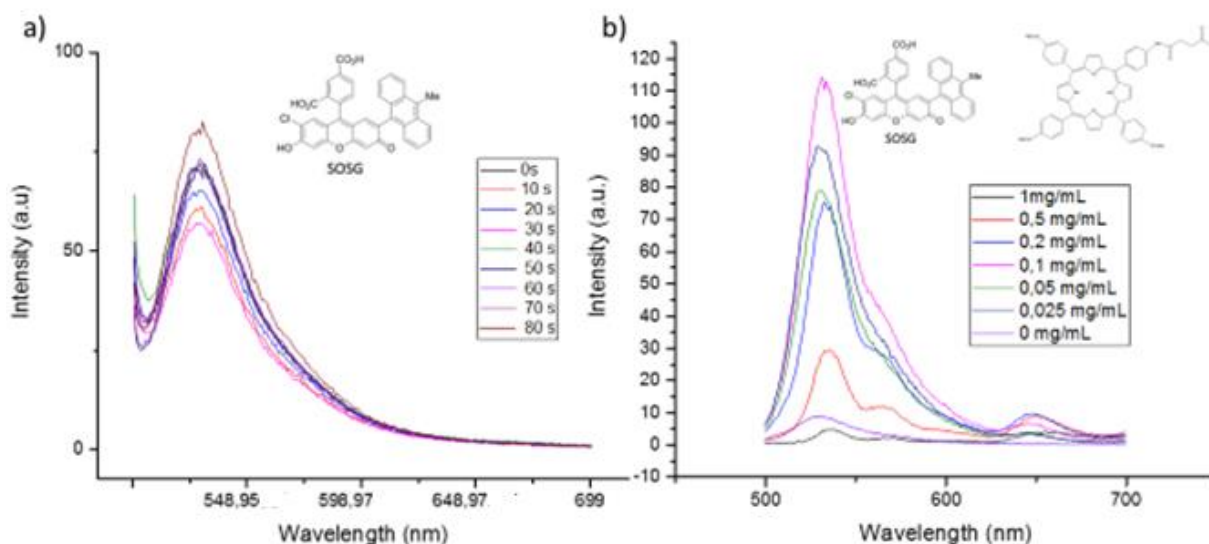
For the detection of the generation of Reactive Oxygen Species (ROS) by the porphyrin inside the hydrogel matrix we used the SOSG (Singlet Oxygen Sensor Green Reagent) as a probe for ROS. SOSG is a dye composed of fluorescein and anthracene moieties. Unlike other fluorescent and chemiluminescent singlet oxygen detection reagents, the Singlet Oxygen Sensor Green reagent is highly selective for singlet oxygen ( $^1\text{O}_2$ ); it show no appreciable response to other reactive oxygen species, including hydroxyl radical ( $\text{HO}\cdot$ ), superoxide ( $\cdot\text{O}_2^-$ ) and nitric oxide (NO) (KIM; FUJITSUKA; MAJIMA, 2013). Before reaction with singlet oxygen, this probe initially exhibits weak blue fluorescence with excitation peaks at 372 and 393 nm and emission peaks at 395 and 416

nm. In the presence of singlet oxygen, however, it emits a green fluorescence similar to that of fluorescein (excitation/emission maxima ~504/525 nm).

In the figure 55 a) we can observe that there is no significant increment in the intensity of SOSG absorption that after the exposure of the fibroin to red light. The intensity corresponds to a weak blue fluorescence around 416 nm, indicating that in the absence of porphyrin the reaction of the probe with singlet oxygen is negligible. This shows that the fibroin hydrogels without the addition of the photosensitizer does not generate singlet oxygen.

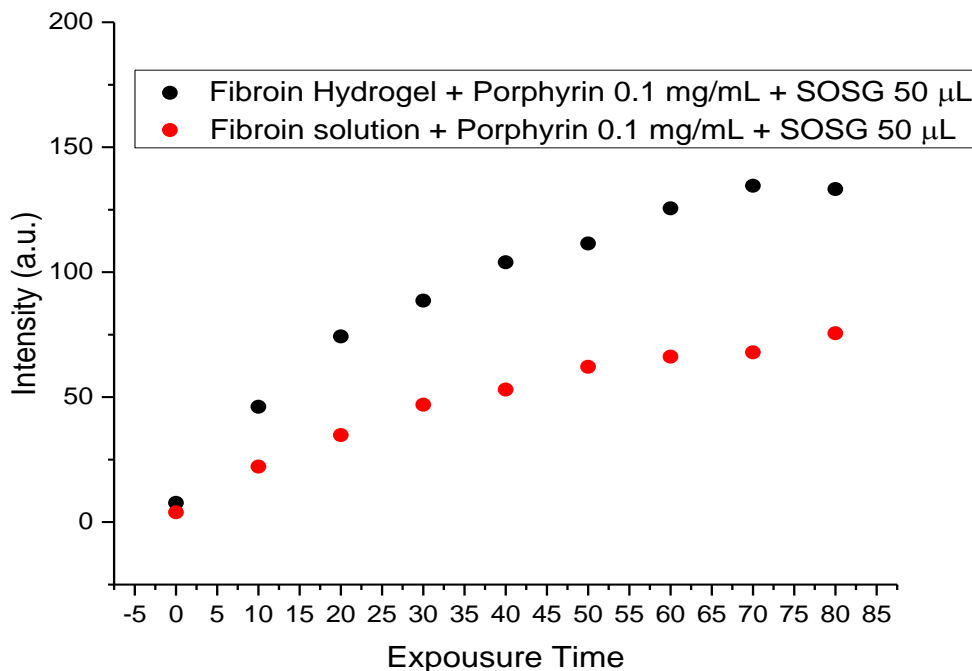
On the other hand, in the figure 55 b) we can notice that after addition of porphyrin to the hydrogels the fluorescence spectrum of the probe shifts from a weak blue fluorescence to a green fluorescence around 525 nm. This shift occurs due the presence of singlet oxygen in the material, generated by the porphyrin following irradiation with red light and activation from a “ground state” to an “excited state”. As it returns to the ground state, the released energy can be transferred to oxygen to form the ground singlet state PS and the excited state  $^1\text{O}_2$ , which then oxidizes various substrates (type II PDT reaction). Is possible to say that the type of reaction generated with this porphyrin inside the matrix is the type II (energy transfer), because the SOSG is specific to detect singlet oxygen and this ROS is generated during the type II reaction. We can also observe an influence of the porphyrin concentration on the fluorescence intensity of SOSG: this could be an indirect measure of the amount of singlet oxygen generated by the effect of the porphyrin. Notably, at higher concentrations of the porphyrins the intensity of the SOSG decreases, which could be due a quenching effect produced by the high amount of porphyrin in the hydrogel. The light is dispersed by the porphyrin in the outer layers of the hydrogel as was observed in the previous test (figure 21). The hydrogel with 0.1 mg/mL fibroin presented the most intense fluorescence because the amount of porphyrin in the hydrogels is not enough to disperse the light, and irradiation causes the excitation of all the porphyrin in the hydrogel which results in a higher generation of singlet oxygen.

**Figure 56.** Fluorescence spectrum of the hydrogels with SOSG for singlet oxygen detection a) Generation of reactive Oxygen species in a 7.2 mg/mL fibroin hydrogel with different times of exposure, b) Generation of reactive Oxygen species in a 7.2 mg/mL fibroin hydrogel (0 mg/mL porphyrin) with different concentrations of porphyrin 1mg/mL, 0.5mg/mL, 0.2mg/mL, 0.1 mg/mL, 0.05 mg/mL, 0.025 mg/mL and a blank with only fibroin, after a 80 exposure to red light. With 50  $\mu$ L of SOSG in each test.



In figure 56 we can observe a difference between the intensity of the porphyrin solutions and the hydrogels with porphyrin. With the addition of fibroin to the solutions to form hydrogel we can observe that the intensities of the samples with 0.1 mg/mL are higher than the intensities of the solutions after being exposed to red light from 0 to 80 seconds. This increment in the singlet oxygen species generation could be due to a lack of aggregation of the porphyrin within the hydrogel structure. Porphyrins often suffer from aggregation caused quenching (ACQ) which limits their maximal imaging ability. In solution porphyrins tend to form  $\pi$ - $\pi$  stacking aggregates via driving forces such as hydrogen bonding, van der Waals interactions, electrostatic interactions and hydrophobic effects, leading to fluorescence quenching (ANDRADE; COSTA, 2006; GUO et al., 2016). One of the approaches used to avoid this quenching is to fix the porphyrins in 3-D networks like silica, metal organic frameworks and as like we proved in this work in hydrogels matrix (MAKARSKA-BIALOKOZ, 2012; ZENKEVICH et al., 2006).

**Figure 57.** Kinetic curve of Fibroin /Porphyrin hydrogel (●) and porphyrin solution (●) after being expose to red light from 0s to 80s.

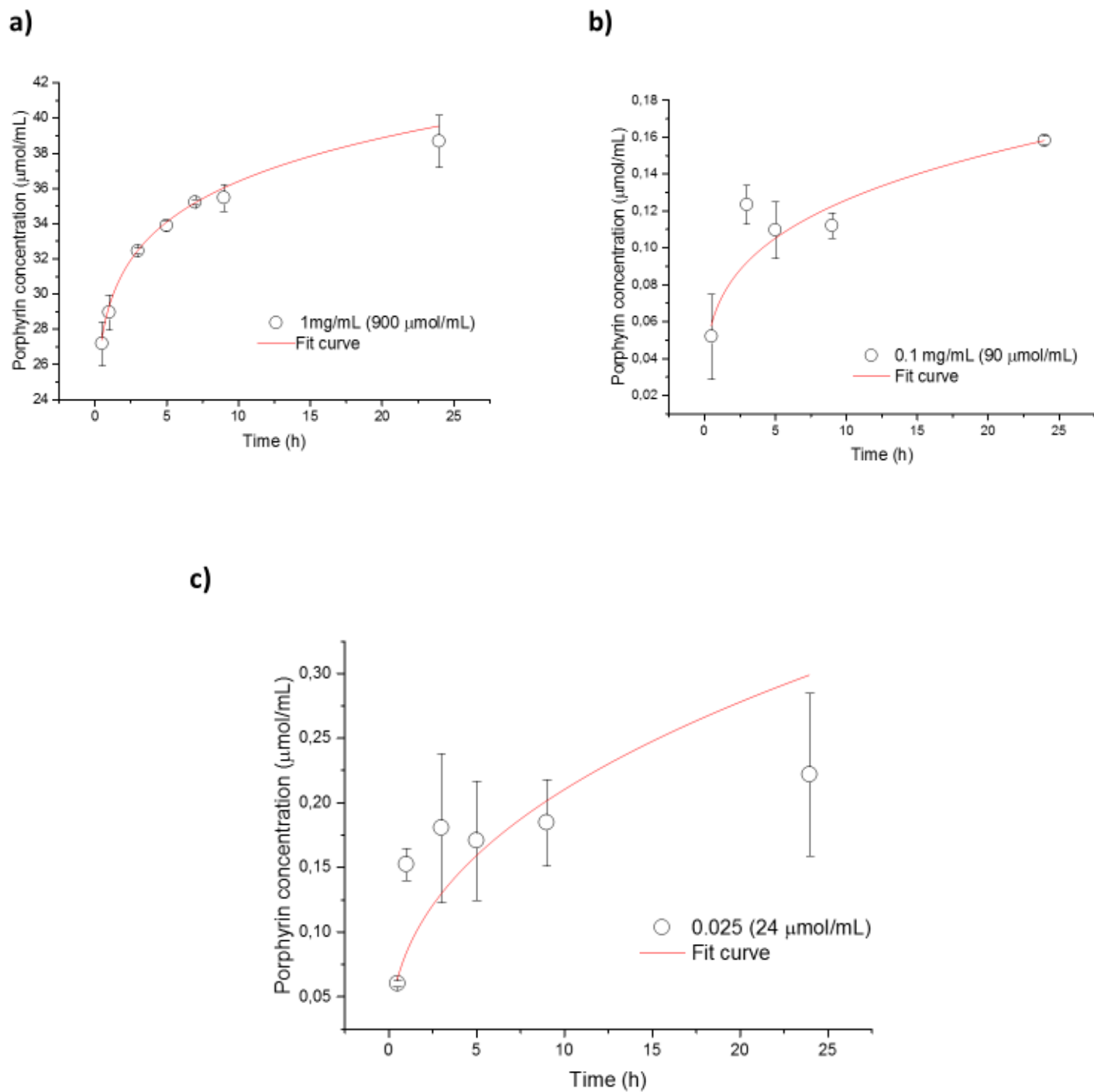


### 5.12. In vitro Porphyrin release studies

Data of the drug release evaluation are shown in figure 57, we can observe that at higher concentration of porphyrin in the fibroin hydrogel more porphyrin is released to the solution. The amount of porphyrin liberated is independent from the initial concentration loaded in the hydrogel, the release time does not present difference between samples. In all the samples, then the porphyrin is freed from the hydrogel after 30 min. The Fibroin hydrogel with 1mg/mL of porphyrin presents a regular release profile than the hydrogels with lower concentrations of porphyrins, this could be due a thermal or photodegradation of the porphyrin in the medium.



**Figure 58.** Porphyrin release curves from a fibroin hydrogel matrix containing a) 1mg/mL, b) 0.1 mg/mL and c) 0.025 mg/mL of porphyrin, obtained by Uv-vis spectrometry.



The obtained experimental data was fitted into the Ritger-Peppas equation. A Fickian diffusion of first-order is observed when  $n$  has the limiting value of 0.5; when  $n = 1$ , case II transport (polymer relaxation/degradation) occurs leading to zero-order release (DOS SANTOS et al., 2015). When  $n$  lies between 0.5 and 1 anomalous transport is observed, this means that the anomalous transport occurs where the polymer relaxation as well as Fickian diffusion control the drug release, and the drug release rate is time-dependent. In our case, all the  $n$  values for all the fibroin concentrations were lower than 0.5 meaning that the diffusion follows an abnormal transport (Table 10).

Sample	$n$	$R^2$
1mg/mL(900 $\mu$ mol/mL)	0,09153	0,99
0.1 mg/mL (90 $\mu$ mol/mL)	0,261	0,85
0.02 mg/mL (24 $\mu$ mol /mL)	0,4	0,46

**Table 10.** Porphyrin release kinetic data obtained from fitting experimental release data to Ritger-Peppas equation where “ $n$ ” is the diffusion exponent and  $R^2$  is the correlation coefficient.

### 5.13. Permeability studies

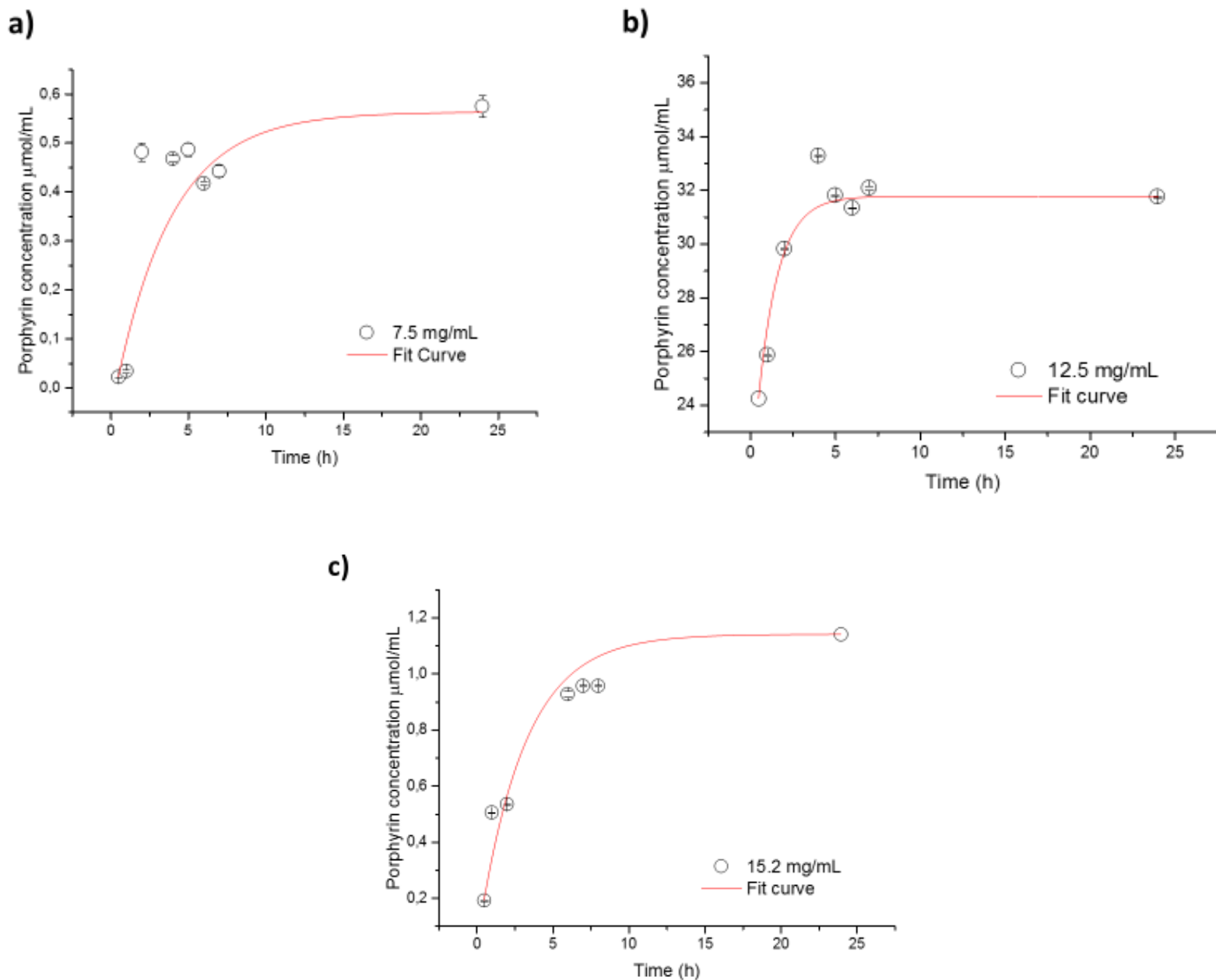
For the in vitro permeability studies, we used a Franz’s cell chamber. The Franz Cell chamber is an in vitro skin permeation assay frequently used in formulation development. The Franz Cell apparatus consists of two primary chambers separated by a membrane. Although animal skin can be used as the membrane, human skin is preferred. The test product is applied to the membrane via the top chamber. The bottom chamber contains fluid from which samples are taken at regular intervals for analysis. This testing determines the amount of active that has permeated the membrane at each time point. The chamber is maintained at a constant temperature of 37° C.

Data of the drug release evaluation in  $\mu\text{mol/mL}$  are shown in figure 58, we can observe that in all the cases the porphyrin was capable to pass through the synthetic membrane. The Strat-M® membrane is a non-animal based model for transdermal diffusion testing that is predictive of diffusion in human skin without lot-to-lot variability. This mean that the porphyrin used in this test is compatible with the human skin therefore is capable to permeate through the outer skin layers. This compatibility allows the hydrogel to release the drug continuously and the porphyrin permeability through the skin allows a greater effect and efficiency during a photodynamic therapy. The irregular variation of the porphyrin concentration in the receptor chamber could be due to an increase in the crosslinking of the hydrogel and this could cause a decrease in the amount of porphyrin capable to be released from the hydrogel.

The liberation of the porphyrin not only depend from the fibroin concentration, it is also dependent on the changes in the hydrogel that modify the crosslinking of the matrix this result in irregular release profiles. These changes in the hydrogel crosslinking could be provoked by the rise in the crosslinking caused by the singlet oxygen species generated by the matrix and the evaporation of the ethanol used to prepared the hydrogels. Previous studies have shown that concentrations of  $2 \pm 1 \mu\text{M}$  ( $0.002 \mu\text{mol/mL}$ ) and  $5 \pm 1 \mu\text{M}$  ( $0.005 \mu\text{mol/mL}$ ) for TMPyP (Tetra(N-methyl-4-pyridyl)porphyrin chloride) and TPPS4 (tetra(4-sulfonatophenyl)porphyrin-Na salt) inhibit biological process in tumorigenic line cells (TITA; PERUSSI, 2001),also Lamer *et al.* (2015) found that concentrations around  $9\mu\text{M}$  ( $0.009 \mu\text{mol/mL}$ ) of gold(III)porphyrin complex shows promising anticancer activity, they report a  $\text{IC}_{50}$  of 9 mM for the A2780 human ovarian cancer cell line. For the inactivation of Gram (-) and Gram (+) microorganisms Gyulkhandanyan *et al.* (2009) report that concentration  $0.14 \pm 0.01 \mu\text{g/mL}$  of St. aureus cause the 50% of the inhibition of biological process in  $\text{IC}_{50}$  and a concentration of  $0.75 \pm 0.05 \mu\text{g/mL}$  cause the 100% of the inhibition of the biological process. In the Figure 58 we can observe that the concentration of porphyrin in the receptor compartment were from  $0.02 \mu\text{mol/mL}$  ( $20 \mu\text{g/mL}$ ) to  $34 \mu\text{mol/mL}$  ( $35000 \mu\text{g/mL}$ ). If we compare our permeation results with the previously reported in the literature, we can confirm that the used porphyrin in these studies is capable to pass through the human skin at a sufficient concentration to

cause an effect in the growth of cancer cells and be used in photodynamic therapy. It also may be used to inhibit microorganisms by photodynamic inactivation.

**Figure 59.** Porphyrin permeation across a skin alike membrane, after 24 h, with different concentrations of fibroin a) 7.5 mg/mL, b) 12.5 mg/mL and c) 15.2 mg/mL. All the hydrogels contain 1 mg/mL (0.09 mmol/mL) of porphyrin.



## 6. Conclusions

*Bombyx mori* (silkworm) silk is a unique material that has gained attention as a biomaterial because of several desirable properties like biocompatibility, its slow rate of degradation in vivo and its ability to be processed into multiple material formats from either aqueous solution or an organic solvent. These properties make it an excellent candidate to form hydrogels for different applications. The successful generation of SF materials depended on the in vivo and in vitro processing conditions that can greatly influence the structural organization and packing of the molecules.

In this study, we were capable of forming translucent hydrogels from raw silk fibers and used them as matrix to incorporate porphyrin for future application in PDT. The hydrogels obtained were characterized by rheology and spectrophotometry to identify the factors involved in the formation of the hydrogel and to have a better notion of the behavior of the SF after adding a fluorescence molecule to the hydrogel. All the concentrations of porphyrins used except the one with 2.5 mg/mL of fibroin were capable to form hydrogels. The hydrogel behavior was confirmed by oscillatory analysis where the values of  $G'$  were higher than the  $G''$ , this modulus in the case of the fibroin hydrogel are dependent of the concentration of the hydrogel at higher concentration higher  $G'$  and  $G''$  values were obtained, this means that it is possible to obtain stronger SF hydrogels increasing the concentration of the protein. The set of obtained results shows that the silk fibroin hydrogels have a shear thinning behavior (the viscosity of the Gel decreases with the increase of the shear rate) and can be classified as a thixotropic materials, the structure of the material needs time to recover after experience shear deformation. This thixotropy behavior is desirable for material for topical applications like the hydrogel prepared in this work.

The secondary structure of the Fibroin is not affected by the addition of porphyrin in any concentration and the  $\beta$ -sheet secondary structure prevails, this was confirmed by the negative Cotton signal around 220nm in the Circular Dichroism analysis. Silk Fibroin hydrogels are an excellent matrix to encapsulate other molecules to be applied in different areas for example photodynamic therapy. After being incorporated to the hydrogel

the porphyrin is still capable to generate singlet oxygen. From the permeability and release studies we conclude that the fibroin hydrogel can be used as matrix to form hydrogels for PDT that allow the generation of ROS and the permeability and release of the compound through the skin in effective amounts. After compare the obtained results with reported in other studies is possible to affirm that the used amount porphyrin that pass through the skin is enough to produce inactivity in microorganism and to provoke cell death in cancer tissues. To confirm this observation is necessary to compare the results obtained with other porphyrins incorporated in a fibroin hydrogel.

The set of results showed that the obtained translucent fibroin hydrogels have great potential to be applied in photodynamic therapy with the objective of causing the death of cancerous tissue and the inactivation of microorganisms, due to its ability to allow the generation of oxygen free radicals and the release and permeability of the porphyrin through the skin. Thought more *invitro* and *in vivo* studies are needed to achieve a better understanding of the process involved.

## 7. References

- AFONSO, S. C.; ENRIQUEZ DE SALAMANCA, R.; DEL, A. M. The photodynamic and non-photodynamic actions of porphyrins. **Brazilian Journal of Medical and Biological Research**, v. 32, n. 3, p. 255–266, 1999.
- AGOSTINIS, P. et al. Photodynamic Therapy of cancer: an update. **CA Cancer J Clin.**, v. 61, n. 4, p. 250–281, 2011.
- AJISAWA, A. STUDIES ON THE DISSOLUTION OF SILK FIBROIN. (1) STUDIES ON THE DISSOLUTION OF SILK FIBROIN BY  $\text{CaCl}_2$ -1120-R- (OH)  $n$ , TERNARY SYSTEM SOLUTIONS. By Akiyoshi Ajisawa (Omiya Research Laboratory, Katakura Industry Co. Ltd., Omiya City, Saitama Prefecture, Japan. **SEN-I GAKKAISHI**, v. 24, 1968.
- AKHTAR, M. F. Methods of Synthesis of Hydrogels. **Saudi Pharmaceutical Journal**, p. 554–559, 2016.
- ALLISON, R. R.; MOGHISSI, K. Photodynamic Therapy (PDT): PDT Mechanisms. p. 24–29, 2013.
- ALTMAN, G. H. et al. Silk-based biomaterials. **Biomaterials**, v. 24, n. 3, p. 401–416, fev. 2003.
- ANDRADE, S. M.; COSTA, S. M. B. Spectroscopic studies of water-soluble porphyrins with protein encapsulated in bis(2-ethylhexyl)sulfosuccinate (AOT) reverse micelles: Aggregation versus complexation. **Chemistry - A European Journal**, v. 12, n. 4, p. 1046–1057, 2006.
- APPLEGATE, M. B. et al. Photocrosslinking of Silk Fibroin Using Riboflavin for Ocular Prostheses. p. 2417–2420, 2016.
- ARAKAWA, T.; TIMASHEFF, S. N. Mechanism of Protein Salting In and Salting Out by Divalent Cation Salts: Balance between Hydration and Salt Binding? **59 Biochemistry**, v. 12, n. 59, p. 12–5923, 1984.
- ASAKURA, T.; NAKAZAWA, Y. Structural Analysis of Silk Fibroins using NMR. **Modern Magnetic Resonance**, 2008.
- ASAKURA, T.; OKUSHITA, K.; WILLIAMSON, M. P. Analysis of the structure of Bombyx mori silk fibroin by NMR. **Macromolecules**, v. 48, n. 8, p. 2345–2357, 2015.
- BAILEY, K. **Potential Applications of Silk Fibroin as a Biomaterial**. [s.l: s.n.].
- BALA MURALI KRISHNA, M. et al. Synthesis and structural, spectroscopic and nonlinear optical measurements of graphene oxide and its composites with metal and metal free porphyrins. **Journal of Materials Chemistry**, v. 22, n. 7, p. 3059, 2012.
- BALDEA, I. et al. Journal of Photochemistry and Photobiology B: Biology Efficiency of photodynamic therapy on WM35 melanoma with synthetic porphyrins: Role of chemical structure, intracellular targeting and antioxidant defense. **JOURNAL OF PHOTOCHEMISTRY & PHOTOBIOLOGY, B: BIOLOGY**, v. 151, p. 142–152, 2015.

BEXIGA, N. M. **Preparo e avaliação comparativa das propriedades físico- químicas de hidrogéis de fibroína de seda com conteúdo variado de sericina obtidos a partir dos cloretos de cálcio e lítio em sistemas distintos de solventes.** [s.l.] Universidade de São Paulo, 2014.

BIESAGA, M.; PYRZYNSKA, K.; TROJANOWICZ, M. Porphyrins in analytical chemistry. A review. **Talanta**, v. 51, n. 2, p. 209–224, 2000.

BOISLY, M. et al. General Aspects of Yield Stress Fluids – Terminology and Definition of Viscosity Abstract : v. 24, p. 1–11, 2014.

BOYLE, N. M.; ROCHFORD, J.; PRYCE, M. T. Thienyl — Appended porphyrins : Synthesis , photophysical and electrochemical properties , and their applications. v. 254, p. 77–102, 2010.

CALANDRINI, V. et al. Role of hydrophobic interactions on the stabilisation of native state of globular proteins. **Chemical Physics Letters**, v. 324, n. 5–6, p. 344–348, 2000.

CALIXTO, G. et al. Polyacrylic acid polymers hydrogels intended to topical drug delivery: preparation and characterization. **Pharm Dev Technol**, p. 1083–7450, 2014.

CHEN, D. T. N. et al. Rheology of Soft Materials. **Annu. Rev. Condens. Matter Phys**, v. 1, p. 301–22, 2010.

CHEN, J.-J.; GAO, L.-J.; LIU, T.-J. Photodynamic therapy with a novel porphyrin-based photosensitizer against human gastric cancer. **Oncology letters**, v. 11, n. 1, p. 775–781, 2016.

CHEN, X. et al. Conformation transition kinetics of regenerated Bombyx mori silk fibroin membrane monitored by time-resolved FTIR spectroscopy. **Biophysical Chemistry** 89, v. 89, p. 25–34, 2001.

COSMA, E. UV-VIS and Fluorescence Spectra of Meso-Tetraphenylporphyrin and Meso-Tetrakis-(4-Methoxyphenyl) Porphyrin in THF and THF-Water Systems. The Influence of pH. v. 58, n. REV. CHIM, 2007.

DE MORAES, M. A. et al. Formation of silk fibroin hydrogel and evaluation of its drug release profile. **Journal of Applied Polymer Science**, v. 132, n. 15, p. 1–6, 2015.

DOS SANTOS, A. C. M. et al. Poloxamer-based binary hydrogels for delivering tramadol hydrochloride: Sol-gel transition studies, dissolution-release kinetics, in vitro toxicity, and pharmacological evaluation. **International Journal of Nanomedicine**, v. 10, p. 2391–2401, 2015.

ETHIRAJAN, M. et al. The role of porphyrin chemistry in tumor imaging and photodynamic therapy. **Chemical Society reviews**, v. 40, p. 340–362, 2011.

FALLIS, A. . J. V. **Biochemistry V**. [s.l.: s.n.]. v. 53

FRANCIS, R.; SAKTHI, K. **Biomedical Applications of polymeric Materials and Composites**. [s.l.] Wiley- VCH, 2013.

GALEOTTI, F. et al. Precise surface patterning of silk fibroin films by breath figures. **Soft**



**Matter**, v. 8, n. 17, p. 4815, 2012.

GIUNTINI, F. et al. Conjugatable water-soluble Pt(II) and Pd(II) porphyrin complexes: novel nano- and molecular probes for optical oxygen tension measurement in tissue engineering. **Photochemical & photobiological sciences : Official journal of the European Photochemistry Association and the European Society for Photobiology**, v. 13, n. 7, p. 1039–51, jul. 2014.

GREABU, M.; VIRLAN, M. Silk Fibroin and Potential Uses in Regenerative Dentistry-a Systematic Review. **Stomatology Edu ...**, v. 1, p. 32–39, 2015.

GRYCZYN, Z. Spectrochimica Acta Part A : Molecular and Biomolecular Spectroscopy Physicochemical properties of potential porphyrin photosensitizers for photodynamic therapy. v. 146, p. 249–254, 2015.

GUO, B. et al. Decoration of Porphyrin with Tetraphenylethene: Converting Fluorophore with Aggregation-Caused Quenching to Aggregation-Induced Emission. **J. Mater. Chem. B**, v. 4, n. 4, p. 4690–4695, 2016.

HARDY, J. G.; LEAL-EGAÑA, A.; SCHEIBEL, T. R. Engineered spider silk protein-based composites for drug delivery. **Macromolecular Bioscience**, v. 13, n. 10, p. 1431–1437, 2013.

HONG, E. J.; CHOI, D. G.; SHIM, M. S. Targeted and effective photodynamic therapy for cancer using functionalized nanomaterials. **Acta pharmaceutica Sinica. B**, v. 6, n. 4, p. 297–307, 2016.

HUANG, X.; NAKANISHI, K.; BEROVA, N. Porphyrins and Metalloporphyrins: Versatile Circular Dichroic Reporter Groups for Structural Studies. **Chirality**, v. 12, p. 237–255, 2000.

JANMEY, P. A.; SCHLIWA, AND M. Rheology. v. 18, n. 15, p. 1–5, 2010.

JOANA, A.; VASCONCELOS, C. Andreia Joana Costa Vasconcelos Protein matrices for wound dressings. 2010.

JOSEPH, B.; RAJ, S. J. Therapeutic applications and properties of silk proteins from Bombyx mori. **Frontiers in Life Science**, v. 6, n. 3–4, p. 55–60, 2012.

KAPOOR, S.; KUNDU, S. C. Silk protein-based hydrogels: Promising advanced materials for biomedical applications. **Acta Biomaterialia**, v. 31, p. 17–32, 2016.

KAROLCZAK, J. et al. Photophysical Studies of Porphyrins and Metalloporphyrins : Accurate Measurements of. p. 4570–4575, 2004.

KEARNS, V. et al. Silk-based Biomaterials for Tissue Engineering. **Topics in Tissue Engineering Tissue Engineering**, v. 4, n. 4, 2008.

KHAN, M. M. R.; TSUKADA, M. **Silk Biomaterials for Tissue Engineering and Regenerative Medicine**. [s.l: s.n.].

KIM, D.-H. et al. Dissolvable films of silk fibroin for ultrathin conformal bio-integrated electronics. **Nature Materials**, v. 9, n. 6, p. 511–517, 2010.

KIM, S.; FUJITSUKA, M.; MAJIMA, T. Photochemistry of singlet oxygen sensor green (supporting information). **Journal of Physical Chemistry B**, v. 117, n. 45, p. 13985–13992, 2013.

KOH, L.-D. et al. Structures, mechanical properties and applications of silk fibroin materials. **Progress in Polymer Science**, v. 46, p. 86–110, 2015.

KUMARI, P.; GAUTAM, R.; MILHOTRA, A. Application of Porphyrin nanomaterials in Photodynamic therapy. **Chemical Biology Letters**, v. 3, n. 2, p. 32–37, 2016.

KUNDU, B. et al. Silk fibroin biomaterials for tissue regenerations. **Advanced Drug Delivery Reviews**, v. 65, n. 4, p. 457–470, 2013.

KUNDU, B. et al. Silk proteins for biomedical applications: Bioengineering perspectives. **Progress in Polymer Science**, v. 39, n. 2, p. 251–267, 2014.

KUNDU, J. et al. Silk fibroin/poly(vinyl alcohol) photocrosslinked hydrogels for delivery of macromolecular drugs. **Acta Biomaterialia**, v. 8, n. 5, p. 1720–1729, 2012.

LAWRENCE, B. D. **Processing of Bombyx mori silk for biomedical applications**. [s.l: s.n.].

LE, V. H. et al. Bcl-2 Promoter Sequence G-Quadruplex Interactions with Three Planar and Non-Planar Cationic Porphyrins: TMPyP4, TMPyP3, and TMPyP2. **PLoS ONE**, v. 8, n. 8, 2013.

LEE, Y.; BARON, E. D. Photodynamic Therapy: Current Evidence and Applications in Dermatology. **Seminars in Cutaneous Medicine and Surgery**, v. 30, n. 4, p. 199–209, 2011.

LIHUI WENG, X. C.; CHEN, W. Rheological Characterization of in situ Crosslinkable Hydrogels Formulated from Oxidized Dextran and N-Carboxyethyl Chitosan. **NIH Public Access**, v. 8, n. 4, p. 1109–1115, 2008.

LIU, Y. et al. Thixotropic silk nanofibril-based hydrogel with extracellular matrix-like structure. **Biomater. Sci.**, v. 2, n. 10, p. 1338–1342, 2014.

LOVELL, J. F. et al. Porphyrin-Cross-Linked Hydrogel for Fluorescence-Guided Monitoring and Surgical Resection. 2011a.

LOVELL, J. F. et al. Porphysome nanovesicles generated by porphyrin bilayers for use as multimodal biophotonic contrast agents. **Nature Materials**, v. 10, n. 4, p. 324–332, 2011b.

LV, Q. et al. Preparation of Insoluble Fibroin Films Without Methanol Treatment. n. March, p. 3–8, 2004.

MACOSKO, C. W. **RHEOLOGY Principles , Measurements and Applications**. [s.l: s.n.].

MAITRA, J.; SHUKLA, V. K. Cross-linking in Hydrogels - A Review. **American Journal of Polymer Science**, v. 4, n. 2, p. 25–31, 2014.

MAKARSKA-BIALOKOZ, M. Spectroscopic study of porphyrin-caffeine interactions. **Journal of Fluorescence**, v. 22, n. 6, p. 1521–1530, 2012.

MALKIN, ALEXANDER YA.; ISAYEV, A. I. **Rheology : Concepts, Methods and Applications**. 2. ed. [s.l.] ChemTec Publishing, 2012.

MARELLI, B. et al. Silk Fibroin as Edible Coating for Perishable Food Preservation. **Scientific Reports**, v. 6, p. 25263, 6 maio 2016.

MEINEL, L. et al. The inflammatory responses to silk films in vitro and in vivo. **Biomaterials**, v. 26, p. 147–155, 2005.

MELKE, J. et al. Silk fibroin as biomaterial for bone tissue engineering. **Acta Biomaterialia**, v. 31, p. 1–16, 2015.

MICHELLE NOGUEIRA, G. et al. Hydrogels from silk fibroin metastable solution: Formation and characterization from a biomaterial perspective. 2011.

MITROPOULOS, A. N. et al. Transparent, Nanostructured Silk Fibroin Hydrogels with Tunable Mechanical Properties. **ACS Biomaterials Science & Engineering**, v. 1, n. 10, p. 964–970, 2015.

MOHAMED, M. I. Optimization of Chlorphenesin Emulgel Formulation. **The AAPS Journal** 2004;, v. 3, n. 6, 2004.

MOREIRA, L. M. et al. Photodynamic therapy: Porphyrins and phthalocyanines as photosensitizers. **Australian Journal of Chemistry**, v. 61, n. 10, p. 741–754, 2008.

MOTTA, A. et al. Fibroin hydrogels for biomedical applications: preparation, characterization and in vitro cell culture studies. **Journal of biomaterials science. Polymer edition**, v. 15, n. 7, p. 851–864, 2004.

MURATA, H. Rheology – Theory and Application to Biomaterials. **INTECH**, 2012.

MYUNG, S. J. et al. Fluorescent silk fibroin nanoparticles prepared using a reverse microemulsion. **Macromolecular Research**, v. 16, n. 7, p. 604–608, 2008.

NOGUEIRA, G. M. et al. Preparation and characterization of ethanol-treated silk fibroin dense membranes for biomaterials application using waste silk fibers as raw material. **Bioresource Technology**, v. 101, n. 21, p. 8446–8451, nov. 2010.

O'CONNOR, A. E.; GALLAGHER, W. M.; BYRNE, A. T. Porphyrin and nonporphyrin photosensitizers in oncology: Preclinical and clinical advances in photodynamic therapy. **Photochemistry and Photobiology**, v. 85, n. 5, p. 1053–1074, 2009.

OCHI, A. et al. Rheology and Dynamic Light Scattering of Silk Fibroin Solution Extracted from the Middle Division of Bombyx mori Silkworm. **Biomacromolecules**, v. 3, n. 6, p. 1187–1196, 2002.

OSSWALD, T. **Polymer Rheology**. [s.l.: s.n.].

OSUKA, T. T. AND A. Chem Soc Rev and applications for functional materials. 2014.

PANILAITIS, B. et al. Macrophage responses to silk. **Biomaterials**, v. 24, p. 3079–3085, 2003.

PARTLOW, B. P. et al. Dityrosine Cross-Linking in Designing Biomaterials. **ACS Biomaterials Science and Engineering**, v. 2, n. 12, p. 2108–2121, 2016.

PÉREZ-MORALES, M. et al. Soret emission from water-soluble porphyrin thin films: effect on the electroluminescence response. **Journal of Materials Chemistry**, v. 19, n. 24, p. 4255, 2009.

PRITCHARD, E. M. et al. Encapsulation of oil in silk fibroin biomaterials. **Journal of Applied Polymer Science**, v. 131, n. 6, p. n/a-n/a, 15 mar. 2014.

RAQUEL, J.; ACIARI, F. Preparação de micropartículas de fibroína da seda calcificadas. 2013.

REKAS, A. et al. PAMAM Dendrimers as Potential Agents against Fibrillation of  $\alpha$ -Synuclein, a Parkinson's Disease-Related Protein. p. 230–238, [s.d.].

ROCKWOOD, D. N. et al. Materials fabrication from Bombyx mori silk fibroin. **NATURE PROTOCOLS**, n. September, 2011.

SAUER, M.; HOFKENS, J.; ENDERLEIN, J. Basic Principles of Fluorescence Spectroscopy. In: **Handbook of Fluorescence Spectroscopy and Imaging**. Weinheim, Germany: Wiley-VCH Verlag GmbH & Co. KGaA, 2011. p. 1–30.

SCHARAMM, G. **Practical approach reology**. [s.l.: s.n.].

SCHMID, F.-X. Biological Macromolecules: UV-visible Spectrophotometry. **ENCYCLOPEDIA OF LIFE SCIENCES**, 2001.

SO, P. T.; DONG, C. Y. Fluorescence Spectrophotometry. **ENCYCLOPEDIA OF LIFE SCIENCES** /, 2002.

SWINERD, V. M. et al. Silk inverse opals from template-directed  $\beta$ -sheet transformation of regenerated silk fibroin. **Soft Matter**, v. 3, n. 11, p. 1377, 2007.

THURBER, A. E.; OMENETTO, F. G.; KAPLAN, D. L. In vivo bioresponses to silk proteins. **Biomaterials**, v. 71, p. 145–157, 2015.

TITA, S. P. S.; PERUSSI, J. R. The effect of porphyrins on normal and transformed mouse cell lines in the presence of visible light. **Brazilian Journal of Medical and Biological Research**, v. 34, n. 10, p. 1331–1336, 2001.

TRIANTAFILLOPOULOS, N. Measurement of Fluid Rheology and Interpretation of Rheograms Second Edition. [s.d.].

UDDIN, J. (ED.). **Macro To Nano Spectroscopy**. [s.l.] InTech, 2012.

ULLAH, F. et al. Classification, processing and application of hydrogels: A review. **Materials Science and Engineering C**, v. 57, p. 414–433, 2015.

UQI, Y. et al. A Review of Structure Construction of Silk Fibroin Biomaterials from Single

Structures to Multi-Level Structures. **International Journal of Molecular Sciences**, v. 18, n. 3, p. 237, 2017.

VEPARI, C.; KAPLAN, D. L. Silk as a biomaterial. **Progress in Polymer Science (Oxford)**, v. 32, n. 8–9, p. 991–1007, 2007.

VIOLETA GHICA, M. et al. Flow and thixotropic parameters for rheological characterization of hydrogels. **Molecules**, v. 21, n. 6, 2016.

WALKER, J. M. **The Protein Protocols Handbook**. [s.l: s.n.].

WENK, E.; MERKLE, H. P.; MEINEL, L. Silk fibroin as a vehicle for drug delivery applications. **Journal of Controlled Release**, v. 150, n. 2, p. 128–141, 2011.

WRAY, L. S. et al. Effect of processing on silk-based biomaterials: reproducibility and biocompatibility. **Journal of biomedical materials research. Part B, Applied biomaterials**, v. 99, n. 1, p. 89–101, out. 2011.

WYSS, H. M. R. J. L. Oscillatory Rheology Measuring the Viscoelastic Behaviour of Soft Materials. **G.I.T. Laboratory Journal**, p. 68–70, 2007.

YANG, Y. et al. Optical spectroscopy to investigate the structure of regenerated Bombyx mori silk fibroin in solution. **Biomacromolecules**, v. 5, n. 3, p. 773–779, 2004.

ZAHARIA, C. et al. Silk fibroin films for tissue bioengineering applications. **Journal of Optoelectronics and Advanced Materials**, v. 14, n. 1–2, p. 163–168, 2012.

ZENKEVICH, E. et al. Photophysical properties of self-aggregated porphyrin: Semiconductor nanoassemblies. **International Journal of Photoenergy**, v. 2006, p. 1–7, 2006.

ZHENG, Z. et al. Lithium-free processing of silk fibroin. **Journal of Biomaterials Applications**, v. 0, n. 0, p. 1–14, 2016.